PUT YOUR BACK INTO IT: A STRUCTURAL AND MECHANICAL CHARACTERIZATION OF ILIAC CREST AND CERVICAL SPINE AUTOGRAFT FOR ACDF SURGERIES

Jackson Simon Comer

Thesis submitted to the faculty of the Virginia Polytechnic Institute and State University in partial fulfillment of the requirements for the degree of

Master of Science

In

Biomedical Engineering

Caitlyn J. Collins, Chair
Andrew R Kemper
David Gray

6/20/24
Blacksburg, VA
Keywords: ACDF, Autograft, Cervical Spine, Iliac Crest, Bone Mechanical Characterization

PUT YOUR BACK INTO IT: A STRUCTURAL AND MECHANICAL CHARACTERIZATION OF ILIAC CREST AND CERVICAL SPINE AUTOGRAFT FOR ACDF SURGERIES

Jackson Simon Comer

ABSTRACT

Anterior cervical discectomy and fusion (ACDF) is one of the most common cervical spine surgery procedures performed worldwide. ACDF utilizes autologous bone graft (autograft) from the iliac crest to induce fusion between neighboring vertebrae following the procedure. The iliac crest is widely considered the gold-standard autograft for ACDF procedures due to its osteoinductive, osteoconductive, and osteointegrative properties. However, harvesting from a second surgical site, as seen with iliac crest autograft, is commonly associated with short- and long-term complications.

To mitigate iliac crest harvest site complications, a novel autograft location must be identified. The adjacent cervical vertebral body has been identified as a potential alternative donor site to the iliac crest. Previous studies have shown that this novel autograft site does not biomechanically compromise the vertebral body harvest site and has demonstrated clinically successful fusion rates comparable to those of the iliac crest. Despite prior successful fusion, a direct morphological and mechanical comparison between autograft from the adjacent cervical vertebra and iliac crest has not been thoroughly investigated.

The primary goal of this thesis was to morphologically and mechanically compare the cervical spine and iliac crest. It was hypothesized that the cervical spine and iliac crest would not significantly vary in their morphological properties; however, due to daily physiological

loading at each graft location, it was hypothesized that the two graft locations would differ mechanically.

A clinical model utilizing iliac crest and cervical vertebral bone from human donors was characterized at the meso- and microscale to quantify morphological properties and collagen organization using micro-computed tomography (microCT) and second-harmonic generation (SHG) imaging modalities, respectively. A pre-clinical large animal model was used to characterize the mechanical and material properties of lumbar spine tissue, under similar physiological loading as the cervical spine, relative to the iliac crest through uniaxial compression testing.

No significant difference was identified in the morphological and collagen organization properties in tissue from a human clinical cohort; however, directionality and anatomical location significantly impacted the mechanical and material properties in a bovine comparative anatomy model. Here, trabecular bone from the lumbar vertebra was found to be transversely isotropic whereas iliac crest trabecular bone was nearly isotropic; thus, directionality and anatomical location should be considered and quantified when selecting autograft tissue for future ACDF surgeries.

Further characterization of the mechanical properties of cervical vertebral tissue and determination of correlations between directionality, anatomical location, and morphology through microCT and compression testing should be completed before adopting the cervical vertebra as the gold standard autograft for ACDF procedures.

PUT YOUR BACK INTO IT: A STRUCTURAL AND MECHANICAL CHARACTERIZATION OF ILIAC CREST AND CERVICAL SPINE AUTOGRAFT FOR ACDF SURGERIES

Jackson Simon Comer

GENERAL AUDIENCE ABSTRACT

Anterior cervical discectomy and fusion (ACDF) is a common upper spine surgery that helps to stabilize the spine by fusing two or more vertebrae together. To achieve this fusion, surgeons often use bone grafts taken from the patient's own hip, specifically the iliac crest. While this method is effective, it can lead to complications at the hip bone harvest site.

To avoid these complications, researchers are exploring the possibility of using bone from a nearby vertebra in the upper spine as an alternative graft source. Early studies suggest that using bone from the upper spine does not weaken the spine and achieves similar success rates in fusion as the hip bone. However, a detailed comparison between both graft sites has not been thoroughly investigated until now.

The main goal of this thesis was to compare the bone from the upper spine and the hip in terms of structure and strength. It was expected that the two types of bone would be similar in structure but different in strength due to difference forces they experience in the body.

The research involved examining human bone samples from both the upper spine and hip using advanced imaging techniques to analyze their structure and collagen organization. Additionally, a large animal comparative model was used to test the strength and material properties of bone from the lower spine and hip, which experience similar forces as the human upper spine and hip.

The findings showed no significant difference in the structure and collagen organization of the human bone samples. However, in the animal model, the strength and material properties of the bone significantly varied depending on the direction and location. Bone from the lower spine was found to be significantly stronger in one direction in comparison to two other directions in the lower spine and all three directions in the hip.

These results suggest that when choosing bone for fusion in ACDF surgeries, it is important to consider the direction and location of the graft. Further research is needed to fully understand the mechanical properties of upper spine bone and to confirm its suitability as a standard graft for ACDF procedures.

Acknowledgements

First and foremost, I would like to thank Dr. Caitlyn Collins for taking a chance on a Junior in college and for helping him thrive within the world of research. Her expertise and love of bone is shown through her passion to lecture the material and ability to make knowledgeable bone puns, and I hope I can achieve a similar level of mastery in any field. Thank you for your constant guidance and support through school, careers, and life.

I would also like to thank my committee members, Dr. Andrew Kemper and Dr. David Gray, for their time and guidance in helping me complete my thesis. I was constantly pushed to expand my thought process, something that is invaluable to use in future fields. I appreciate Dr. Kemper for giving me my first professional teaching experience and I appreciate Dr. Gray for introducing me to the world of interdisciplinary design.

Next, I would like to thank the members of the ACDF3 team who I collaborated with over the last couple of years. I extend my gratitude to Haseeb Goheer, the medical student I had the pleasure of working with throughout this process and someone who I look up to for their extraordinary work ethic.

I would like to thank my collaborators at Virginia Tech Carillion Clinic and Dr. Jonathan Carmouche for giving me the ability to perform a clinical trial as a master's level student. I would like to thank my collaborators at Virginia Tech Fralin Biomedical Research Institute and Dr. Sharon Michelhaugh for her constant help and kindness during sample prep. I would like to thank Dr. Vincent Wang and Dr. Jake Socha for their mentorship and access to the testing instruments in their labs. I would like to thank Emily Rogers, Dylan Easley, Raffae Ahmad, and Aileen Suarez for their mentorship of the instruments I utilized to complete this thesis.

I would like to acknowledge the financial support I received from the Carilion Clinic Research Acceleration Program and the National Center for Advancing Translational Science of the NIH to complete this thesis. I would also like to acknowledge the help of BioRender for creating plenty of figures in this paper and my defence.

I would not have had the drive to complete this thesis without the support from my lab mates in the Collins Lab. They made research a joy and I will cherish the plentiful number of hours spent together in the lab.

Finally, I would like to Meg Comer, Mike Comer, Nick Comer, Sarah Comer, and Emily Maida for their constant support and encouragement throughout the thesis project. Their love and support was more than I could ever ask for.

Table of Contents

List of Tables

List of Equations

List of Figures

Chapter 1 - Introduction

The cervical spine plays a critical role in mobility and support of the head and neck. Specifically, the cervical spine serves as the junction between the head and the back, protecting the spinal cord as well as the vessels providing blood flow to the brain, and enables a wide range of motion essential for our quality of life [1]. Due to the high utilization of the cervical spine in everyday life, most humans will experience neck and upper back pain in their lifetime. Neck pain, ranging from a small twinge to debilitating pain, is a pervasive condition reported to impact over 203 million people across the globe and is expected to rise to 269 million by 2050 [2]. In addition to neck pain, the upper back, arms, chest, and shoulders may experience pain due to cervical radiculopathy (pinched nerves), impacting patient quality of life and daily function [3]. Deteriorated, degenerated, and herniated cervical spinal discs are most associated with neck pain, cervical radiculopathy, and cervical myelopathy (compressed spinal cord). Neck pain resulting from these conditions not only negatively affects quality of life but is also associated with a high health care economic burden with a total spending estimate over $134.5 billion [4].

Effective in treating lower levels of neck pain, initial conservative steps are taken at the onset of treatment for most cases of degenerative disc disease, including physical therapy, pain medication, and local injections [5]. While effective in managing minor symptoms, conservative approaches to treating chronic neck pain only reduce the pain rather than eliminating it. Thus, more invasive approaches are most commonly utilized to treat chronic neck pain. Specifically, Anterior Cervical Discectomy and Fusion (ACDF) is a treatment performed 137,000+ times

annually to treat chronic neck pain for patients with damaged cervical discs [6]. To induce fusion between neighboring vertebrae following an ACDF procedure, damaged discs are removed and replaced with a spacer containing an osteoinductive material. Traditionally, this material is autologous bone graft (autograft), which promotes bone growth and fusion throughout the spacer, thereby fusing the neighboring vertebrae together. The standard-of-care autograft is typically taken from the iliac crest for ACDF surgeries, necessitating a secondary surgical incision. ACDF is consistently used for its minimal risk, consistent clinical results, and high fusion rates, ranging from 83-99% [7], [8], [9], [10]. Despite these benefits, ACDF is associated with a high rate of morbidity at the autograft donor site with 91.3% of patients reporting pain there [8], [9], [11]. Moreover, secondary donor graft sites are associated with longer operation times, increased time under anesthetic agents, and additional time for surgical complications to surface [8].

Currently, autograft alternatives, such as xenografts, allografts, and artificial grafts, have been utilized and analyzed; however, each graft has its own unique set of complications to mitigate when used in ACDF surgeries [7]. Given the limitations of autograft alternatives and complications associated with secondary surgical sites, experiments have been conducted in the last 7 years at Virginia Tech and Carillion Clinic to determine the feasibility of a novel autograft donor site; namely the inferior vertebral body adjacent to the operative space [8], [9]. Walterscheid et. al. proved that this location was biomechanically viable and can withstand the excision of autograft without compromising the integrity of the vertebral body [8]. O'Neill et. al. preliminarily studied the fusion rates in a clinical study utilizing inferior adjacent vertebral autograft, reporting that the treating surgeon, a blinded radiologist, and a senior spine surgeon

all confirmed fusion from radiographs taken 1-year post-operation [9]. Harvest site stability following graft resection and fusion rates are comparable to the standard-of-care autograft taken from the iliac crest for the ACDF procedure [9]. While these preliminary results are promising, further research is needed to understand why the inferior adjacent cervical vertebral bone exhibits comparable fusion rates to the standard iliac crest autograft. This understanding is crucial for adopting cervical vertebral bone as the gold standard for ACDF, which could mitigate all morbidities associated with secondary surgical incisions. Characterizing the tissue level, micro level, and mechanical properties of bone is crucial for considering cervical vertebrae as the new standard-of-care for ACDF surgeries.

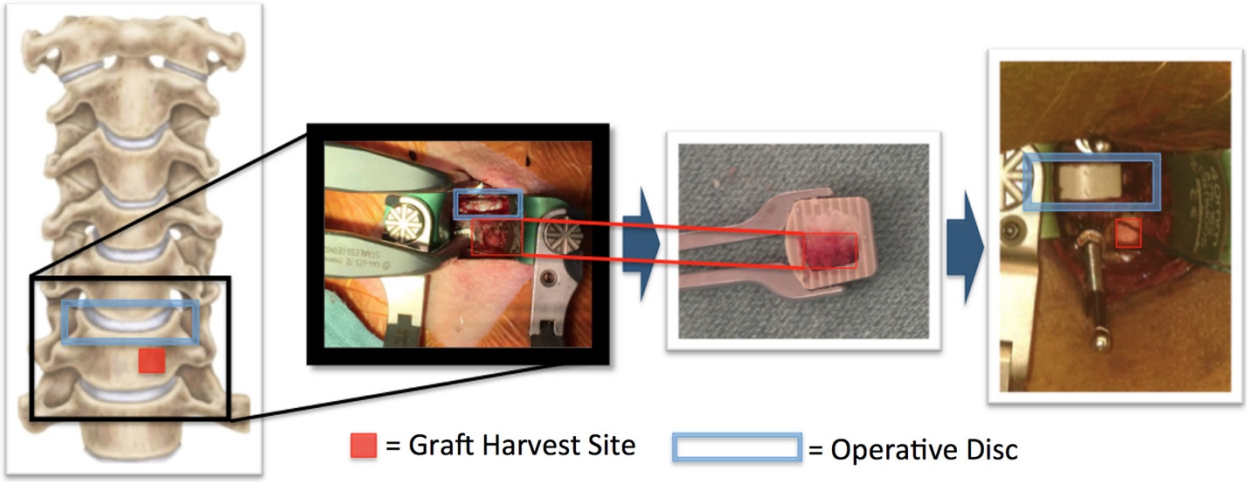

Figure 1: An ACDF surgery utilizing a novel autograft site found at the adjacent cervical spine [9].

Trabecular bone, irrespective of its donor location, is traditionally used as autograft material in ACDF and other surgeries. Its extensive surface area and porous nature promote revascularization and integration at the recipient site [12], [13]. Additionally, the high concentrations of osteoblasts and osteocytes within the tissue facilitate bone growth for fusion. Of the methods utilized in characterizing the tissue level of trabecular bone, micro-computed tomography (microCT) is an established tool utilized to study the micro-architecture of bone to

evaluate its structure and quality [13], [14], [15]. As noted, the porosity and micro-architecture of trabecular bone can help us better understand potential differences in cellular metabolic activity associated with growing bone within a trabecular bone autograft for stable fusion [12], [13].

To supplement the tissue level characterization, micro level characterization of the collagen structure within trabecular bone is necessary to understand potential bone growth patterns for newly formed bone and the stiffness and toughness properties of trabecular bone under loading [16]. Collagen alignment and organization has been proven to be directly correlated with bone strength and its mechanical integrity [17], [18], [19]. Due to the different loading patterns within the iliac crest and cervical spine, different collagen alignments may occur, resulting in weak randomly arranged fibers or strong, highly organized fibers [16], [20], [21]. Thus, collagen organization may impact bone integrity and quality should osteoblasts parallel a weak collagen alignment utilized in autograft bone [16].

The mechanical properties of trabecular bone, including its stiffness and strength, are essential for characterizing its ability to withstand physiologically mechanical loads it will experience during and after healing post-ACDF [22], [23], [24]. The iliac crest and cervical spine undergo vastly different physiologically compressive loads; however, the two have not been directly compared. As the bone fuses following an ACDF procedure, the mechanical properties of the autograft may impact how newly formed bone grows in response to varied mechanical loads.

Objective

The present study follows the experimental work performed by Walterscheid et. al. and O'Neill et. al. which identified and tested in-vivo the inferior adjacent cervical vertebra as an alternative autograft donor source to be utilized in an ACDF surgery. The goal of the present research was to compare the morphological, mechanical, and osteogenic properties between the iliac crest and cervical spine autograft locations. This work was achieved through the following aims:

1. Characterize and compare the osteogenic properties within the microarchitectural niche of human iliac crest and cervical spine autograft tissue via microCT and SHG data;
2. Characterize and compare the mechanical properties of cow iliac crest and cervical spine trabecular bone via compression testing.

The primary objective of the study was to be the first direct comparison of iliac crest and cervical spine autograft tissue to support the usage of an autograft donor site that mitigates current complications with secondary surgical sites and promotes interbody fusion. To accomplish this objective, a radiological analysis of experimental results for human autograft tissue from both donor locations and a mechanical analysis of experimental results for cow trabecular bone tissue from both donor locations were conducted. Should the cervical spine autograft demonstrate similar morphological, mechanical, and osteogenic properties in comparison to the iliac crest, it can be concluded that the cervical spine is a viable autograft donor site and should continue to be tested in-vivo for ACDF surgeries. If significant differences are found between the iliac crest and cervical spine autograft sites, further characterization is

necessary to analyze why the cervical spine autograft displayed similar fusion rates to iliac crest for ACDF surgeries in a preliminary study and to better understand what characteristics greatly impact spinal fusion using autograft.

Chapter 2 - Background

Physiological Loading in the Spine

The spine, made up of 33 vertebra, 23 spinal discs, and soft tissues, is the central support structure for the body. Spanning the back and connecting the head, chest, pelvis, shoulders, arms, and legs, the spine provides stability to the entire body [25]. These connections, in addition to body weight, contribute to a multitude of complex dynamic and static loads that are placed on the spine. The multitude of joints associated with each connection allow the body to move freely with dix degrees of freedom: translational – medial-lateral, superior-inferior, and anterior-posterior; flexion-extension, twist, and lateral bending [25].

Of the 33 vertebra, the superior seven make up the cervical spine, titled C1-C7. C1, known as the atlas, connects the skull to the neck and bears the load of the head [26]. C2, the axis, bears the load of the atlas and increases the range of motion of C1's movements [26]. C3-C7, also called the subaxial cervical spine, have a traditional trabecular bone body and cortical dorsal vertebral arch enclosing the spinal cord (**Figure 2**) and associated vascular structures [26], [27].

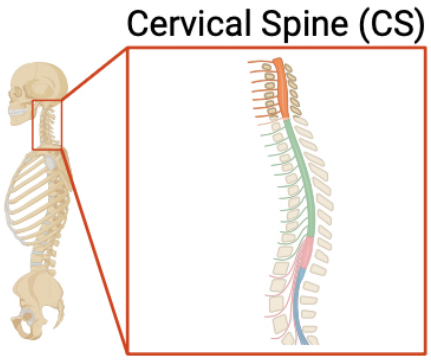

Figure 2: The cervical spine location highlighted on both a sagittal view of the human skeleton and the whole spine.

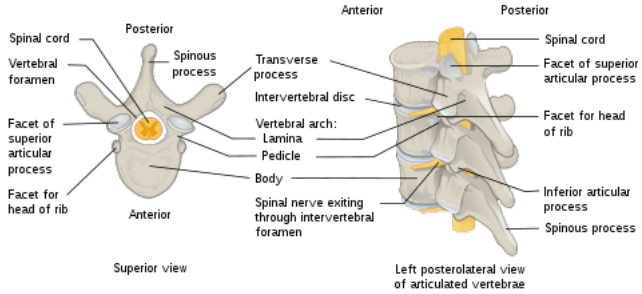

Figure 3: The anatomical features of the spinal column and vertebra in two different views [28].

These cervical vertebrae also have intervertebral discs, comprised of an annulus fibrosus and nucleus pulpous, to distribute loads within the spine. In comparison with the vertebrae in the thoracic spine, the 12 vertebrae following the cervical spine, and the lumbar spine, the 5 vertebrae following the thoracic spine, the cervical vertebral bodies are smaller due to lighter loads associated with only supporting the head and neck at this section of the spine, rather than other limbs and organs [27]. In turn, this increases the mobility of the cervical spine [27]. The cervical spine range of motion (ROM) includes four movements in the sagittal, coronal, and transverse planes: flexion that bends the head toward the chest, extension that bends the head backward with the face looking towards the sky, axial rotation that turns the head left and right,

and lateral flexion-extension, also known as side-bending, that tips the head to the side as seen when the ear touches the ipsilateral shoulder (**Figure 4**) [26].

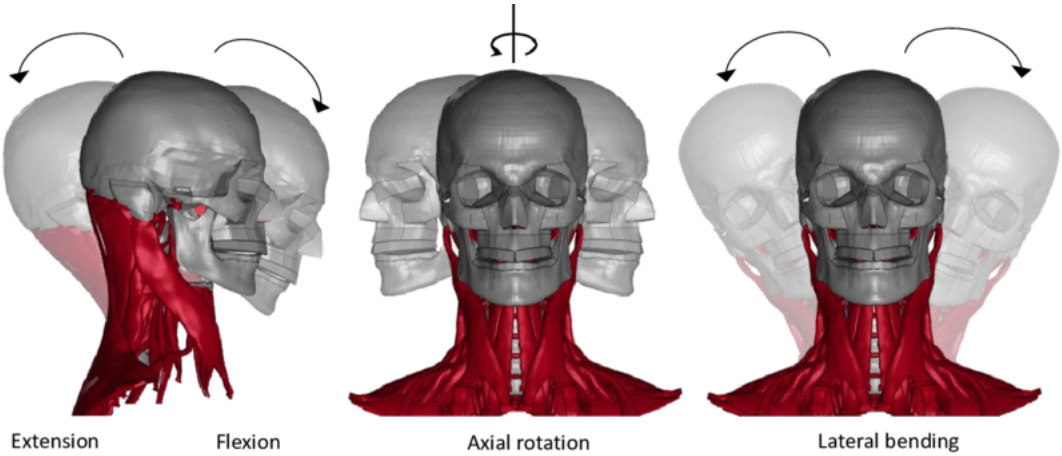

Figure 4: The anatomical features of the spinal column and vertebra in two different views [29].

This elevated mobility and flexibility leads to a greater risk of injury to the cervical spine as loads shift during daily life [27]. For example, compressive loads increase as the cervical spine flexes and extends from a neutral alignment [30]. Shear and torsional forces, which are roughly 10% and 1.5% of the compressive force, also contribute to the combined loading acting on the spine [30], [31]. Extra strenuous activities, such as contact sports and weightlifting, may increase the cervical spine's compressive force; nonetheless, individuals with healthy discs can typically withstand the excessive loading [30]. Additionally, age and sex contribute to the shape of the vertebral bodies', impacting the distribution of the forces within the cervical spine. Notably, aging reduces the water content in discs by approximately 16% in comparison to newborns, increasing the rigidity and stiffness of the aged discs [32]. Cervical vertebral bodies also elongate, widen, and shorten as they age reducing their ability to absorb shock [32], [33]. Sex-based differences in cervical vertebral body size have also been observed, with consistently larger dimensions in males than in females in every metric [33].

Healthy discs play a large part in dispersing physiological loads to ensure that the individual does not experience pain. Discs are designed to combat torsional and shear forces attempting to lengthen or compress the spine [34]. In doing so, the discs protect the vertebrae from unnecessarily large forces that could result in tissue degeneration and the increased risk of vertebral body fractures [34].

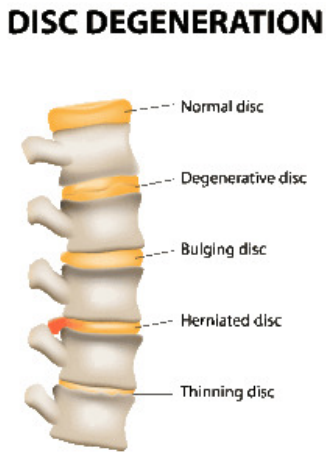

Figure 5: The anatomical features of the spinal column and vertebra in two different views [28].

Disc composition changes as individuals age, increasing their risk of cervical spinal disc injuries. 53.3 years old is the average age of patients undergoing spinal fusion to treat injuries such as degenerative disc disease and disc herniation [35]. Degenerative disc disease, which is attributed mostly to aging and genetic factors, has debilitating stages of dysfunction, instability, and over-stiffening associated with water and proteoglycan supply loss in the annulus fibrosus and nucleus pulpous [36]. As the water content decreases, the nucleus pulpous gel-like consistency thickens, reducing its resistance to physiological loading [36]. This promotes radial and circumferential tears in the annulus, disc herniation, joint degeneration, and extreme stiffness in the discs that can cause myelopathy, the compression of the spinal cord, and radiculopathy, pinching of the nerve roots exiting the spinal cord, in the cervical spine [36].

Along with degenerative disc disease, herniated discs can also cause massive amounts of pain to individuals. Herniated discs occur when the annulus fibrosus remains intact but bulges from the disc or when it cracks and ruptures [37]. Disc herniations can be attributed to the dysfunction and instability phases of degenerative disc diseases because of bony overgrowth narrowing the disc space or to violent compressive trauma seen in car crashes or contact sports [37], [38]. Herniated discs can press against the nerves, causing radiating pain within the back and surrounding limbs and leading to cervical myelopathy and radiculopathy [37], [38]. Treatments for these conditions can range from conservative physiotherapy to surgical intervention, depending on the severity of pain and degeneration.

ACDF Surgery

When determining how to manage pain associated with herniated discs and disc degeneration, the extent of the pain, progression of the disease/herniation, and loss of function in the neck are first considered [37], [38], [39]. Physical evaluation can be performed to assess an individual's ROM to identify the severity of pain and degeneration [39]. The normalized ROM index for C5-C6 vertebra levels has been reported to increase from 10.4% to 27.1% to 56.8% in flexion, and from 3.7% to 16.2% to 41.2% in extension as disc degeneration disease worsens, highlighting the impact of worsening spinal stability between mild and severe disease states. [40]. Identifying symptoms such as muscle pain, radiating pain, decrease in overall mobility, numbness, and muscle spasms can also help with the evaluation of an individual's cervical spine pain [8], [37], [38], [39]. For a more in-depth analysis and clearer understanding of the current level of herniation and disc degeneration, imaging modalities such as x-rays, computed

tomography (CT) scans, and magnetic resonance imaging (MRI) can be performed [37], [38], [39].

After determining the patient's levels of pain, treatments and management can be proscribed. Conservative treatments, such as collar immobilization, traction, pharmacotherapy, physical therapy, cervical manipulation, and steroids, are traditionally applied prior to invasive techniques [37], [38], [39]. Conservative treatments serve as inexpensive options to help mediate initial mild to moderate pain associated with herniated and degenerated discs. However, 10-25% of patients don't see improvement from conservative treatments, resulting in the need for surgical treatment [37], [38], [39].

With varying effectiveness rates, surgery is recommended to patients who don't see improvement within 6 weeks of beginning conservative therapy [41]. There are three major surgical techniques to treat myelopathy and trauma within the surgical spine: laminectomy, spinal fusion, and anterior cervical discectomy and fusion (ACDF).

ACDF, the gold standard for degenerative and herniated conditions within the cervical spine, is the most used spinal fusion technique for the cervical spine, making up 80.6% of all cervical spine surgeries [42]. The procedure involves an anterior incision in the cervical region, lateral to the midline, followed by the dissection of the disc; replacement of the disc with an intervertebral spacer with fusion inducing material; and a plate screwed in to reduce mobility as fusion occurs in healing post-surgery [9].

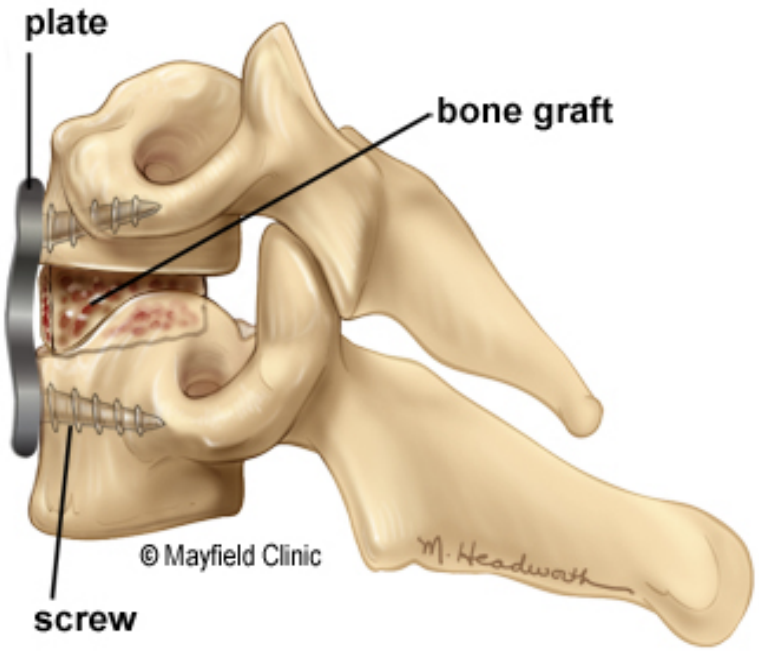

Figure 6: A single level spinal fusion utilizing a plate, bone graft, and screws [37].

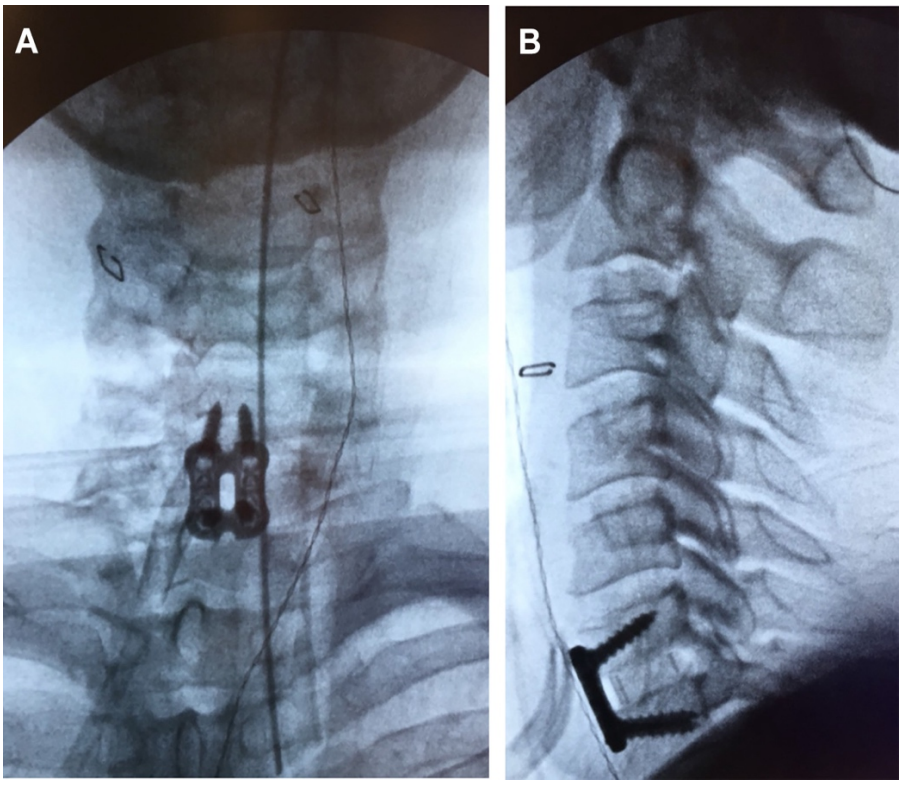

Figure 7: An X-ray of a single level ACDF in the coronal (A) and sagittal planes (B) [43].

This surgery produces high fusion rates ranging from 83% to 99%, improving the alignment in your spine and space between discs post decompression all while reducing disruption to the bodies surrounding the cervical spine [7]. While the fusion rates are impressive, patients often have morbidities such as dysphagia, esophageal perforation, and postoperative hematomas at the surgical site [6]. In addition to this, failure of bony fusion stemming from non-union can lead to steep costs associated with physical therapy, injections, and revision surgeries [44]. In turn, this can induce longer hospital stays and more pain at the surgical site [44]. Nonetheless, ACDF has become the superior cervical spine surgery for its consistent post-operative outcomes and reduced risk to patients [10]. However, complications and morbidities associated with the graft site can be reduced via novel approaches to graft choice and location.

Fusion Tissues Utilized in ACDF

Effective and efficient materials that encourage fusion are essential to the success of ACDF, preventing the need for extra care should a non-union occur. In a comprehensive study of ACDF graft selection by surgeons, 94.6% of surgeons consider fusion important to a successful ACDF surgery [45]. Here, roughly 75% of ACDF surgeries worldwide were reported to use a nonstructural component to encourage fusion between the two vertebra [45]. Nonetheless, 89.3% of surgeons believe that graft selection impacts fusion rates [45]. A multitude of graft materials have been utilized since ACDF was introduced in 1958; however, only some are utilized currently [12], [46]. These sources fall into four main categories: synthetic, xenograft, allograft, and autograft bone material.

Synthetic bone material substitute can be utilized to emulate the osteoconductive nature of bone and to promote bone healing at the surgical site [46]. Synthetic materials can range from titanium alloys to ceramic alloys; however, matrices of inorganic material such as collagen, tricalcium phosphate, calcium sulfate, and hydroxyapatite, ceramic alloys appear to be more prevalent in spinal fusion [47]. Ceramic alloys each have different binding, degrading, and mechanical properties due to their composition, porosity, and structure [47], [48]. As these alloys can be easily manufactured, the porosity can be adjusted to ensure that it falls within the optimal pore size, 150 – 500 micrometers, to improve osteointegration and osteoconductive properties of the material [47], [49]. Ceramic alloy bone grafts benefit patients by preventing inflammatory responses, offering adaptable graft size and shape, reducing costs, and avoiding morbidity from secondary surgical sites, unlike the gold standard in ACDF surgeries [47]. Despite their advantages, ceramic alloys lack osteoinductive qualities, are susceptible to fracture, have low tensile strength, and, critically, have lower fusion rates than other graft options [47].

Xenograft, also known as animal allograft, is made up of decellularized cancellous bone from animals and has been shown to encourage the fusion between two vertebrae [7]. Osteoconductive in nature, xenograft exhibits similar fusion rates to other bone grafts such as human allograft and autograft tissue [7]. Xenograft benefits include biocompatibility, ease of use, and safety [50]. Typically taken from adult cattle, the xenograft undergoes treatment to ensure it has no antigenic, immunogenic, or pyrogenic effects on the patient receiving ACDF [50]. With plentiful availability, an array of shapes and sizes, and the ability to reshape the graft, xenograft is easy to use [50]. Moreover, there are no human infectious agents associated with xenograft making it safer in terms of biocompatibility than human allograft [50]. Much like

synthetic ceramic grafts, there is no morbidity associated with secondary surgical sites. However, some studies have shown reduced biocompatibility and an increase in potential viral transmission, leading to increased reoperation rates for patients that received xenograft during their ACDF surgery [7]. Nonetheless, conflicting opinions about xenograft typically eliminate it from being selected as the graft for the ACDF surgery.

Allograft, allogenic bone transplanted from human cadavers or human donors, is traditionally considered the second-best graft choice option [7]. Allograft has both osteoconductive and osteoinductive properties if prepared properly [7]. Allograft is also widely available in high volumes, making it a very viable option when autograft harvesting is limited [51]. Mineralized allograft, which undergoes strict cleansing procedures to remove and/or attenuate potentially antigenic material, maintains its inorganic composition and crystalline structure [51]. Following cleansing, further actions are taken to ensure pathogens are deactivated [51]. Outside of mineralized allograft, demineralized bone matrix (DBX) is commonly utilized for its osteoinductive properties, although variable, and its paste-like nature that makes it easy to apply [7], [51], [52]. Both allograft substitutes come with major issues that make surgeons hesitant to use them: there is a low immunologic response from the grafts, infection frequency is heightened, it is expensive, disc height may deteriorate, fusion rate is less than the gold standard, and there is a potential risk for human disease transmission [7], [50], [51].

The three previous material groups contain the alternatives to the gold standard: autograft tissue. Autograft tissue, autologous bone transplanted from the patient's own body to another part of their body, has been proven to be the gold-standard for the surgery having the

highest fusion rates recorded between 83-99% [7], [45], [51], [53], [54]. Donor sites can include the proximal tibia, distal radius, distal tibia, and greater trochanter; nonetheless, the iliac crest is the most cited source of autograft for ACDF surgeries [9], [55]. Particularly, cancellous autograft tissue will be in focus being the most common nonstructural component used in single and complex ACDF surgeries [45]. Autograft has also been shown to improve the fusion rates of other materials when partnered with them. If paired with synthetic ceramic bone grafts, the fusion rate of the synthetic material improves as osteoinductive properties are introduced [47]. In addition to this, DBX is paired with autograft bone to fill the spacer to prevent extensive movement of the graft [9]. Leading to its high fusion rates, autograft bone has no risk of outside viral infections, is histocompatible, and is completely osteointegrative [53]. Autograft is void of most morbidities associated with grafts in an ACDF surgery; however, there is great morbidity at the graft's secondary surgical location harvest site [7], [45], [51], [53], [54], [56], [57], [58]. Morbidity associated with autograft harvesting sites involve longer operating time, longer time under anesthesia for the patient, increased blood loss, pain at donor site, hematoma at the donor site, infection at donor site, and disruption to the donor site [7], [53], [56], [58]. These morbidities have been reported in 10-20% of surgeries involving iliac crest autograft in the ACDF surgery [6], [53].

Implant Design and Mechanics for ACDF

While effective in encouraging fusion, bone grafts for spinal fusion are non-structural and are not designed to carry the load of the spine immediately when replacing the deteriorated cervical disc [45]. Instead, these grafts are designed to encourage fusion via bone

ongrowth and ingrowth; thus, the grafts must be combined with a structural component that allows them to encourage growth in a healthy and mechanically stable environment. As such, a structural graft or cage is utilized to mechanically stabilize the vertebral bodies undergoing fusion and maintain sufficient spacing to decompress the spinal cord. An effective cage maintains its structural properties, does not react to the biological action occurring within it, and must remain stable to not interfere with fusion [59]. However, should the material be too stiff, aseptic loosening may occur resulting in resorption. Should the material be too soft, the implant fails, and the nonstructural implant can become loose ruining an effective chance at fusion. In turn, an ideal cage must prevent subsidence, loss of correction, and have a high fusion rate [59]. In addition to this, design, shape, and size need to be considered when designing the cage [60]. Of these surgeries, there are two major categories for these cages: metallic and Polyetheretherketone (PEEK) cages [45].

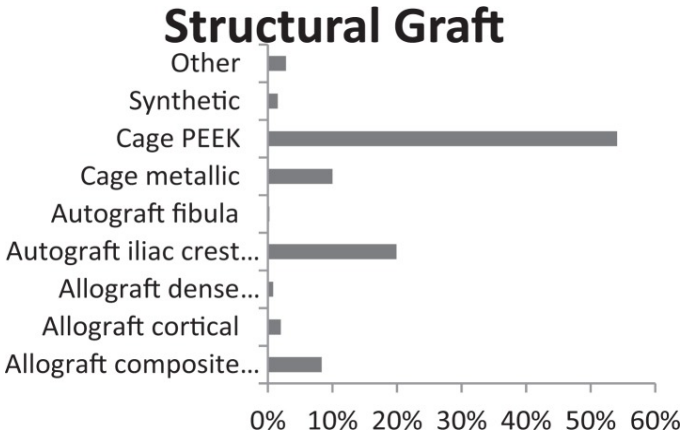

Figure 8: A graph showing the use of different structural grafts for simple ACDF [45].

Metallic cages are typically made from titanium, the standard metal of choice for implant surgeries for its ability to oxidize within the body to become biologically inert [61]. This leads to the retention and easy predictability of the material's mechanical properties, a lack of

biologic response from the host, and extended material stability [61]. This also leads to the titanium cage having a higher modulus of elasticity than PEEK cages [60].

Successfully used in the late 1990s, PEEK is a high strength, high thermal stability, highly biocompatible, engineered thermoplastic making it a great material for medical implants [60], [62]. In addition to this, PEEK has a resists corrosion and lacks cytotoxicity [59].

As reported in literature, titanium and PEEK cages have very similar fusion rates leading to conclusions that either material is acceptable as an implant [59], [60], [63]. However, 85% of ACDF surgeries that use cages select PEEK as their material of choice [45]. This can be attributed to multiple characteristics that support PEEK's usage over titanium. PEEK's elastic modulus, comparable to that of bone, reduces the risk of resorption and failure, unlike titanium cages with a higher modulus [62]. In addition to this, PEEK does not attenuate x-rays (***Figure 10***), MRI, or CT scans, unlike titanium, that are needed for analyzing fusion and healing of the surgical site [64]. Also, PEEK cages are less expensive and quicker to make, reducing costs for the patient [64]. PEEK cages, having a several advantages over titanium cages, are only effective if the autograft implant encourages effective osseous fusion between the two vertebrae together.

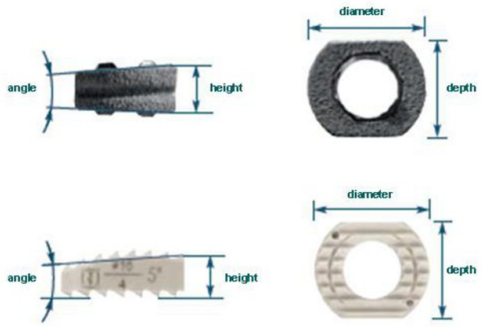

Figure 9: A comparison in shape between titanium and PEEK spacers [60].

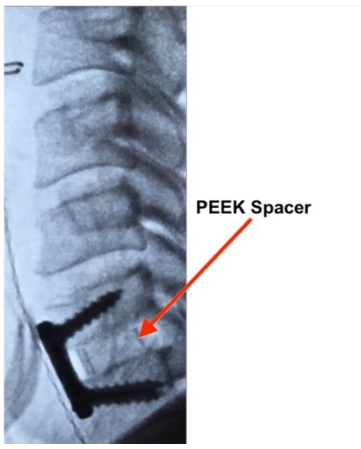

Figure 10: A sagittal view of an X-ray of a single level ACDF. This ACDF utilized a PEEK spacer (Red Arrow) that does not show attenuation (Edited from [37]).

Bone Healing, Bone Cells, and Fusion Pathways

The end-goal of ACDF is to have a completely healthy patient 9 months post-surgery with complete bony fusion at the surgical site and no other morbidities present. To achieve complete fusion, an integrated osseus complex is necessary. Despite high spinal fusion success rates for ACDF, the surgeries can result in non-union also known as pseudarthrosis. In literature, 7-60% of ACDF patients are reported to develop a nonunion following primary surgery [65]. Yet, there is no unanimous definition in the radiologic or orthopedic field describing nonunion [66], [67]. A pseudarthrosis diagnosis has described the absence of solid bony fusion at a minimum 6-months following lumbar spine surgery [68]. Factors increasing the likelihood of nonunion include nicotine use such as smoking, steroid use, radiation, chemotherapy, segmental bone defects, and a poor microenvironment, leading to potential infection, fractures in adjacent tissues, and congenital deformities [69], [70]. With autograft transplantation in ACDF, most risks are mitigated due to the stable fracture site and autograft tissue [69]. The process of fracture

healing and fusion for ACDF patients can be broken into three major stages, inflammation, proliferation, and differentiation [70].

Table 1: Terms and associated definitions associated with Bone Healing Pathways [12], [68], [71], [72].

Term	Definition
Osteoconduction	Cells, vasculature, and tissue are grown into the scaffold
Osteoinduction	The process where MSCs differentiate into osteoblasts via promotion from growth factors
Osteointegration/Osseointegration	Incorporation of the graft at the fusion site as it binds to the surrounding bone
Osteogenesis	Host or graft utilizes donor cells to synthesize new bone
Pseudarthrosis Diagnosis	Diagnosis of the absence of solid bony fusion at a minimum follow-up of 6 months following surgery

The inflammation stage spans roughly the three weeks following surgical intervention [70]. In these three weeks, the major event is the formation of a hematoma at the surgical site. The hematoma utilizes mesenchymal stem and osteoprogenitor cells in addition to a combination of platelets and macrophages, blood-derived immunocompetent and osteogenic cells, and proinflammatory cytokines to promote cell migration and increase vascular permeability within the fracture site [70]. The mesenchymal stem cells (MSC), known for their role in morphogenetic/tissue forming events and embryonic development, have the unique ability to differentiate into bone forming cells under the correct stimulation [71], [73], [74]. The first cell the MSCs differentiate into is the osteoprogenitor cell. The osteoprogenitor cell, the foundation to specialized bone cells such as osteoblasts and osteoclasts, are spindle bone cells that activate multifunctional stages of bone remodeling [75]. These cells, found in the autograft tissue, assist in promoting cell migration to and vascular permeation of the fracture healing site. Osteoinduction, the capability of autograft material to simulate the recruitment and differentiation of MSCs from surrounding tissues into bone-forming cells, contributes to the success of autograft tissue in remodeling bone [71], [73].

As the hematoma begins to subside, the new resident cells, mediated by growth factors, begin proliferation and differentiation into preosteoblasts, osteoblasts, and osteoclasts [70]. Transformed from MSCs and osteoprogenitor cells, preosteoblasts contribute to osteogenic induction by recruiting, guiding the differentiation of, and organizing more immature cells [73]. Following differentiation, these cells, now osteoblasts, begin to produce and deposit extracellular matrix proteins, such as collagen, onto the autograft scaffold, forming a soft callus [69], [70], [71], [73]. Simultaneously, osteoclasts, another form of differentiated MSC, act to dissolve and resorb the damaged bone cells to provide space and stimulation for osteoblasts to continue to grow the soft callus [71]. This soft callus is permeated by newly formed blood vessels, providing nutrients and new cells to continue to grow the soft callus and replenish the osteoblasts and osteoclasts. Although the soft callus grows, it cannot maintain stability on its own in the autograft until hydroxyapatite is mineralized into the extracellular matrix [70]. Hydroxyapatite, the main mineral in bone regeneration, will help grow the callus into woven bone and lead to further bone cell differentiation.

Following the introduction of extracellular matrix to the autograft scaffold, vascular ingrowth of capillaries into the scaffold leads to further differentiation of mesenchymal cells into osteoblasts [70]. The autograft has osteoconduction properties, initiating new bone formation and acting as a permanent scaffold to support vessel ingrowth and bone growth [71], [73]. These osteoblasts continue to put down extracellular bone matrix as the bone matrix begins to grow bone spicules. These spicules, after growing larger, will fuse together into trabeculae, weaving together to form fragile woven bone [70]. This woven bone will be remodeled with deposition and resorption to become biomechanically competent lamellar

bone [69]. As the bone continues to grow and fuse to the autograft, osteointegration will become complete throughout the fracture site as the graft acts as an anchor to incorporate the growth of new fibrous tissue [16], [71], [73]. The bone will continue to replace itself, remodeling constantly to maintain a healthy nature and respond to mechanical stimuli. This response to mechanical stimuli is mediated by osteoblast and osteoclast activity [70]. The production of new bone is known as osteogenesis [71].

Bony fusion in ACDF surgeries relies on a graft's ability to promote osteoinduction, osteoconduction, and osteointegration. Bone structure and microarchitecture influence trabecular bone's potential for growing new bone as it acts as a graft for the ACDF surgery. Specifically, bone structure and mechanical properties have been used for the assessment of potential osteointegration at various stages of bone healing [16] Morphologically and mechanically characterizing a graft's attributes can improve the understanding of which properties impact osteogenesis and bony fusion at an ACDF surgical site.

Bone Morphology and Micro-Computed Tomography

Bone morphology, the study of trabecular bone microarchitecture, is essential to understanding an autograft's mechanics, response to stimuli, and ability to be conducive to osteointegration that leads to fusion [76]. With this understanding, bone morphology can be used as an indicator of overall autograft quality. According to Wolff's Law, trabecular bone, a tissue with high metabolic activity, will adapt its morphology to the local mechanical environment [13]. Bone morphometry measurements, including Bone Volume Fraction (BV/TV), Specific Bone Surface (BS/BV), Trabecular Thickness (Tb.Th), Trabecular Separation (Tb.S),

Trabecular Number (Tb.N), Connectivity Density (Conn.D), Degree of Anisotropy (DA), and Bone Mineral Density (BMD), can be effective predictors in determining the efficacy of autograft tissues when analyzing different autograft sites [13], [76], [77], [78], [79], [80], [81], [82].

Trabecular bone architecture has been consistently studied since the 1970s, traditionally utilizing quantitative histologic techniques to analyze bone microarchitecture [79]. Beginning in the late 1980s, Feldkamp introduced the use of micro-Computed Tomography (microCT) to study ex-vivo bone microarchitecture [83]. MicroCT is a non-desctructive, high resolution 3-Dimensional imaging technique that provides rapid digitization of structures [79], [84]. The process of acquiring and analyzing the images can be broken into three major steps: generate x-ray projection images from attenuation data at multiple consecutive viewing angles, reconstruct these projection images into a 3D stack, and analyze the newly generated 3D image stack [78], [79]. Ensuring the highest quality pictures is crucial to the analysis of the 3D stack and morphometric properties calculated from the images.

Porosity within graft material is crucial for cells and vasculature to grow through as fusion is attempted [70], [85] Pore size, in controlled synthetic scaffold experiments was varied to determine which size facilitates the most cell migration and bone growth. Scaffolds with 100 – 400 micrometer pore sizes were reported to be viable in the recruitment of cells and promoting vascularization which results in effective bone growth [70], [85], [86]. These scaffolds attempted to replicate autograft bone which has varying sizes of pores that increase its efficacy to recruit cells and vascularization. To measure this within autograft bone, trabecular separation (Tb.S) is utilized. Tb.S, measured as the mean distance between trabeculae and assessed using

direct 3D methods, represents the porosity of the trabecular bone for cells and vasculature to grow through [79], [81].

In addition to studying porosity as an indication of graft osteoinductive properties, one must also analyze where the bone will lay its extracellular matrix that eventually forms into bone. Trabecular thickness (Tb.Th) measures the mean thickness of trabeculae utilizing direct 3D methods [79]. The trabeculae it measures act as the scaffold upon which bone can grow during osteointegration. Trabecular thickness was reported to vary after the scaffold is implanted, especially seen two and four weeks after the surgery, due to the growth of lamellar bone fibers that thicken the trabeculae [77].

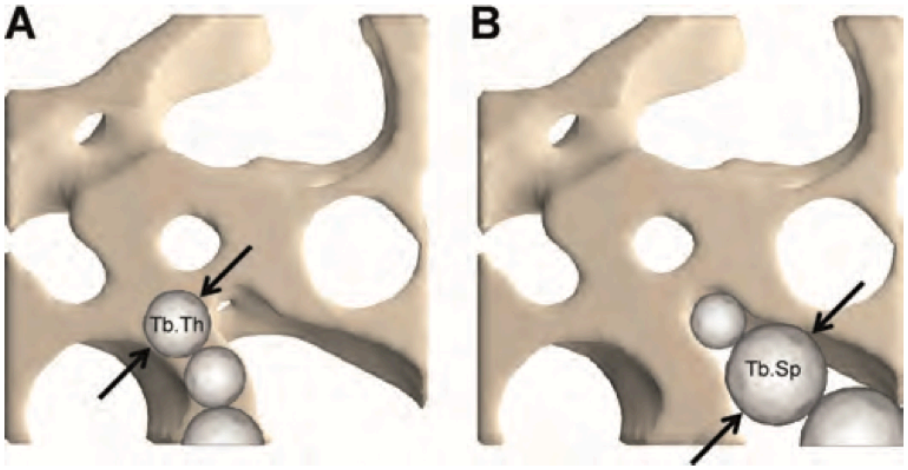

Figure 11: A visual representation of the direct 3D method for calculating trabecular thickness (A) and trabecular separation (B) [79].

Unlike Tb.S and Tb.Th, bone volume fraction (BV/TV), also known as bone volume to tissue volume ratio, does not have a consensus definition in literature. In some sources, BV/TV is a ratio of the segmented bone volume to the total volume, including marrow, tissue, and other non-bone tissues, that is correlated with the amount of bone implant contact in PEEK and titanium cages [79], [87]. BV/TV helps improve the understanding of the balance between

trabecular bone formation and resorption to better assess bone quality and cancellous bone connectivity [88]. Surgeons currently use BV/TV to predict trabecular failure in local parts of trabecular bone [89]. Whether it is used to describe connection to implants, formation and resorption, or fracture risk, BV/TV is used to better understand the efficacy of grafts utilized in spinal fusion.

Many other measurements can be utilized to continue to morphologically characterize the autograft bone. Bone surface density (reported as BS/BV or BS/TV) is the ratio of bone surface to bone volume that assists in determining the amount of mineral exchange that can occur between a graft and its surroundings [90].

Table 2: Trabecular Bone Microarchitecture and Morphology Variable Definitions and [79], [81], [82], [91], [92], [93], [94], [95].

Abbreviation	**Variable**	**Description**	**Standard Unit**	**Reported Iliac Crest Averages (in standard units)**	**Reported Cervical Spine Averages (in standard units)**
TV	Total Volume	Volume of the entire region of interest, including bone and its surrounding tissues	mm^3	Varies based on graft harvest methodology	Varies based on graft harvest methodology
Tb.Th	Trabecular Thickness	Mean thickness of trabeculae	mm	151-170	138-212
Tb.S	Trabecular Separation	Mean distance between trabeculae utilized when studying porosity	mm	532.1-906.3	400 – 630
BV/TV	Bone Volume Fraction	Bone Volume to Tissue Volume Ratio	%	20.1	20.9-33.0
BS/BV	Specific Bone Surface	Bone Surface to Bone Volume Ratio	mm^2/mm^3	13.66	11.1-15.5

Studying bone morphometry requires continuous improvement in microCT scanners, which now have the capability to scan at a resolution of 0.1 micrometers and up to 200 millimeters in diameter [96]. Currently, microCT scanners can provide resolutions of 1-20 micrometers per voxel while also allowing for larger resolutions for larger objects. Trabecular bone and their structures are traditionally scanned from 10-20 micrometers [78]. Following

resolutions, voltages and currents may be changed to better improve the attenuation obtained from the samples via the x-rays. Peers recommended to always have the highest power possible, 10 W in the case of a Bruker SkyScan 1172 microCT scanner, and it was reported that 50-60kV should be utilized for the voltage [78]. Thus, the current should be set in the range of 166-200 uA to obtain maximum scanning power. Additionally, microCT scanners, especially the SkyScan 1172, have a multitude of correctional settings that may be utilized to improve the taken images and reduce the need for rescans. These features include geometrical correction, median filtering, flat field correction, post alignment, gaussian filters, ring artifact correction and beam hardening correction, all of which mostly improve the accuracy of the morphological values calculated from the scan.

While these features attempt to combat the pitfalls of microCT, it is important to recognize the few flaws of the imaging system. In comparison with histomorphometeric measures, improper image resolution and segment thresholding may risk overestimates of sample Tb.Th [79]. Segment thresholding may be influenced by image artifacts on the microCT scans, most commonly from ring and beam hardening artifacts. Ring artifacts, appearing as an out-of-place ring on the image, occur due to a faulty detector whereas beam hardening artifacts, appearing as streaks, dark bands, or flare artifacts, occur from the absorption of select low energy photons [79], [97], [98]. The artifacts caused by faulty detectors and select photon absorption may confuse automatic thresholds, resulting in portions of bone being excluded from or background being included in the threshold. Nonetheless, microCT has countless benefits that outweigh these few pitfalls. MicroCT is non-invasive and non-destructive; thus, the sample will not change after undergoing microCT allowing for imaging pre and post

experimentation. Additionally, microCT imaging provides a faster direct 3D measurement of trabecular morphology over a much larger area in comparison to histological analyses [79]. It is reported that Tb.Th, Tb.S, and Tb.N should be calculated utilizing volumetric measurements given the complexity of bone microarchitecture in 3D space [79]. Supplementing the morphological measurements from microCT images with measurements describing the micro-architecture of trabecular bone would further enhance its characterization.

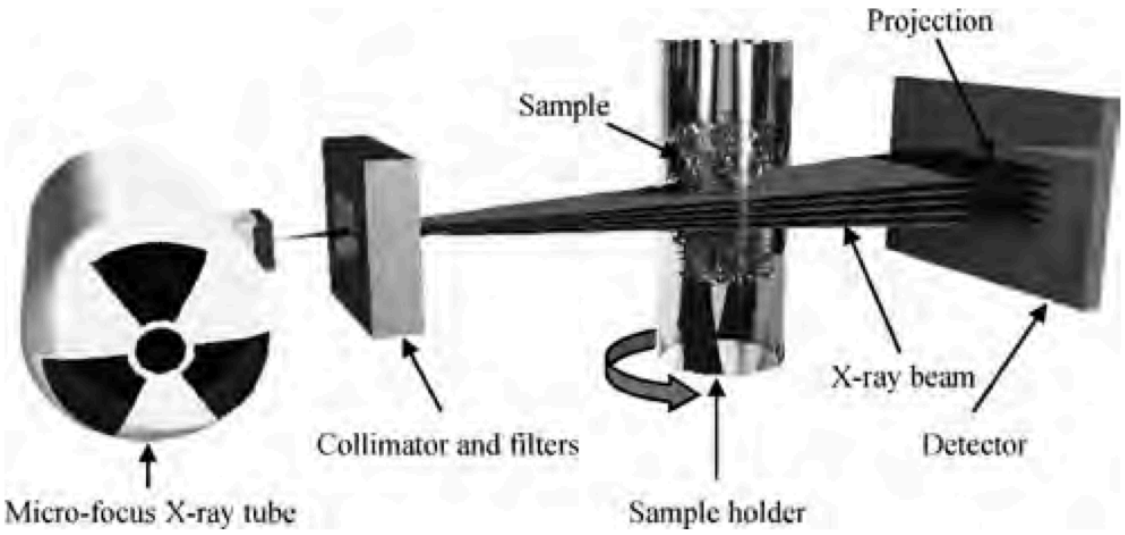

Figure 12: Key mechanisms for standard desktop microCT scanner [79].

Bone Collagen Alignment and Second Harmonic Generation (SHG) Characterization

To improve our understanding of early-middle stage graft healing, it is important to supplement microarchitecture assessment with an understanding of what impacts an osseous callus phase and the growth of minerals and proteins within an autograft.

Bone is made up of hydroxyapatite, collage, proteoglycans, non-collagenous proteins, and water, all of which contribute to its mechanical properties [99]. Hydroxyapatite is crucial for bone structural strength and regeneration. Collagen, making up 90% of bone's organic matrix, contributes to a multitude of bone's properties, including its ductility, toughness, force transmission, bone structure, bone maintenance, mechanical support, and maintenance of bone strength [100], [101], [102].

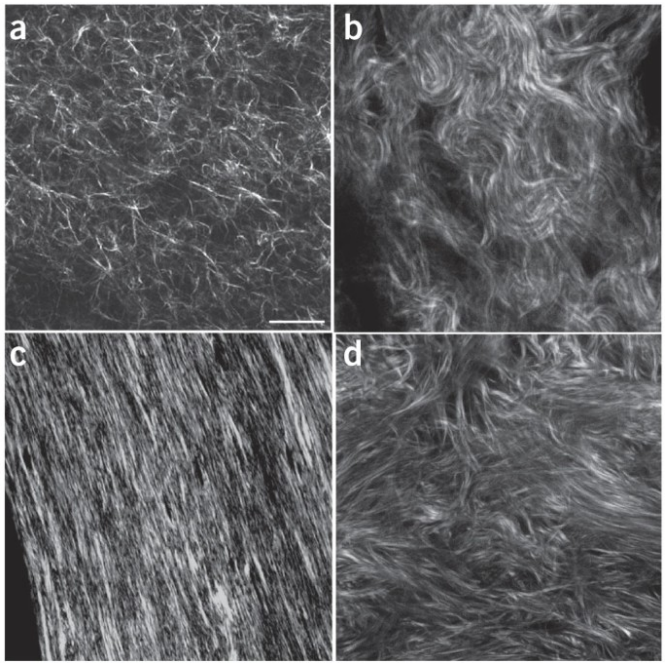

Figure 13: Collagen alignments for different samples (a. Self-Assembled Collagen Gel; b. Mouse Dermis; c. Mouse Bone; d. Human Ovary) that experience various physiological loads using SHG imaging [103].

Across all its uses within the body, collagen is most responsible for maintaining the structural integrity of the tissues in which it is found [101]. Collagen fibrils are formed from a triple-helix structure of hydrogen-bonded polypeptide chains and arranged into different fibril types [101], [103]. Types I, II, III, and V, being the most prevalent in bone, impact the bone's ability to resist tensile, shear, or compression forces after arrangement into concentric weaves [101], [102].

In the process of fracture and graft healing, deposition of unorganized collagen in the form of callus tissue begins as the inflammation stage recedes. MSCs, recruited during the inflammation stage, begin laying down extra-cellular matrix proteins, such as collagen, to form the soft tissue callus [16], [70], [71]. These collagen fibers, after self-assembly, cannot provide mechanical stability due to a lack of organization, random arrangement, and lack of mineralization of hydroxyapatite [16], [70]. With time, this callus matures with longer and more aligned collagen fibers that begin to mineralize to form osteoid and ultimately mature bone.

Analyzing collagen alignment during healing is difficult as the minimal reports of in-vivo imaging of bone collagen dynamics are novel studies [104]. Traditional imaging techniques such as x-ray and MRI have not been proven successful at imaging collagen. However, dyes and stains applied to thin tissue sections (histology) in conjunction with fluorescence and bright-filed microscopy and second-harmonic generation (SHG) microscopy can effectively image collagen alignment and direction [101], [102], [103], [104], [105], [106], [107], [108], [109], [110], [111], [112]. SHG, rather than fluorescence and bright-field microscopy, imaging offers label-free detection, relying solely on the auto-florescence of the collagen when excited with a laser [105], [109]. Additionally, SHG has high resolution and specificity when imaging collagen structures, solidifying it as the most attractive choice for imaging collagen structure and alignment in ex-vivo tissues.

First utilized on biological tissues in 1971 by Fine and Hansen, SHG of collagen alignment within biological tissues was not completed until 1986 by Freund and Deutsch [113], [114]. SHG microscopy utilizes two lower energy photons from high energy laser pulses to generate an emission signal at twice the excitation frequency of the collagen in the targeted sample [105],

[110], [111]. Ensuring that the emission signal is twice the excitation frequency of the collagen is crucial for high resolution and contrast for image processing following imaging.

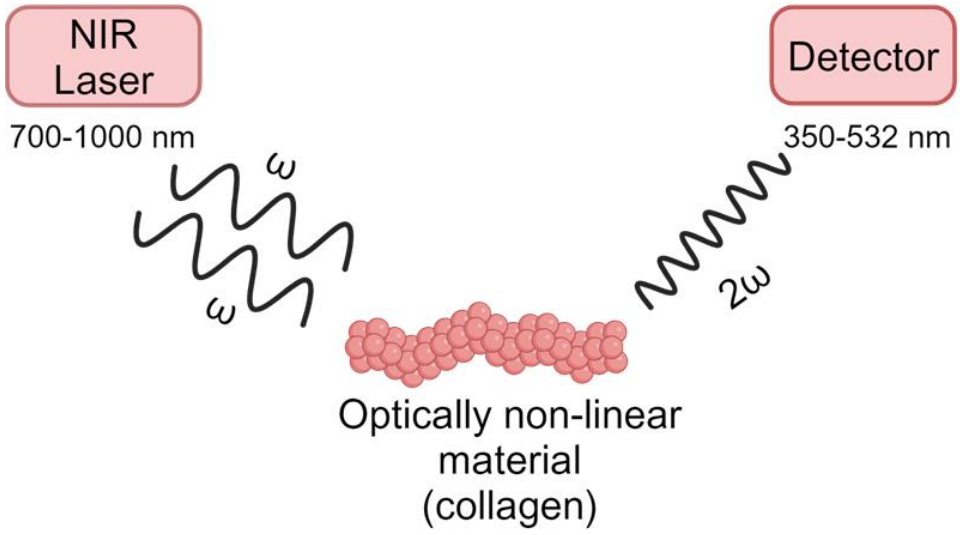

Figure 14: Schematic of SHG imaging laser being produced and detected from a collagen source [115].

While SHG has been established as the premier imaging modality for collagen alignment, it does not come without limitations. First, SHG works at a very shallow depth to avoid scattering; thus, samples can only be efficiently analyzed on depths at which SHG can work, ranging from 100 to 300 microns [111]. Additionally, this short depth prohibits in-vivo scanning of musculoskeletal tissues, necessitating the use of histological tissue prep or samples. Prepping the samples for slicing involves fixation and dehydration, both of which can alter the tissue's normal micro-architecture and material properties [112].

Despite these challenges, CHG does not suffer from the pitfalls of more tradiational histological characterization such as photo-bleaching as it can conduct label-free characterization, eliminating the need for extensive processing prior to imaging [105], [110]. With a sharper contrast, high-resolution images, a lack of sample alteration post sample-prep, and live-imaging capabilities, SHG is more than suitable to image collagen alignment within

bone and provide characterization of the collagen mesh micro-architecture. Combined with microCT imaging analysis, SHG imaging analysis enables a multiscale characterization of tissue architecture. Tissue architecture, linked to both structure and function, should be mechanically characterized to understand the correlation between architecture and mechanics.

Bone Mechanical Testing in Comparable Animal Models

With the help of MicroCT and SHG imaging modalities, one can develop a better understanding of the first 3 weeks of healing post-ACDF surgery by analyzing the micro-architecture associated with the morphology and collagen alignment of bone. However, as the soft callus stage transitions into the hard callus, bony callus formation, and bone remodeling stages, understanding the mechanical properties of bone and how bone heals under different mechanical loads is critically important. Thus, supplementing morphological analysis from radiographic imaging with mechanical testing is necessary to understand the mechanical properties of trabecular bone autografts that may impact fusion following ACDF surgery.

Mechanical testing, often in the forms of bending, torsion, shear, tension, and compression tests, is effective in characterizing bone's load-bearing capacity to better understand bone fractures, adaptation, and healing [22], [23], [24]. Trabecular bone experiences predominantly compressive physiological forces, making its role to transfer and distribute these mechanical loads form the bone's surface to the cortical bone [24], [89], [116]. While trabecular bone does experience shear and torsion forces, they are minimal in comparison to dominant compressive forces [23]. This dominance is further highlighted by observed mechanical properties, where mean tensile strengths are 30% lower than mean

compressive strengths [117]. While trabecular bone does undergo tension and bending forces, these loading mechanisms require complicated fixtures, equipment, and more complicated modifications to the samples prior to testing [118]. Thus, compressive properties of trabecular bone are of primary interest when determining mechanical competence of the tissue. For the most optimal specific characterization of trabecular bone at the tissue level, uniaxial compression testing is utilized to find elastic modulus, ultimate strain, and ultimate stress to determine stiffness and strength [22], [23], [24], [119], [120], [121]. Note, trabecular bone is considered an anisotropic material with high porosity and architectural variability, which impacts its elastic behavior [23], [89], [116], [122]. Studying the elastic behaviors of strength and stiffness of trabecular bone in multiple directions is crucial to assess how the bone will remodel and potential failure of the bone under new loading conditions [22], [24], [89], [116], [122].

A uniaxial compression test involves two fixed, parallel stainless-steel platens compressing the trabecular bone under displacement control as seen in ***Figure 15***. A Materials Testing System (MTS) is traditionally utilized to control the displacement to which the platens move and compress the bone sample.

Figure 15: A standard platen compression testing setup for a bone specimen.

Although strict ISO or ASTM standards are not set for testing trabecular bone under uniaxial compression, the test is quite straightforward to perform to produce timely mechanical measurements [22]. To improve upon the accuracy of the measurements, one can implement cyclic preloading and repeated elastic region compression tests prior to a compression test to failure. Cyclic preloading, also called preconditioning, ranging from 0.2-1% has been proven to increase reproducibility of mechanical testing by achieving a steady viscoelastic state and ensuring the strain is zeroed [22], [89], [118]. Additionally, cyclic preloading ensures that the bone sample is uniformly contacting both platens prior to compression testing [22]. As these cycles are in the elastic range, cyclic preloading can be a check to see if any plastic damage has occurred to the sample before repeating testing [22]. Following cyclic preloading, repeated elastic region compression tests can be utilized to develop an average modulus for the sample in

multiple directions as the individual tests are non-destructive. Trabecular bone exhibits elastic properties during daily physiological loading and demonstrates linear behavior in experimental settings; therefore, its bulk elastic properties can be assumed to follow linear elasticity [89]. Exhibiting linear elasticity, these averages can be assumed to not impact the yield and failure points of the sample. Finally, compression tests to failure are used to understand fracture risk and determine the loads that may cause trabecular bone to mechanically collapse [123].

In previous trabecular compression test studies, iliac crest trabecular bone is utilized as a standardization point to compare other bones as it is a nonloadbearing bone, and its anisotropy does not change with age [124]. While utilized as a standardization point, iliac crest trabecular bone compression testing is not as extensively studied as spine trabecular compression tests. The lumbar, followed by thoracic, region appears to be the most studied portion of the spine due to its extensive loadbearing responsibilities, the commonness of lower back pain, and the larger size of lumbar spine vertebra [23], [125], [126], [127], [128]. While most of these studies utilize trabecular cores for compression testing, some studies utilize the whole vertebra to simulate in-vivo conditions [24], [129]. Although less frequently documented, the strength and stiffness of cervical spine trabecular bone cores have been characterized via compression testing as seen in Table 3.

Table 3: Mechanical Characterization of Human Iliac Crest and Spine Trabecular Bone [130], [131], [132], [133], [134], [135], [136].

Study	Region	Specimen Configuration	Comments	Properties
Struhl et al (1987)	Iliac Crest	6 or 8 mm cubes	Orthogonal Preload, Uniaxial Stress	Strength: 0.12-8.2 Mpa Modulus: 5-282 Mpa
Struhl et al (1987)	Vertebral Body	8 and 6 mm cubes	Orthogonal Preload, Uniaxial Stress	Strength: 0.06-15 Mpa Modulus: 10-428 Mpa
Hans et al (1999), Cendre et al (1999)	Vertebral Body	Cube, 29 subjects, 23-95y	Assumed to be tested in Inferior-superior direction	Ulitmate Strength: 1.28-1.6 Mpa Modulus: 58.5-134 Mpa
Hans et al (1999)	Vertebral Body	Cube, 7 subjects, 23-67y	Anterior-posterior and medial lateral directions	Modulus: 32.7 and 33 Mpa respectively
Shim et al (2005)	Cervical Vertebra	8 subjects, 40-79y	N/A	Modulus: 286 ± 157 MPa
Liu et al (2013)	Cervical Vertebra	5 male subjects, 47-79y	N/A	Ultimate Stress: 5.8 MPa

While commonly used in the biomechanical testing community, compressive tests can have inaccuracies due to the end-artifact associated with the bone interacting with the testing machine [126]. Even if samples are kept the same size, end-artifacts may also be impacted by the roughness of the sample's machined surfaces [22], [126]. Nonetheless, ensuring that sample size is regulated reduces variability between trials. Regulating sample size also normalizes load and deformation variables used to calculate mechanical properties of the bone samples [24].

To ensure that the samples are analyzed correctly, directionality and anisotropy of the trabecular bone should be considered. The iliac crest trabecular bone exhibits inherent anisotropy; however, it is considered to have less significant differences across properties between anatomical directions due to the lack of physiological forces impacting trabecular bone architecture [137]. In comparison, cervical, as well as lumbar and thoracic, spine trabecular bone has adapted to have a clear loading direction, leading to anisotropic properties in the

principal axial loading direction and nearly isotropic properties in the horizontal direction to account for daily physiological loading [22], [23], [89], [116], [122], [124], [125], [127], [130], [137].

Utilizing human specimens for biomechanics research is the gold standard; however, there is limited availability and multiple associated restrictions. Commonly utilized in preclinical biomechanics research, animal models have become an effective substitute for their ability to mimic biomechanical data found in human specimens [138]. While there are no established standards for bone biomechanical testing due to the wide variety of bone shapes and sizes, it is important to consider the species' bone tissue microarchitecture and physiological loading patterns when designing an animal model for trabecular bone compression experiments. [138]. Additionally, deciding between large and small species animal models each have their own benefits. Small animal models, such as rats and mice, come with decreased cost, faster healing time, and the ability to generate a larger data pool whereas large animal models, such as dogs and cows, more closely resemble the human body in size and bony anatomy but come with elevated costs [138].

Having shown high reliability, bovine (cow) bone has been used to model human bone [139]. Bovine trabecular bone has been utilized to study yield strain and modulus in addition to analyzing yield strain anisotropy at different anatomical sites [138]. Additionally, bovine bone has been utilized for its osteoinductive properties to study tissue response to new osteoinductive proteins and what proteins impact lumbar vertebral interbody autograft fusion [140], [141]. Skeletal differences are seen between humans and cows primarily due to the bipedal and quadrupedal gait, respectively, and difference in size of each species. Mature adult

bovine vertebral columns are on average approximately 209 cm longer than mature adult human vertebral columns, approximately 280 cm to 71 cm respectively [142]. Additionally, cows have two more vertebra than humans, 35 to 33 respectively, when excluding the vertebra in the tail [142]. To achieve closer analysis and avoid variances in size, 6–8-week-old dairy calves have been utilized for their relatively similar size in vertebral column to that of mature humans [142]. In contrast, humans and cows have relatively similar sizes of pelvises, having an internal pelvic width of 12.9 cm and 15.8 cm and an internal pelvic height of 13.7 cm and 19.3 cm respectively [143], [144], [145].

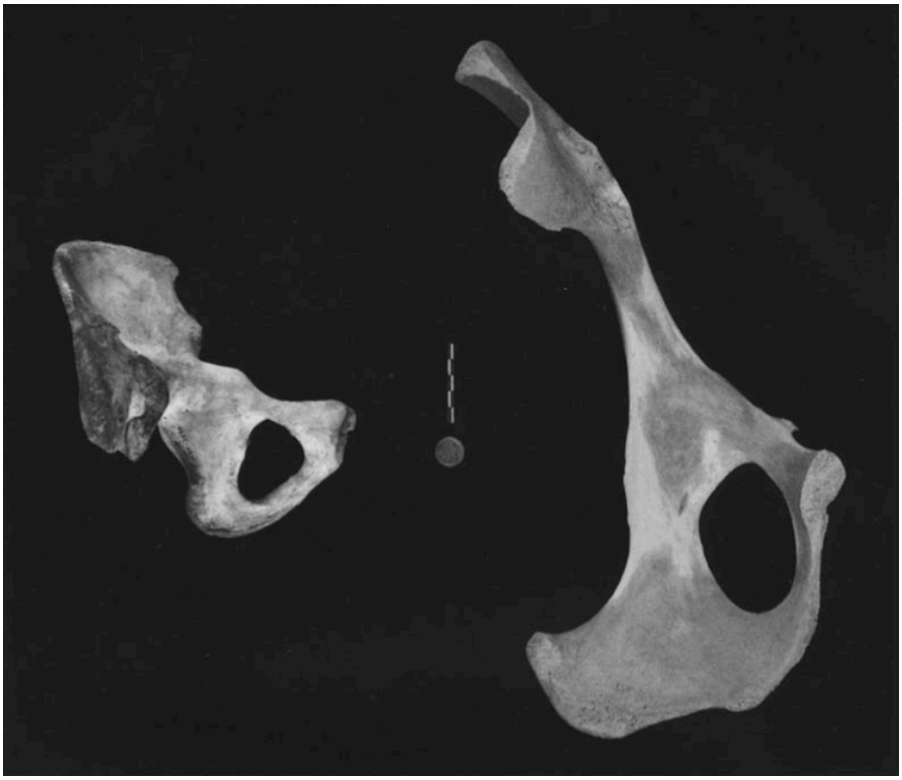

Figure 16: Medial View of the human pelvis (left) vs a cow pelvis (right) [146].

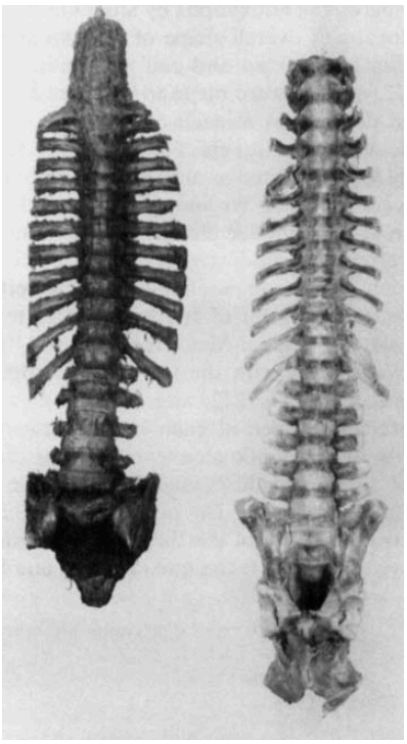

Figure 17: An adult human spine (left) and a calf spine (right) from an anterior view [142].

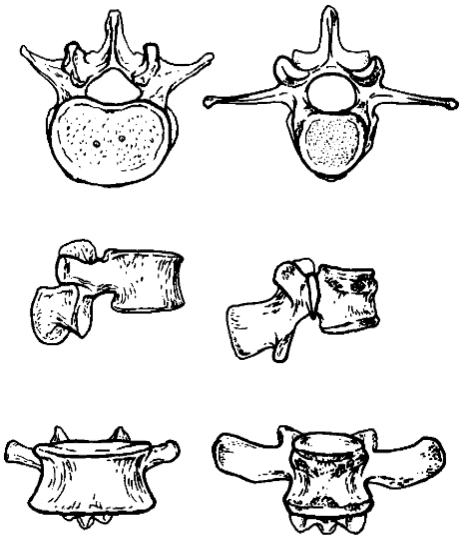

Figure 18: Comparison of human and bovine L3 vertebra from superior, lateral, and anterior views [142].

While prevalent in research, cow bone poses limitations in its composition and ratio of cortical to trabecular bone in its bone structures. Bovine bone exhibits plexiform qualities, a more densely vascularized form of cortical bone arranged into a “brick wall” appearance, rather than traditional Haversian qualities exhibited by human bone [147], [148]. Note that this

increased density from the plexiform bone increases the difference between cow and human cadaver studies which tend to utilize more elderly patients with greater bone density loss. Also, this plexiform bone is utilized in the cow's cortical structure of the vertebra, giving it a higher ratio of cortical to trabecular bone in comparison to human vertebra (***Figure 18***).

Chapter 3 - Aim 1: Characterize and Compare the Osteogenic and Morphological Properties within the Microarchitectural Niche of Human Iliac Crest and Cervical Spine Autograft Tissue: a Micro-Computed Tomography and Second Harmonic Generation Image-Based Analysis

Introduction

Standard-of-care ACDF utilizes trabecular autograft from the iliac crest, yielding impressive fusion rates of 83% to 99% [7]. Although success rates are often high, increased levels of donor site morbidity and loss of quality of life due to said morbidities are commonly associated with iliac crest autograft usage for ACDF surgeries [11], [53]. To mitigate donor site morbidities associated with the secondary surgical sites or autograft resection, a novel autograft location was proposed: harvesting bone from the inferior adjacent cervical vertebra to the operative disc space [8]. This novel autograft location for ACDF has been investigated using biomechanical analyses of surrogate tissue following simulated surgery and, in a pilot, clinical patient cohort, revealing minimal impact on the mechanical properties of the donor site and equivalent fusion rates to the iliac crest autograft location [8], [9]. With the elimination of the need for a secondary surgical site, there was a decrease in reported morbidities in the pilot ACDF cohort when utilizing the novel autograft location [9]. While preliminary evidence suggests the inferior cervical vertebra is a suitable autograft location for ACDF, there remain open questions related to the osteogenic properties of tissue from the cervical vertebra relative to the gold standard iliac crest. As such, it is necessary to characterize fusion inducing properties of the cervical spine and directly compare it to iliac crest properties before adapting the standard-of-care for patients worldwide.

Osseous fusion, the ultimate goal of all ACDF surgeries, is a healing process where newly formed bone fuses the two neighboring vertebrae impacted by the removed degenerative disc following surgery. This healing process can be broken into three major stages: inflammation, proliferation, and differentiation [70]. To ensure that the major stages proceed without complications, autograft tissue with osteoinductive, osteoconductive, and osteointegrative properties is utilized as a bioactive scaffold to promote fusion in ACDF. Osteoinductive properties, promoting recruitment of surrounding bone and bone precursor cells, are utilized to recruit MSCs for differentiation into osteoblasts, osteoclasts, and osteocytes [71], [73], [74]. Following osteoinduction, the osteoconductive properties of the autograft bone initiate new bone and blood vessel growth throughout the trabecular bone structure [71], [73]. Finally, the osteointegrative properties of trabecular bone then integrate this new woven bone at the surgical site into the autograft, anchoring the new fibrous tissue leading to two fully fused vertebra upon healing [16], [71], [73].

The morphological shape of trabecular bone, which continuously adapts to the physiological loads it undergoes, impacts its ability to generate new bone and, consequently, its ability to achieve healthy fusion [12], [13], [76], [78], [79], [80], [81], [82]. Trabecular bone porosity facilitates cell migration, leading to bone ingrowth and vascularization throughout cancellous autograft [70], [85]. Trabecular thickness and bone surface area influence where MSCs can lay down bone matrix, allowing woven bone to deposit and grow [77], [79]. Additionally, bone volume fraction (BV/TV) has been shown to impact bone connectivity, formation, and resorption [88]. To capture these properties, micro-computed tomography (microCT), a non-invasive and non-destructive imaging modality, is commonly used to study

bone tissue architecture from ex vivo samples. The resultant, high-resolution images of the microarchitecture of bone, can then be processed to quantify the morphological features of trabecular bone described above [13], [14], [15].

In addition to morphological shape, trabecular bone collagen alignment, follows similar adaptation principles under physiological loading; can impact bone's stiffness and influence the location and quality of newly formed bone during healing [17], [18], [19]. Traditionally, imaging collagen content and alignment on ex-vivo bone tissue is performed using histological staining and microscopy. However, these approaches require significant sample preparation and can suffer from photobleaching during imaging. As an alternative for visualizing collagen fibers, second harmonic generation (SHG) imaging microscopy modality that can take high resolution pictures of the collagen content and alignment within bone without the need for dyes or fluorescent stains [101], [102], [103], [104], [105], [107], [108], [109].

In the present research, the morphological and microarchitectural properties of trabecular bone from the two autograft locations, the iliac crest and cervical spine, were compared utilizing analyses of the microCT and SHG imaging data.

Methods

ACDF Surgical Procedure and Patient Cohort

Patients (n=12) between the ages of 21 and 65 with cervical radiculopathy or myelopathy underwent a standard-of-care 1 or 2 level ACDF in which combined iliac crest and cervical spine autograft was utilized [9]. Patients provided bone samples from both cervical vertebrae and iliac crest., which were divided for use as autograft tissue (1/2), gene expression (1/4), and tissue microstructural characterization (1/4). Exclusion criteria was as follows: previous spinal surgery, diagnosed osteoporosis, pregnancy, or anyone unable to give consent [9]. This study was approved by the Institutional Review Board (IRB) at Carilion Clinic (Roanoke, VA, USA) and informed and written consent was obtained from all patients per governmental guidelines.

Following intubation, a standard-of-care surgical approach was taken to perform the discectomy. Autograft tissue was recovered from the iliac crest as seen in traditional ACDF surgery. The cervical spine autograft was retrieved as described in O'Neill et. al. [9]. Post autograft tissue resection, the sections of the autograft tissues isolated for microarchitectural analysis were placed in separate labeled 2.0 mL Graduated Microtubules (Olympus Plastics from Genesee Scientific) and placed in an ice chest for transport.

Sample Prep for MicroCT

Once the samples were retrieved from the operating room, the samples were either placed in a -80˚C freezer to preserve the tissue's structural properties or taken to a chemical fume hood for preparation. Thawed or never frozen tissue samples were individually secured in

screw-cap microtubules with sterile gauze pads (Med Pride) and hydrated with approximately 20 mL of

refrigerated phosphate-buffered saline (PBS) solution (Apex BioResearch Products, Genesee Scientific) per two bone grafts, and an ice chest were utilized to prep the samples for microCT under the chemical fume hood (**Figure 19**). PBS solution was added in excess to reduce air bubbles within the microtubule that could affect attenuation occurring during scanning, resulting in beam hardening artifacts. Following sample prep, samples were transported on ice and placed in a -80˚C freezer up until scanning. On the scanning day, samples were transported and kept on ice until 15 minutes prior to the scan to preserve the tissue and thaw only once for the scan. Following thawing and patting dry to ensure no water droplets were on the outside, Parafilm (Parafilm M Film Roll) was placed on the cap and stretched around the sample to ensure no evaporation from the PBS would damage the microCT scanner.

MicroCT Imaging

To acquire the microCT images, a Bruker SkyScan 1172 high-resolution micro-computed tomography (microCT) scanner was used with the following settings: Source Voltage = 60 kV, Source Current = 167 µA, Power = 10 W (max), Filter = Aluminum 0.5 mm, Image Pixel Size (Resolution) = 17.42 µm, Image Rotation = 0.5460, Exposure = 3751 ms, Rotation Step = 0.700 degrees, and Geometrical Correction, Median Filtering, and Flat Field Correction were all turned on. A light-dark flat field correction scan was utilized to initialize the properties of the scan. The voltage and current were set to maximize power and were optimized for scanning ex-vivo trabecular bone.

MicroCT was performed on all 24 samples, one from the iliac crest and cervical spine for each patient. The microtubule with sample secured inside was placed firmly in a vertical position in clay on a small sample holder. Following the flat field correction scan, the sample holder with microtubule attached was placed in the scanner. A scout scan was performed to choose the location of scan, centering data capture to the sample within the microtubule. Once the sample location was designated, the scan was started.

Following the scan, samples were stored at -80˚C until further analysis. NRecon (Bruker) was utilized to reconstruct the microCT scans. Misalignment compensation was set by analyzing the profile windows of the sample at 0 and 180 degrees and aligning the two of them together. Ring Artifact Correction was set to 10, and thresholding was adjusted when necessary to enhance the contrast of the sample.

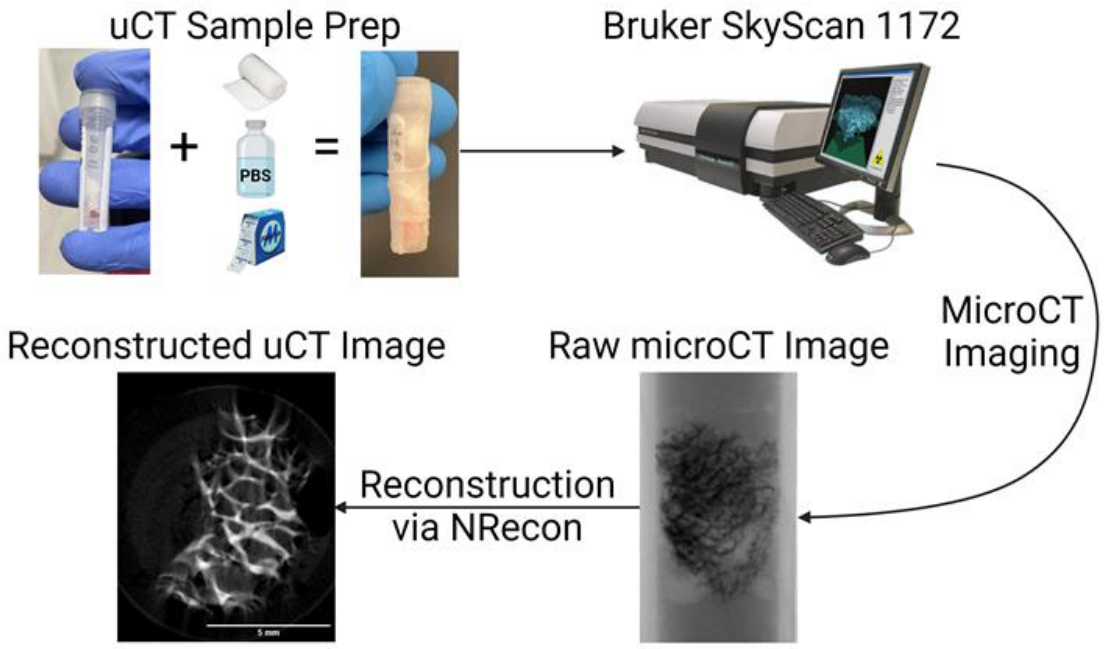

Figure 19: Methodology displaying sample prep, imaging, and image reconstruction for microCT imaging.

Analysis of MicroCT Images

Post-processing of the reconstructed images was done using 3D Slicer 5.4.0, Python 3.9.12, and Fiji/ImageJ 2.14.0 softwares [149], [150]. Reconstructed microCT images were first uploaded to 3D Slicer. Second, a volume of interest was identified using the ImageStacks module by SlicerMorph 4.10 to automatically crop the image volume to the space directly surrounding the sample in order to reduce file size and save on computational time [151].

The cropped volume image was then thresholded using the automatic "OTSU" threshold, retaining everything above an automatically detected lower bound and identifying the bone tissue volume of the sample. The “OTSU” threshold stems from Otsu’s method, a discriminant analysis of a gray level histogram to maximize separating the object in focus and the background [152]. The bone volume (BV), represented by the OTSU thresholded volume, was recorded. The lower bound of the OTSU threshold was noted for future application in Python for each sample. The cropped volume was exported as a DICOM series.

Within Python, the DICOM files were opened and the “OTSU” threshold was reapplied. Utilizing the thresholded image, a convex hull representing the gross “tissue volume” was generated. The convex hull identified the boundary of the thresholded sample, and the resulting boundary was filled using the flood fill method. The convex hull was eroded 20 times to ensure that it represented a tissue volume that did not encompass extra background pixels which would skew morphological measurements.

The thresholded bone within the convex hull and convex hull tissue volume masks were then exported to 3D Slicer. The Bone Morphomety Features function within

BoneTextureExtension 2.0 was utilized to compute bone volume fraction (BV/TV) and bone surface to bone volume ratio (BS/BV) [153].

Following the use of 3D slicer to calculate BV/TV and BS/BV, the raw cropped image stack was uploaded to ImageJ. The image stack was further cropped to the beginning and the end of the bone as seen in the 2D orthogonal plane. Within ImageJ, the "OTSU" threshold was applied to binarize the cropped image stack. Utilizing the BoneJ2 7.0.19 plugin, the trabecular thickness (Tb.Th) of the sample was calculated by averaging the diameter of the largest sphere that fits inside each trabecula and contains the point for each voxel in the sample [154]. Trabecular separation (Tb.S) was calculated using a smaller region of interest that included a portion of the sample rather than sampling the background. The region of interest was analyzed by inverting the voxels of the image and performing the same calculations as Tb.Th using the BoneJ2 7.0.19 plugin [154].

Sample Prep for SHG

The samples, having been frozen in a -80˚C freezer to preserve its structure, were thawed and placed in new microtubules for sample washing prior to embedding in methylmethacrylate. Sample preparation followed the 45359 Epoxy-Embedding Kit (Hexion, Inc, Sigma-Aldrich) normal embedding instructions [155]. The bone samples were fixed in 1:10 diluted formalin for at least 48 hours at 4˚C to ensure effective fixation. Samples were washed with DI water, followed by a wash in PBS after fixation. Next, the sample, under a chemical fume hood, underwent six acetone washes: 30%, 60%, 90%, and three changes at 100%, each for 10 minutes [155]. After the acetone washes, the samples were treated with an acetone and final epoxy mixture in polyethylene Peel-A-Way™ Embedding Molds (Polysciences, Inc, Sigma-

Aldrich). First, a 1:1 ratio was applied for 30 minutes, followed by a 1:2 ratio added on top for an additional 30 minutes [155]. The capsules were polymerized at 45˚C for 12 hours followed by an additional 24 hours at 60˚C [155].

Post-epoxy-embedding and sample hardening, the samples were kept at 4˚C prior to sectioning. A Buehler Isomet Low Speed Saw (Buehler, Lake Bluff, IL) instrumented with a diamond-coated saw blade (Buehler IsoCut® Wafering Blades, Buehler, Lake Bluff, IL), were utilized to cut thin sections from the embedded samples. Following a facing cut, the 8 samples (4 paired iliac crest and cervical vertebra) were sliced into 0.65 mm thin sections. Samples were dried, placed in sample bags, and kept at -20˚C prior to SHG imaging. Before imaging, samples are placed onto a Fisherbrand™ InkJet Microscope Slide (Fisher Scientific).

SHG Imaging

SHG imaging was performed on the thin sections. SHG imaging was similar to the setup described in McGuire et. al. [156]. The thin sections were placed on a microscope slide onto the motorized stage of a Zeiss LSM 880 upright confocal microscope (Zeiss, Thornwood, NY). A Ti:Sapphire laser (Ultra 1, Coherent Inc., Santa Clara, CA) was utilized to perform backward-SHG imaging. The laser produced linearly polarized, 140-fs duration pulses, spectrally centered at 780 nm at 80-MHz repetition rate [156]. Following beam deflection and passing through a 690-nm short-pass dichoric mirror, the beam focused onto the tissue specimen with a 20x microscope objective [156]. Excitation power was kept to less than 30 mW [156]. Before generating the two-dimensional images for collagen fiber organization and orientation analysis, the backscattered SHG signals from the tissue travelled through the objective, a 690-nm short-pass dichoric mirror, a secondary dichoric mirror, a 390-nm bandpass filter (Semrock FF01-

390/18-25, IDEX Health & Science, LLC, Rochester, NY), and collected by a detector (BiG.2 module, Zeiss, Thornwood, NY) [156]. The generated two-dimensional images were 512 x 512 pixels^2 (1700.38 x 1700.38 μm^2). Two samples, S002H-2 and S002H-3 were imaged at 256 x 256 pixels^2 (850.19 x 850.19 μm^2).

Three image stacks, containing twenty images each, were acquired for each sample for a total of 24 (= 8 x 3) image stacks. Image stacks were taken at three different regions determined by searching for the neck and shoulder of a trabeculae (**Figure 20**).

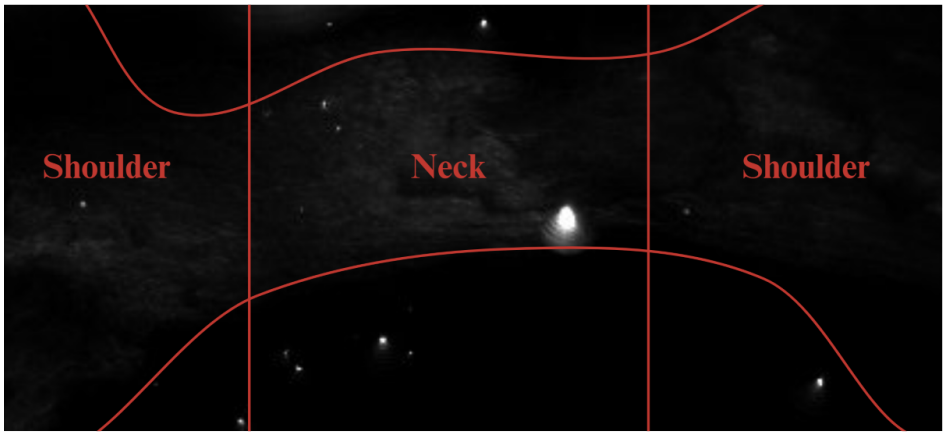

Figure 20: Trabecular locations, neck and shoulder, identified on a trabeculae.

Analysis of SHG Images

The orientation of collagen fivers within each of the 24 image stackes were quantified by means of a z-project image generated in ImageJ 2.14.0 [150]. The z-project image utilized the max intensity of each image in the stack to generate one composite image from the stack. Should the z-project image appear too dark, the contrast and maximum of the image was adjusted (S001H-2, S001H-3). The new z-projection image utilized the Slice Geometry module in BoneJ to determine the long-axis of the individual trabeculae within the image [154]. The axis were utilized to generate a perpendicular line to the collagen fibers running across the

trabeculae, allowing for trabecular thickness (Tb.Th) to be approximated. Following Tb.Th approximation, the z-project image was cropped into two ~375.28 x 225.83 μm^2 regions of interest representing the clearest collagen alignment at the shoulder and neck regions of the trabeculae. The region of interest was adjusted if highly attenuated air pockets were present at the shoulder or neck regions. The mean intensity (I_{ROI}) and max intensity (I_{ROI}^{max}) were calculated from the grayscale histogram for region of interest. Within each ~375.28 x 225.83 μm^2 region of interest, a smaller region of interest, ~16.61 x 13.28 μm^2, was utilized to determine the mean intensity (I_{ROI}) of four different collagen fibers, two higher in intensity and two lower in intensity. The average of the four lamellae was recorded. **Eq. (1)** was used to interpret the orientation of the collagen fibrils within the transverse plane relative to the sample preparation [157].

Equation 1: Collagen Angle

$$Collagen\ Angle = \arccos\left(\sqrt{\frac{I_{ROI}}{I_{ROI}^{max}}}\right) \quad (1)$$

Statistics

Statistical analysis for tissue meso- and microstructural parameters was performed using Rstudio 4.1.0 and Python 3.9.12. Given the small sample sizes, normality was not assumed for the datasets. A Wilcoxon Signed-Rank Test was performed to determine if any significant differences were observed between meso-scale morphological measurements (BV/TV, Tb.Th, Tb.S, BS/BV, Volume) derived from microCT scans at each graft location. A Kruskal Wallis was performed to determine any significant differences between the graft locations (iliac crest vs cervical vertebra), trabecular locations (shoulder vs neck), and the interaction between graft

location and trabecular locations for the microarchitecture measurements (Collagen Angle). The threshold for statistical significance was set to $p = 0.01$ due to the dataset's small size.

Results

A total of twelve (n=12) consecutive skeletally mature patients were consented for the study. Each patient had autograft harvested from both the iliac crest and cervical spine. Baseline demographics and comorbidities of patients enrolled in this study were noted (**Table 3**). Macroscopically, autograft bone retrieved from the cervical vertebra and iliac crest differed in volume and concavity. Additionally, the cervical vertebral autograft samples were consistently smaller and more prone to fragmentation during sample preparation compared to iliac crest autograft samples.

Table 4: Demographic variables and comorbidities in patients undergoing ACDF. Values reported as mean [range], mean ± standard deviation, or as a ratio, yes:no, of the population.

	Patients n=12
Age (years)	53.9 [38 to 62]
Gender [female:male]	[8:4]
Body Mass Index (BMI)	27.7 ± 5.74
Hypertension	4:8
Chronic Kidney Disease (CKD)	2:10
History of Tobacco Use	6:6
Multilevel Disease	9:3
Preoperative Serum Calcium	9.59 ± 0.49

Analysis of Morphological Shape between Autograft Locations via MicroCT Imaging

MicroCT imaging was utilized to quantitatively describe the morphology of the iliac crest and cervical spine autograft samples (**Table 4**). BV/TV, Tb.Th, and Tb.S were larger in the cervical

vertebra than in the iliac crest; however, these differences were not significant. On average the iliac crest samples had a slightly larger TV than the cervical vertebra, validating the qualitative macroscopic observations made prior to microCT; however, this difference was not significant. A trend for higher BS/BV in the iiliac crest compared to cervical vertebra was observed (p=0.03418), but due to our conservative statistics this was not deemed significant.

Table 5: Bone morphometric properties measured via microCT imaging. Morphological variables reported as mean ± standard deviation.

	Iliac Crest	*Cervical Vertebra*	*p*	
BV/TV (%)	20.73 ± 3.813	24.72 ± 6.023	0.09229	ns
Tb.Th (mm)	0.2671 ± 0.0874	0.3213 ± 0.0732	0.2036	ns
Tb.S (mm)	0.5945 ± 0.0600	0.6337 ± 0.1112	0.4238	ns
BS/BV (mm^{-1})	21.39 ± 4.607	19.46 ± 5.049	0.03418	cs
TV (mm^3)	27.01 ± 29.71	22.15 ± 10.91	0.9697	ns
ns, not significant; cs, close significance, p<0.05; * p<0.01				

Analysis of Collagen Alignment between Autograft Locations via SHG Imaging

SHG imaging was utilized to quantitatively describe the collagen alignment across the width of individual trabecula from the iliac crest and cervical spine autograft samples (**Table 5**). Medial collagen angle across the iliac crest (53.26 [50.90 – 55.13]) was not significantly different from that of the cervical spine. Nor was there any significant difference between pooled median angle at the trabecular neck and shoulder. Further, no significant interaction was detected between graft anatomical location and location along the trabecula (**Table 5**).

Initial collagen angle quantitative measures were validated by taking the average of 4 neighboring lamella within the region of interest utilized for the trabecular locations. The new calculations were named “specific collagen angle”.

The specific collagen angle mean and median were 2.419 and 2.794 degrees less than the initial collagen angle respectively (mean: 50.54 ± 2.645 vs 52.96 ± 4.558; median: 49.86 [48.02 – 53.28] vs 52.66 [50.02 – 55.54]).

Table 6: Bone collagen angle measured via SHG imaging. Collagen Angle (degrees) reported as median [IQR].

		Graft Location (p = 0.617)	
		Iliac Crest	Cervical Vertebra
Trabecular Location (p = 0.611)	Neck	52.81 [50.90 - 55.74]	52.97 [49.60 - 56.24]
	Shoulder	53.34 [50.90 - 54.79]	51.49 [48.79 - 54.55]
Graft Location x Trabecular Location (p = 0.517)			
ns, not significant; * p<0.01			

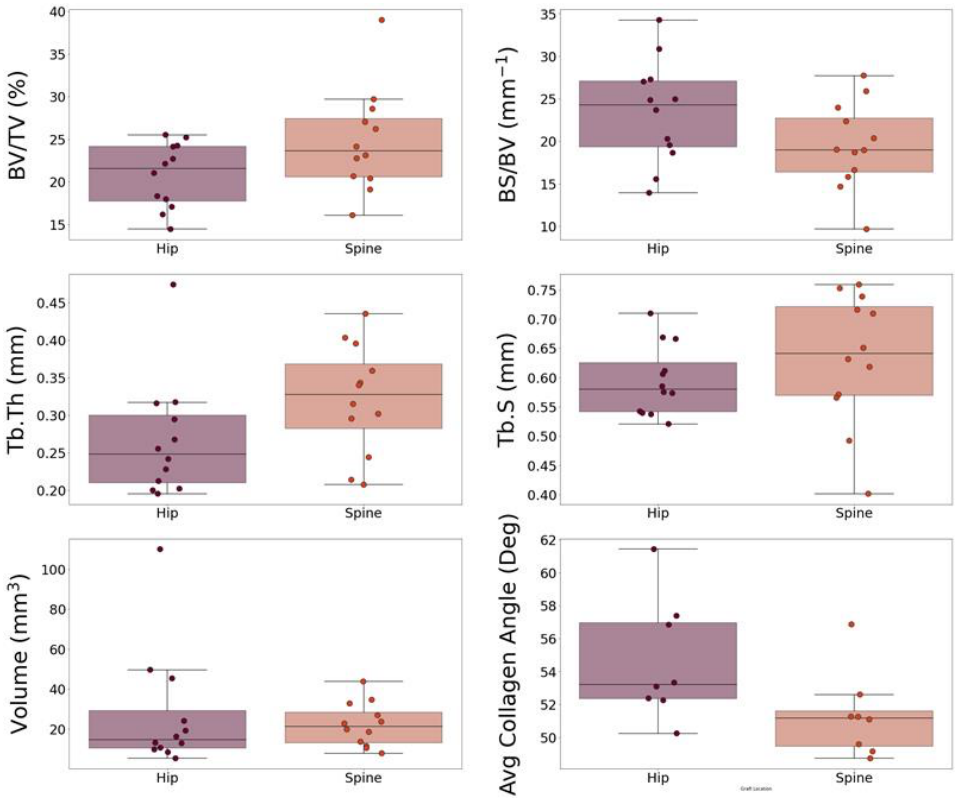

Figure 21: Boxplots and strip plots of the morphometric and micro-architecture measurements between hip and spine autograft locations.

Discussion

In this pilot study, we are the first to compare morphological and collagen microarchitectural characteristics of patient-matched trabecular bone from iliac crest and cervical vertebra. Analyses were performed to assess morphological and microarchitectural characteristics using microCT and SHG image-based analyses. Moreover, in pursuit of the goals of this study - to characterize the morphology and collagen microarchitecture between the standard-of-care autograft location, the iliac crest, and proposed novel autograft location, the cervical vertebra – several sample preparation protocols, and image processing pipelines have also been developed, enabling semi-automatic image processing of high-resolution 3D image data.

In accordance with Wolff's Law, trabecular bone, a tissue with high metabolic activity, will adapt its morphology to thrive within its local mechanical environment [13]. As bone heals and fuses the two vertebrae together following an ACDF, morphology has an impact on how efficiently and effectively new bone can grow. Porosity, often associated with Tb.S, impacts cell recruiting, cell flow, and vascularization of the autograft, all of which are associated with osteoconduction during the inflammation stage [70], [85], [86]. In addition to similar porosity, osteoinduction and osteointegration, often associated with Tb.Th, BV/TV, and BS/BV, impacts the differentiation of MSCs into osteoblasts, the promotion of bone growth, the incorporation of new bone into the fusion site, and the balance between bone formation and resorption via mineral exchange [77], [88], [90]. Notably, no significant differences were detected between the morphometric properties of the iliac crest and cervical vertebra. This suggests that the cervical vertebra autograft exhibits similar osteoconductive, osteoinductive, and osteointegrative

properties to the iliac crest. Consequently, the cervical vertebra has a high likelihood to exhibit similar healing pathways during the inflammation stage and bone growth phases of the bone healing pathway following ACDF surgeries, as supported by a prior clinical study and the lack of adverse events reported to date in the current clinical cohort [9]. Also, the Tb.S values were consistent with prior literature for both the iliac crest and cervical spine [81], [92], [95], [158]. In contrast with the Tb.Th and BS/BV values, the BV/TV values were consistent with prior literature for both the iliac crest and cervical spine [81], [92].

Our study evaluated the collagen angle within the micro-architecture of collagen alignment as it allows for the assessment of osteointegration and bone mechanics to withstand future physiological loads during the inflammation stages of healing following an ACDF surgery [16]. There was no significant difference in the collagen angle found between the iliac crest and cervical vertebra, trabecular location, or the interaction of the graft and trabecular location. When validating the initial collagen angle, the specific collagen angle measurements reinforced the 30-60 degrees plywood layup commonly seen in trabecular bone due to its properties to withstand loads in multiple directions [159], [160]. Thus, both autograft donor sites have the ability to provide mechanical stability to the fusion site, encourage collagen formation, and support bone growth via the continuation of their micro-architectures during healing stages.

Despite showing similar morphometric and micro-architecture properties, this study is limited by its lack of access to ample tissue and resultant small group sizes. As such, findings from the current study should be considered preliminary in nature. Despite the small number of samples, this is the first study to directly compare tissue properties of patient-matched autograft from multiple sites for ACDF. Future studies should increase the number of enrolled

patients, given the comparable success rate and minimal risk, to enable the ability to make comprehensive conclusions. In addition, utilizing one singular software for morphological measurements and validating it utilizing another software would further solidify morphological statistics. Due to time limitations, equipment down time, and extensive imaging protocol development and optimization, a lack of sample preparation timing, SHG imaging was only performed on 1/3rd of the available sample population. Future studies can now utilize the developed streamlined process, enabling more in-depth and robust analysis of the SHG images. Furthermore, the spatial orientation of the autograft tissue was not preserved following excision, prohibiting the comparison of the morphometrics with primary loading direction and other anatomical directions. Collagen alignment is dependent on the sample's orientation to the camera; thus, a lack of orientation reduces our ability to make firm conclusions on the collagen alignment within the trabecular network of the iliac crest and cervical vertebra autograft. Finally, we did not utilize a correction for multi-level comparisons in our statistics; however, we selected conservative statistical tests and utilized a reduced alpha value to account for the pilot nature of the study.

This study quantified the morphological and collagen alignment properties of human iliac crest and cervical vertebra autograft samples. The study found no significant differences in the morphological properties and collagen alignment between the autograft locations. This similarity may have contributed to the comparable fusion rates observed in prior studies, as the healing pathways during the initial stages of bone healing and growth are similar. The lack of significant differences in morphological properties and collagen alignment emphasizes the importance of further characterizing other properties of iliac crest and cervical vertebra bone.

This is crucial to determine if the cervical vertebra might cause complications with fusion if it becomes the gold standard for autograft tissue used in ACDF.

Chapter 4 - Aim 2: Characterization and Analysis of the Compressive Mechanical Properties of Bovine Trabecular Bone from the Iliac Crest and Spine – An Autograft Comparative Anatomy Study

Introduction

Standard-of-care ACDF utilizes trabecular autograft from the iliac crest, yielding impressive fusion rates of 83% to 99% [7]. Although success rates are high, increased levels of donor site morbidity and loss of quality of life due to said morbidities are commonly associated with iliac crest autograft usage for ACDF surgeries [11], [53]. To mitigate donor site morbidities associated with the secondary surgical sites of autograft resection, a novel autograft location was proposed: harvesting bone from the inferior cervical vertebra adjacent to the operative disc space [8]. Additionally, there is a decrease in morbidities associated with ACDF when utilizing the novel autograft location [9].

When used as a bioactive insert within spacers for ACDF surgeries, trabecular bone facilitates fracture repair, stimulates new bone growth, and promotes osseous fusion. This is attributed to its stem cell availability, microarchitecture, self-repair capacity, and internal remodeling properties [16]. In addition, trabecular bone fracture repair is heavily impacted by its response to mechanical stimuli [16], [70], [161], [162]. Mechanical stimulus is greatly associated with bone formation and the speed at which mechanical stability can be restored [16], [161], [162]. Due to its elastic nature, trabecular bone can withstand 3% strain from mechanical stimuli without experiencing irreversible damage [89], [163]. To ensure mechanical stability, trabecular bone should remain in the elastic region to prevent permanent damage. It is

necessary to characterize the mechanical properties of the cervical vertebra and directly compare it to iliac crest properties before adapting the standard-of-care for patients worldwide.

Autograft stiffness, which refers to the resistance to deformation under mechanical stimuli, impacts cell adhesion and differentiation within autografts. This property is often mimicked by scaffolds designed to imitate the structure and mechanical properties of cancellous bone [164]. Trabecular bone, a tissue with high metabolic activity, is constantly adapting to the local mechanical environment associated with the compressive physiological loads it experiences [13]. Trabecular bone is an anisotropic material, adapting its mechanical behavior directionally to improve its strength and stiffness under mechanical loading [23], [89], [116], [122]. In previous studies, it has been found that the lumbar spine is transversely isotropic, differing its mechanics in its axial loading direction versus its other anatomical directions, in comparison to iliac crest which is much more isotropic across all three directions [137], [165], [166]. The difference in anisotropy is traditionally attributed to the differences in function and daily loading between the lumbar spine and iliac crest. Although lumbar and cervical spines inherently have different mechanical properties, they both show similar amounts of anisotropy due to the daily physiological loading directions of the spine [76].

The present study utilizes bovine tissue as a comparative anatomy model to investigate the mechanical properties of iliac crest and lumbar spine, which has similar physiological loading, in both proportional magnitudes and directions, to the cervical spine. The elastic and post-yield mechanical properties of trabecular bovine bone from two locations, the iliac crest and lumbar spine, were compared utilizing analysis of compression testing data. It is hypothesized that the lumbar spine would show differences in stiffness in the primary

physiological loading direction in comparison to its other loading directions due to its inherent anisotropy. It is also hypothesized that the stiffness in the primary physiological loading direction would be higher for the lumbar spine compared to the iliac crest, as body weight forces are consistently greater than anatomical muscle forces.

Methods

Sample Prep

The thoraco-lumbar spine (thoracic vertebra 13 to lumbar vertebra 6, titled lumbar spine due to lumbar spine dominance) and whole pelvic bone from two (n=2) skeletally mature cows were received from the Virginia Tech Meat Center. The received lumbar spines were split down the median sagittal plane and lateral spinus processes were cropped or completely removed, due to the handling and butchering performed at the Meat Center. The left side of the vertebras were utilized. An EXAKT 302 Pathology Saw (EXAKT, Oklahoma City, OK) was utilized to cut the spines into individual vertebra (Thoracic 13 – Lumbar 6) (14 = 2 spines x 7 vertebrae per spine). Two segments from the iliac crest pieces were cut from the left pelvic bones (4 = 2 pelvises x 2 pieces per pelvis). The pubic symphysis was measured to be 9.750 in (24.765 cm) and 9.875 in (25.0825) from the iliac crest for C001 and C002 respectively. Cuts were made 3.375 in (8.57 cm) and 3.75 in (9.525 cm) caudally from the iliac crest for C001 and C002 respectively. These gross cuts were then cut into two different pieces and labelled as cranial or caudal. Directionality of the tissue relative to the primary axes (cranial-caudal (C-C), medial-lateral (M-L), dorsal-ventral (D-V)) for each cut was noted and tracked with each cut (**Figure 22**).

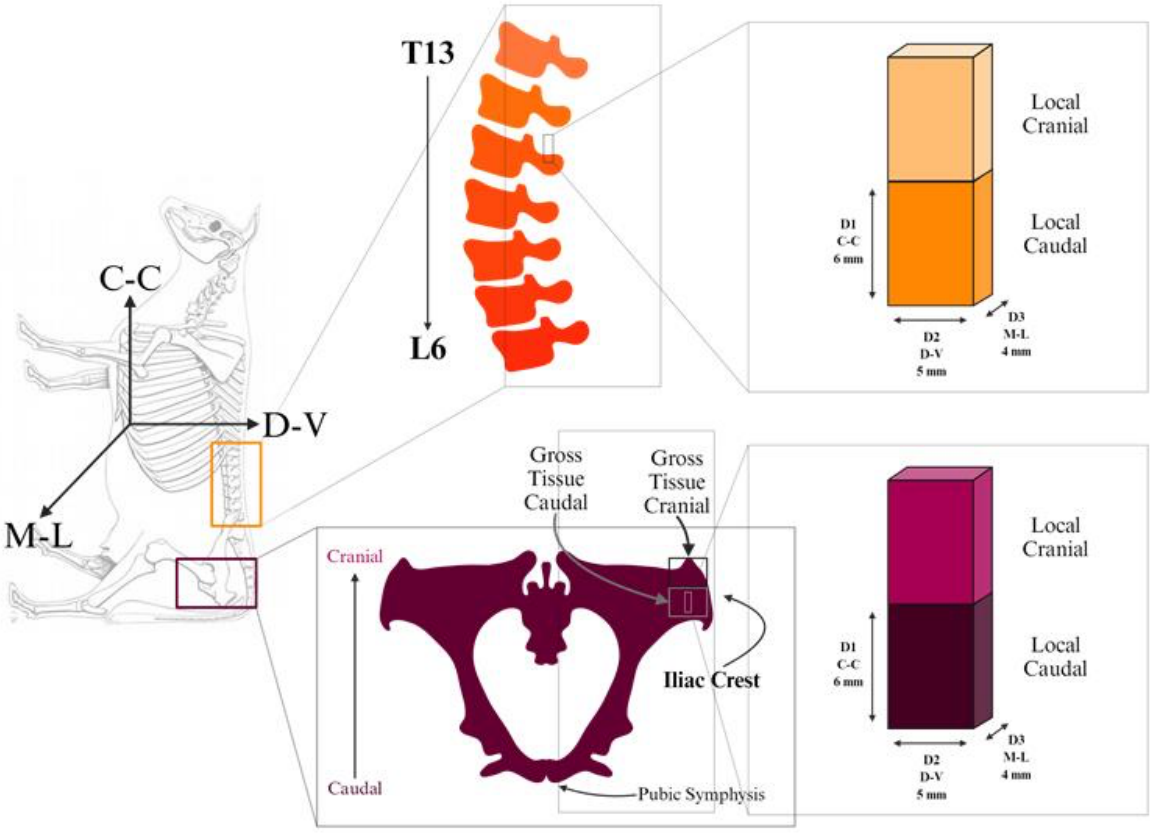

Figure 22: Local cranial and caudal locations taken for the lumbar spine. Gross and local cranial and caudal locations taken for the iliac crest.

A Buehler Isomet Low Speed Saw (Buehler, Lake Bluff, IL) was utilized to precisely cut two cuboid samples of trabecular bone from each piece of vertebral and iliac crest bone segments. The two samples from each subject were taken from adjacent locations, one more cranially and one more caudally (**Figure 22**). The target dimensions of the final test samples were 4 mm in direction 3 (M-L), 5 mm in direction 2 (D-V), and 6 mm in direction 1 (C-C) (**Figures 22, 23**). A series of six cuts, one facing and one for the final dimensional measure, were made in perpendicular directions, increasing by 1 mm with each successive cut (**Figure 23**).

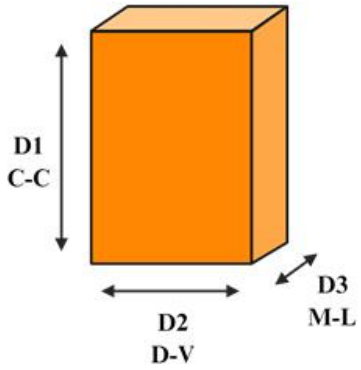

Figure 23: Compression Testing Sample Dimensions and Directionality

Compression Testing

Each sample underwent uniaxial compression testing on an MTS Insight 10 (MTS Eden Prairie, MN) utilizing a 5 kN MTS Servohydraulic System Load Cell (Sensitivity = 2.416 mV/V, recording at 40 samples per second) (MTS Eden Prairie, MN). Displacement control, measured as crosshead deflection, was utilized to control each test. For each sample, 13 tests were performed: one cyclic and 3 repeated-measure tests for each direction, C-C, followed by D-V, followed by M-L, and one final test to failure in the C-C direction.

The cyclic tests performed for the lumbar spine and the iliac crest utilized preload, test, and separation speeds of 0.006, 0.005, and 0.004 mm/s for D1, D2, and D3 respectively. The first cycle of the cyclic test for all lumbar spine samples began with a preload of 20 ± 1 N, loaded to 60 N, and returned to the preload 20 N. The first cycle of the cyclic test for iliac crest samples C001_IliacCrest_01_01_01_D1, -D2, -D3, and C001_IliacCrest_01_01_02_D1 were loaded to 40 N. The first cycle of the cyclic test for iliac crest samples (in all directions) C002_IliacCrest_01_01_01, C002_IliacCrest_01_01_02, C002_IliacCrest_02_02_01, and

C002_IliacCrest_02_02_02 began with a preload of 10 N ± 1 N, loaded to 20 N, and returned to the preload 10 N. The first cycle of the cyclic test for all other iliac crest samples began with a preload of 15 N ± 1 N, loaded to 30 N, and returned to the preload 15 N. The cyclic loading ran for five cycles for each sample in each direction.

The compression tests performed for the lumbar spine and the iliac crest utilized test and separation speeds of 0.006, 0.005, and 0.004 mm/s for D1, D2, and D3 respectively. Each repeated compression test began with the same preload as the cyclic testing (see the paragraph above). Following preloading, the sample was continuously loaded until a linear elastic region was established on a live stress vs strain graph. Once the linear elastic region was identified, the test was stopped, and the sample was immediately unloaded. This test was repeated three times for each direction.

- C-C Direction (D1): Cyclic preload test followed by three repeated compression tests.
- D-V Direction (D2): Cyclic preload test followed by three repeated compression tests.
- M-L Direction (D3): Cyclic preload test followed by three repeated compression tests.

Following the last repeat measure test, a failure test was performed on the C-C direction. This test began with the same preload as the prior tests. The sample was then loaded at the same speed as before, allowing the sample to fail past the elastic limit and into the plastic region of the trabecular bone.

The displacement (mm) and force (N) were recorded for each sample for every test.

Analysis of Compression Testing Data

The data was imported into Python 3.9.12. For each repeated compression test, the elastic modulus was calculated within Python using a linear fit of the elastic region of the stress-strain curve. The last trial for each repeated compression test, trial three, was utilized for analysis as trials 1 and 2 were assumed for precycling use. For the tests to failure, the modulus and maximum stress were calculated.

Statistics

Statistical analysis was performed using Python 3.9.12. A Shapiro-Wilk test was utilized to test for normality. A Levene test was utilized to test for variance homogeneity between samples. A Mann-Whitney U test was performed to compare the means for all samples for its conservative statistical nature. A Kruskal Wallis test was performed to determine if tissue location or directional loading had an impact on modulus and max strain. Dunn's post hoc test was utilized to interpret the results of the Kruskal Wallis test should significance be shown. The threshold for statistical significance was set to $p < 0.05$ due to the dataset's size.

Results

A spine and pelvic bone were retrieved from 2 cows previously sacrificed for teaching material. 41 samples were cut for compression testing: 2 per vertebra (28 = 2 per vertebra x 7 vertebra x 2 cows), 13 from Cow 1's iliac crest and 10 from Cow 2's iliac crest. The average dimensions of the samples, measured using a micrometer, were 4.187 ± 0.249 mm, 5.151 ± 0.313 mm, and 6.002 ± 0.115 mm in height for the D3/M-L, D2/D-V, and D1/C-C directions respectively. Three samples from Cow 2's iliac crest were too soft to record a modulus from the

test to failure; thus, the average of their D1 moduli were utilized. One sample from Cow 2's iliac crest was too soft to produce moduli in the D1 direction and was excluded from analysis.

Comparisons between elastic and post-yield properties of the samples cut from the upper thoracolumbar and lower lumbar spine were not significantly different between or within cows. Similarly, no differences were detected between samples from the cranial vs caudal spatial locations within the vertebra. As such, data was pooled into a single group of lumbar samples, with labels for direction of loading. Similarly, iliac crest tissue was not significantly different between cows or spatial location. As such, these samples were pooled into a single group with labels for direction of loading. Iliac crest gross tissue taken between cranial and caudal locations (**Figure 22**). Normality for different parameters, as determined by the Levene test, is summarized in the table below:

Table 7: Summary of Normality for Different Parameters.

Normality Accepted	Normality Rejected
- C002 D1 - D2 between cows - Lumbar Spine Max Stress - Lumbar Spine Failure Modulus	- Upper vs Lower Lumbar Spine for: C001, C002, and between cows - Iliac Crest between cows - C001 D1 - D3 between cows - D1 vs D2 vs D3 - Iliac Crest Max Stress

Significant differences were found between the moduli of the iliac crest and the cervical spine regardless of directional testing ($p=1.03 \times 10^{-10}$). Significant differences were also found between the moduli of D1, D2, and D3 regardless of anatomical tissue location ($p=3.00 \times 10^{-7}$). Once grouped, the Kruskal Wallis revealed significant differences in elastic modulus associated with the interaction of direction and anatomical location ($p=3.23 \times 10^{-16}$). Additionally, significant difference in max stress was found between anatomical locations.

Table 8: Compressive Properties of Trabecular Bovine Bone Extracted from the Iliac Crest (IC) and Lumbar Vertebra (LS).

Location	Mechanical prop	Testing Direction			P-Value
		D1	D2	D3	
IC (n=22)	Modulus (MPa)	82.5 [50.5 - 153]	81.4 [59.6 - 131]	61.3 [47.4 - 73.4]	-
	Max Stress (MPa)	2.18 [1.74 - 2.94]	-	-	-
LS (n=28)	Modulus (MPa)	603 [436 - 823]	138 [79.0 - 185]	130 [78.2 - 172]	***
	Max Stress (MPa)	12.1 [8.59 - 16.3]	-	-	-

ns, not significant; * p<0.05; ** p<0.01; *** p<0.001

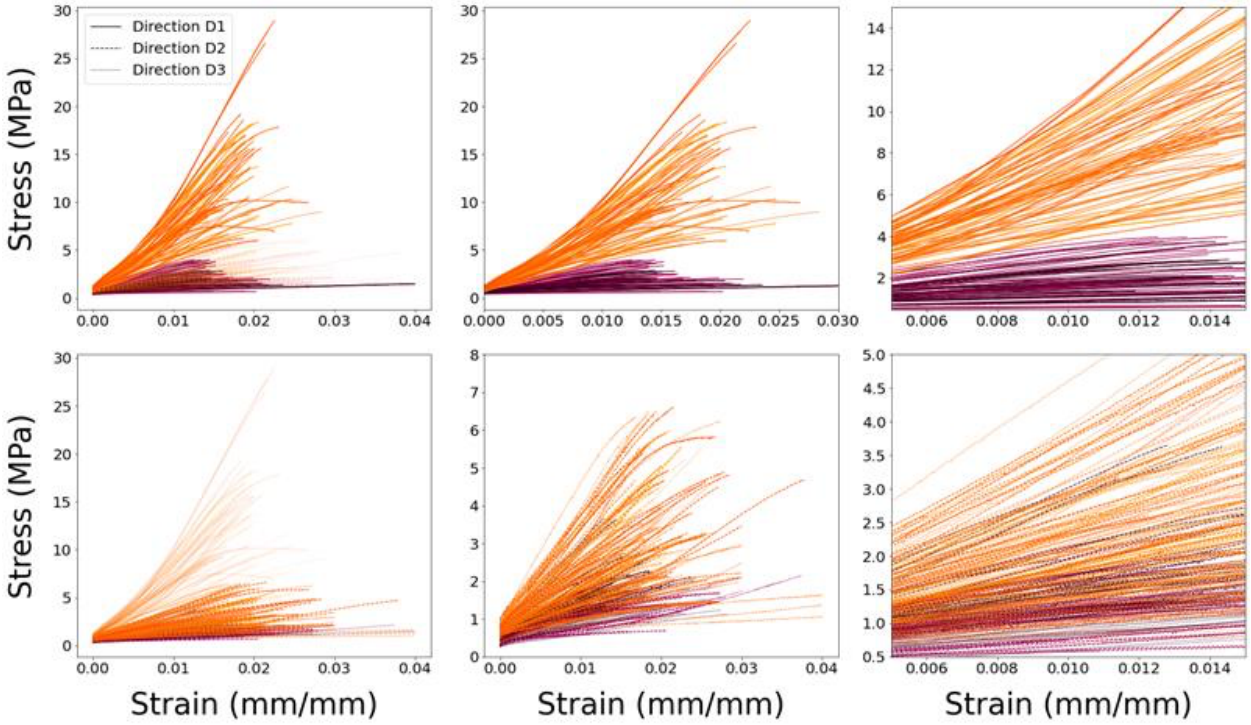

Figure 24: Stress-strain curves of max stress for the last trial of the repeated tests of bovine bone. The Oorange plots represent= lumbar spine trials. and the maroonMaroon plots trials represent= iliac crest trials. The upper left plot highlights D1 tests against other tests. The upper middle plot isolates the D1 tests. The upper right plot zooms to show the linear regions of the upper middle D1 graph. The bottom left plot highlights D2 and D3 tests against other tests. The bottom middle plot isolates the D2 and D3 tests. The bottom right plot zooms to show the linear regions of the D2 and D3the lower middle graph.

Effect of Anatomical Tissue Location Impacting Bovine Bone Modulus and Max Stress

Significant differences were seen between the anatomical tissue location, lumbar spine or iliac crest, for modulus and max stress. Compression testing showed the average modulus of the lumbar spine in each direction was significantly higher, nearly 2.5x larger, than the iliac crest (175 MPa and 71.8 MPa, respectively; $p<0.001$). The lumbar spine modulus median (175 MPa) was 2.44x larger than the median of the iliac crest modulus (71.8 MPa). The variance in modulus is higher in the lumbar spine than that of the iliac crest (**Figure 24**):

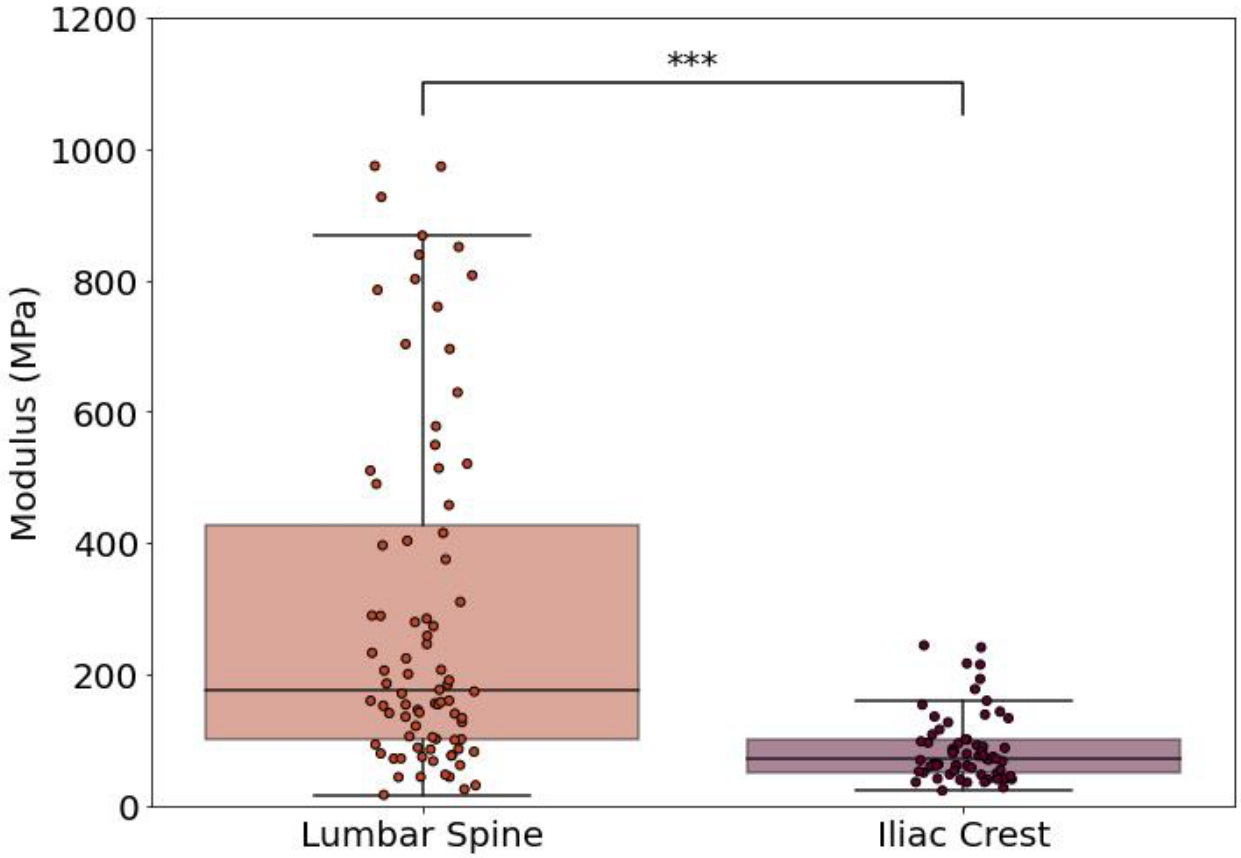

*Figure 25: Boxplot and stripplot of D1 modulus for the anatomical tissue location of bovine bone, significance labeled: (*** p<0.001). The lumbar spine modulus was significantly larger than the iliac crest modulus.*

In addition to modulus, the max stress of the lumbar spine was significantly different than the iliac crest when testing to failure ($p<0.001$). The lumbar spine median max stress (12.1)

was 5.53x larger than iliac crest (2.19). The variance of the max stress was larger in the lumbar spine than the iliac crest (**Figure 25**).

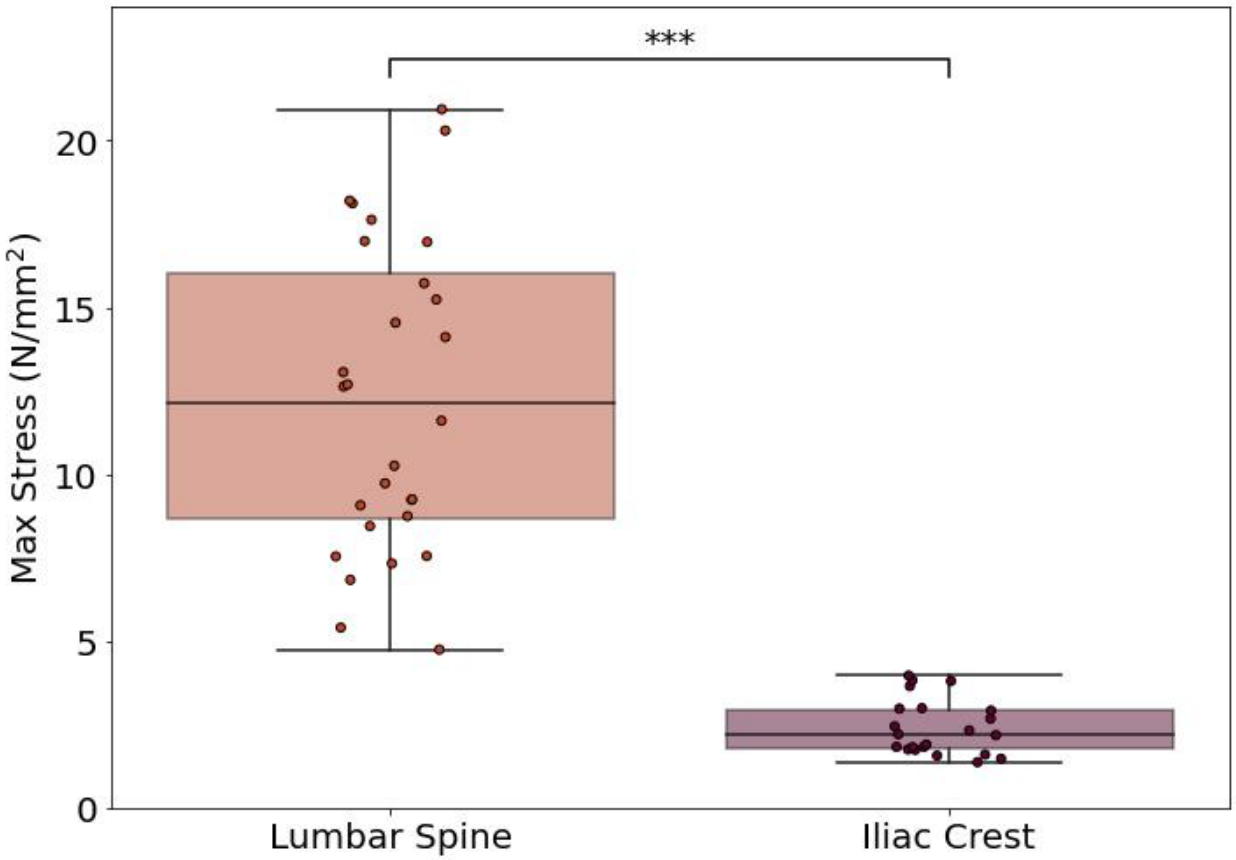

*Figure 26: Boxplot and Stripplot of max stress for the anatomical tissue location of bovine bone, significance labeled: (*** p<0.001). The lumbar spine max stress was significantly larger than the iliac crest max stress.*

Effect of Test Directionality Impacting Bovine Bone Modulus

The modulus varied depending on which direction the compression test was administered (**Figure 26**). The average modulus of D1, the cranial-caudal testing direction, was significantly larger than the modulus of D2 ($p<0.001$), the dorsal-ventral testing direction, and D3 ($p<0.001$), the medial-lateral testing direction, during the last trial of the repeated compression test. However, the modulus of D2 was not found to be significantly different from the modulus of D3 ($p = 0.287$). The median modulus of D1 (375 MPa) is ~3.64x and ~4.72x larger than the medians of D2 (103 MPa) and D3 (79.5 MPa) respectively. In addition to the median, there is a clear qualitatively larger variance in D1 test moduli than there is in D2 and D3 test moduli (**Figure 26**).

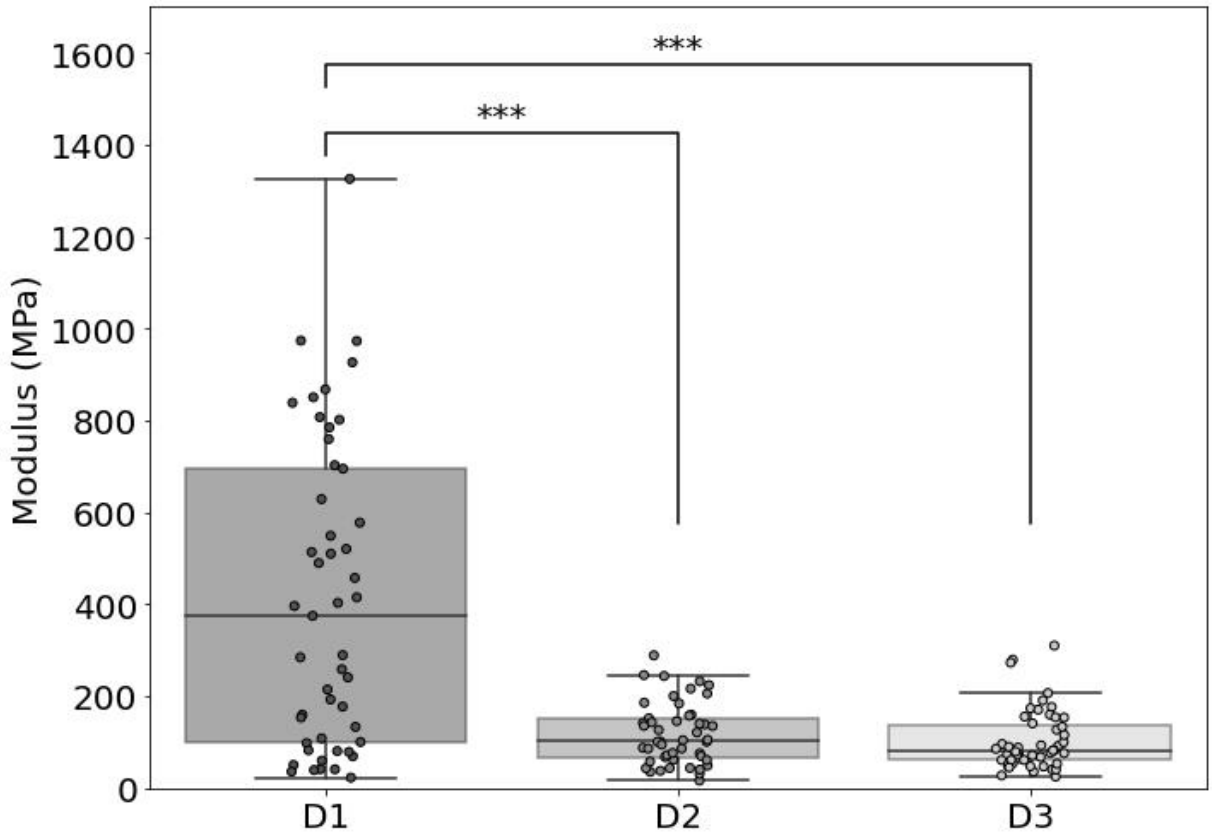

*Figure 27: Boxplot and stripplot of modulus for the direction of bovine bone during the last trial of the repeated compression test, significance labeled: (*** p<0.001). The D1 testing direction modulus was significantly larger than the D2 and D3 testing direction moduli.*

Effect of Test Directionality and Anatomical Tissue Location Impacting Bovine Bone Modulus

The modulus varied significantly when analyzing the interaction of test directionality and anatomical tissue location, peaking with lumbar spine D1. The modulus of lumbar spine D1 was significantly larger than every other combination of testing direction and anatomical location: lumbar spine D2 and D3, and iliac crest D1, D2, and D3 (all $p<0.001$). The median modulus of lumbar spine D1 is 4.37x, 4.64x, 7.31x, 7.41x, and 9.84x larger than lumbar spine D2, lumbar spine D3, iliac crest D1, iliac crest D2, and iliac crest D3 respectively (**Table 6**). The modulus of lumbar spine D2 and D3 were significantly larger, 2.25x and 2.15x respectively, than iliac crest D3 (both $P<0.01$). Also, the modulus of lumbar spine D2 and D3 were not significantly different than iliac crest D1 and D2. However, the modulus of lumbar spine D2 was not significantly different than lumbar spine D3. The modulus of iliac crest D1, D2, and D3 were not significantly different from each other.

The variance of the modulus was larger in the lumbar spine D1 than lumbar spine D2D3, iliac crest D1, and iliac crest D2D3 (**Figure 28**).

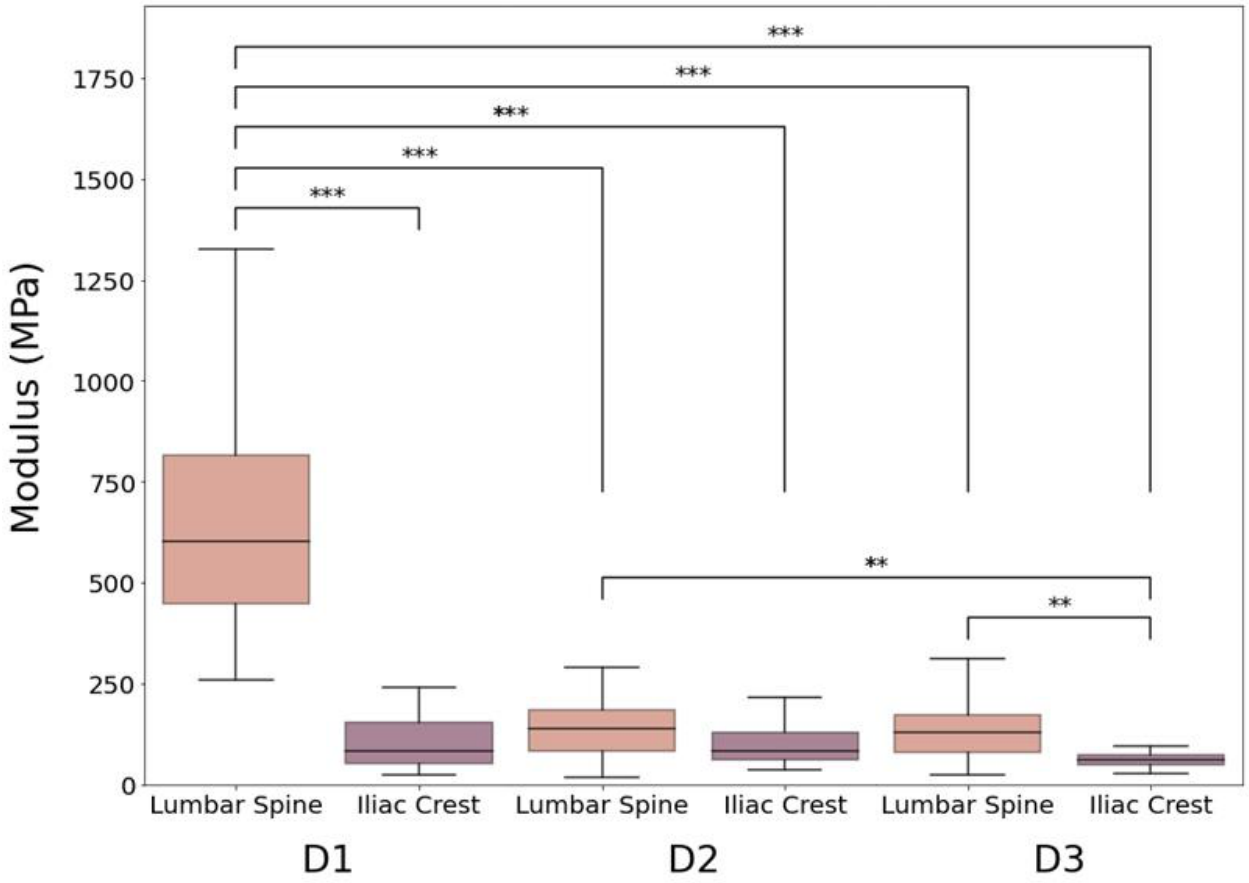

*Figure 28: Boxplot of modulus for the direction (D1, D2, D3) and location of bovine bone during the last trial of the repeated compression test, significance labeled: (** p<0.01; *** p<0.001). The D1 lumbar spine modulus was significantly larger than the D1 iliac crest, D2 lumbar spine and iliac crest, and D3 lumbar spine and iliac crest moduli. The D2 and D3 lumbar spine moduli were significantly larger than D3 iliac crest modulus.*

The modulus of lumbar spine D1 was significantly larger than lumbar spine D2 and D3 combined (D2D3) and iliac crest D2D3 (both $p<0.001$). The modulus of lumbar spine D2D3 was significantly larger than iliac crest D2D3 ($p<0.01$); however, there was no significant difference between the modulus of lumbar spine D2D3 and iliac crest D1. The modulus of iliac crest D1 was not significantly different from iliac crest D2D3.

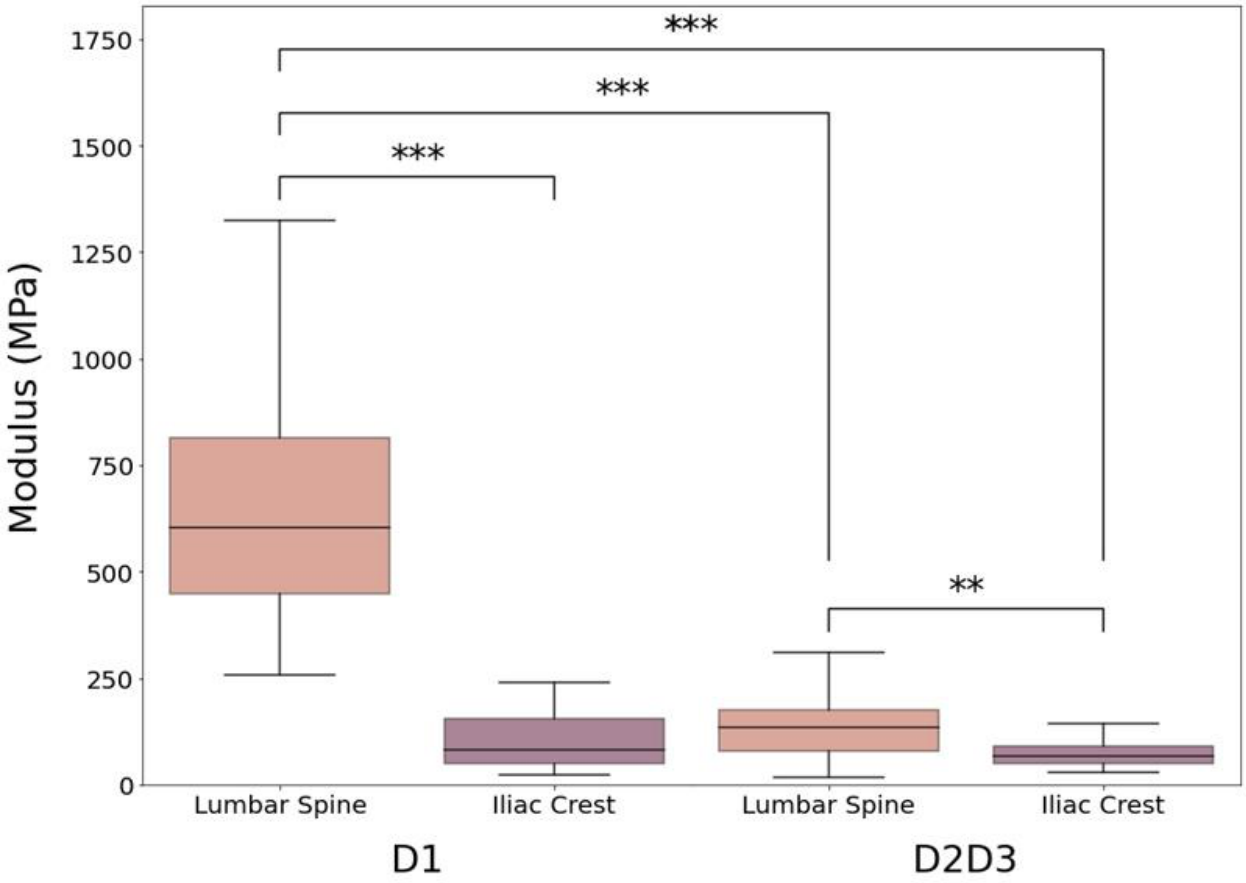

*Figure 29: Boxplot of modulus for the direction (D1, D2D3) and location of bovine bone during the last trial of the repeated compression test, significance labeled: (** p<0.01; *** p<0.001). The D1 lumbar spine modulus was significantly larger than the D1 iliac crest, D2D3 Lumbar Spine, and D2D3 iliac crest moduli. The D2D3 lumbar spine modulus was significantly larger than D2D3 iliac crest modulus.*

Discussion

The goal of this study was to mechanically characterize the material properties of bovine lumbar spine and iliac crest trabecular bone and evaluate the effects of cow subjects, specific locations of the lumbar spine, gross tissue location (cranial vs caudal) for the iliac crest, local tissue location (cranial vs caudal), anatomical tissue location, and test direction on the material properties. For this study, cows, specific locations of the lumbar spine, gross tissue location (cranial vs caudal) for the iliac crest, and local tissue location (cranial vs caudal) did not significantly influence the material properties. Yet, anatomical tissue location and test direction appeared to interact, yielding significant results between modulus and anatomical tissue location and test direction. Significant correlations were also produced between anatomical tissue location and max stress.

Within each anatomical tissue location, there were no significant differences found where the samples were taken. However, lumbar spine modulus was found to be 2-fold larger than iliac crest modulus. Additionally, lumbar spine max stress was found to be 5-fold larger than iliac crest max stress. These significant differences between the anatomical tissue locations may be attributed to the physiological loading of each location. While the load-bearing proportions between the spine and iliac crest may not be the same in humans and cows, the bovine trabecular bone displayed similar load-bearing characteristics to human trabecular bone at both anatomical locations, as compared with values from previous studies (**Table 3**). The only bovine mechanical value in **Table 8** that fell outside the ranges reported in **Table 3** was the inferior-superior (D1) loading direction modulus, which was increased by 30% in the bovine trabecular bone. Despite this difference, the consistent use of bovine trabecular bone in

literature indicates that the scientific community recognizes the similarity in other mechanical values, as evidenced by the congruence between the values in **Tables 3** and **8** [138], [139], [140], [141].

The lumbar spine experiences many compressive physiological loads; however, the main compressive load it experiences is body weight [25]. In previous studies, it has been proven that lumbar and cervical spines are proportionally similar in mechanical properties due to the daily physiological loading of body weight on the spine [76]. In contrast to the lumbar and cervical spine, the iliac crest is relatively non-weight bearing, rather experiencing muscle forces [167]. These differences in physiological loading inherently impact the mechanical properties of anatomical tissue locations in response to compressive loads, as evidenced by the significantly larger modulus and maximum stress associated with the lumbar spine compared to the iliac crest. Consistent with Wolff's law, the lumbar and cervical spine's ability to withstand higher stresses than the iliac crest may influence its candidacy as a novel autograft location should. In contrast, the iliac crest does not require as much stiffness or maximum stress, as it primarily experiences muscle forces. In addition to the magnitude of the physiological loads experienced at each anatomical location, previous literature discussed that the load's direction will cause different anisotropy across the three major perpendicular axis [137], [165], [166]. Lumbar spine D1 represents the loading direction of body weight, the main physiological load on the spine. Muscle forces loading the iliac crest do not result in a primary loading direction. Much like the iliac crest, the spine experiences mostly muscle forces in the non-primary loading directions.

Unlike D1, lumbar spine D2 and D3 do not show any significant differences in modulus. Thus, when characterizing the mechanical characteristics of the lumbar spine, transversely

isotropic behavior can be used to describe lumbar spine trabecular bone. A material is considered transversely isotropic when it exhibits different material properties in one loading direction compared to the other two directions, which display isotropy. Previously stated in literature, lumbar spine is anisotropic in its body weight loading direction versus its muscle force loading directions [137], [165], [166]. While this difference in loading direction moduli is clear in a quadruped cow model, the difference could be even larger in biped human models due to the proportion of weight bared by the spine.

In contrast to the lumbar spine, iliac crest D1, D2, and D3 do not show any significant differences in modulus. The muscle forces acting on the iliac crest load the trabecular bone similarly, which has led previous literature to describe the bone as isotropic [17], [18], [19]. Although no bone is perfectly isotropic, the lack of a principal loading direction on the iliac crest inherently leads to isotropic-esque bone.

In contrast to lumbar spine D1, lumbar spine D2 and D3 moduli show no significant differences to iliac crest D1 and D2. Although lumbar spine D2 and D3 moduli are significantly, 2-fold, larger than iliac crest D3, they are more similar to iliac crest D3 than to lumbar spine D1, with a difference of roughly 2-fold. From this comparison, an assumption can be made that lumbar spine D2 and D3 and similar to iliac crest D1, D2, and D3.

From this assumption, the physiological loads each location and direction experiences may be attributed to the attached anatomical muscle forces acting at the location rather than body weight loads. At lumbar spine D2 and D3, the muscle forces experienced by the lumbar spine optimize the trabecular bone moduli to better withstand these loads rather than a much higher moduli designed to withstand body weight. One muscle that runs along the lumbar spine

and iliac crest within cows, and humans, is the Psoas. In cows and humans, the Psoas acts as a lumbar spine stabilizer and flexor, helping maintain posture and move the (cows: hind) legs and hips [168].

Despite showing significant differences for measurements involving lumbar spine D1 and a relative similarity between lumbar spine D2 and D3 and iliac crest D1, D2, and D3, this study is limited by its lack of readily available tissue. While lumbar and cervical spine experience similar physiological loading mechanisms, there is inherent difference when using a different anatomical location. This limits the conclusions one can draw about cervical spine's mechanical and material properties. With the access to more cow tissue, or even cadaveric tissue, each vertebra within the cow or human could have been tested to further characterization of the lumbar spine. With increased sample processing time, a more streamlined approach could be taken to retrieve more samples per vertebra and iliac crest sample, improving the sample pool and further grounding the statistics. Additionally, sacrificing an iliac crest sample through failure testing would allow for a more effective and consistent preloading methodology, adapting the initial lab protocol tests to such samples. Although the load cell is suspected to have a 1% signal-to-noise ratio, running a compliance test to quantify the noise level and resolution of the load cell could improve measurement accuracy and help account for testing drift.

This study quantified the mechanical material properties of bovine lumbar spine and iliac crest, along with their associated loading directions. The interaction between anatomical tissue location and loading direction was further analyzed, revealing that the modulus was significantly higher in the lumbar spine for the D1 loading direction. The study also found that the median maximum stress was much higher for the lumbar spine compared to the iliac crest.

The lumbar spine exhibited transversely isotropic material behavior, in contrast to the isotropic-like behavior observed in the iliac crest. This difference may have contributed to the higher modulus in the lumbar spine for the D1 loading direction compared to all other testing combinations. The mechanics of the graft material impact its response, such as behavior adaptation, force distribution, and load bearing, to the physiological loads that encourage the fusion healing process during spinal fusion healing. This emphasizes the importance of analyzing how transversely isotropic material may impact bone healing when utilized as a graft for ACDF surgeries. Specifically, transversely isotropic materials should be studied to determine if graft placement relative to the anisotropic loading direction impacts the incidence of pseudoarthrosis in ACDF surgeries.

Chapter 5 - Synthesis

This master's thesis describes the process of morphologically and mechanically characterizing autograft tissue for surgeries, with the aim of finding novel autograft locations to reduce patient morbidities, operation time, and/or operation complexity through exploratory clinical and large animal models. MicroCT and SHG imaging modalities were utilized to morphologically and micro-architecturally characterize clinical autografts to increase our knowledge of potential differences in the initial healing stages following ACDF surgery that could lead to bone growth failure and pseudoarthrosis. Compression testing was used to mechanically and materially characterize physiologically similar large animal trabecular bone to improve our understanding of potential differences that could alter bone growth patterns and cause pseudoarthrosis during the healing stages following ACDF surgery.

Two autograft locations, the gold-standard iliac crest and a novel lumbar spine location, were investigated to determine if a new autograft location could mitigate short- and long-term harvest site complications associated with the gold standard in ACDF procedures. MicroCT and SHG image analysis found no significant differences between the cervical spine and iliac crest for their morphology and micro-architecture. Compression test analysis found that the lumbar vertebra is transversely isotropic, while the iliac crest is isotropic. This distinction should be considered when using these tissues, and other similar physiologically loaded tissues such as the cervical vertebra, for autograft in ACDF procedures.

Further validation of the MicroCT image analysis and SHG sample preparation and imaging should be conducted with more human tissue samples to strengthen the basis for drawing statistical conclusions. Additionally, a sacrificial sample should have been utilized to

validate the initial compression testing methodology to avoid potential complications with various preloading cycles. This will enhance the characterization of anisotropically different materials and improve our understanding of how they may impact ACDF healing outcomes.

Future Work

The immediate next steps for this project are to adjust and improve SHG imaging methodologies and finish SHG image data collection and collagen alignment analysis for all sixteen remaining samples. Additionally, leftover bovine vertebral and iliac crest tissue should be used to correlate morphological properties with directionality and mechanical properties using microCT imaging and compression testing. If more leftover bone is available, SHG samples should be prepared with identifiable directionality to draw correlations between directionality and collagen alignment, as well as to establish a baseline for SHG sample preparation alignment.

Further Characterization of Additional Tissue

A better understanding of the cervical vertebra's mechanical properties, in addition to drawing correlations between the morphological and mechanical properties of cervical vertebra, is necessary prior to further extensive clinical studies. An extensive large animal model or human cadaveric study should be designed to carry out microCT imaging, compression testing, and SHG imaging to draw additional correlations between the tissues and further characterize their properties. Within this study, gaining access to enough tissue to analyze each different vertebra (C3-C7 or L1-L5/T13-L6 in humans/cows) can help us draw further conclusions about whether local autograft tissue could lead to failure in ACDF surgeries involving different vertebra.

Cervical Spine Gold-Standard Initiative

Following further characterization of and comparison between iliac crest and cervical spine autograft tissue, it should be determined if the cervical spine is a safe and responsible alternative to the gold-standard iliac crest autograft for ACDF. If the cervical spine continues to show no significant differences in fusion rate complications, morphological properties, and mechanical properties, apart from anisotropy in the primary loading direction, it should be promoted as the gold-standard autograft for ACDF surgeries due to its potential to reduce morbidities associated with a secondary surgical site. This research should be disseminated throughout multiple conferences and journals. Following dissemination, the surgery should be taught to incoming and practicing orthopedic surgeons to begin phasing out ACDF that utilizes iliac crest as an autograft.

Additional Novel Autograft Locations for Analysis

If the cervical spine autograft were to become the new gold standard for ACDF surgeries, replacing the iliac crest autograft, it is important to determine which experimental studies and characteristics must be compared to deem it acceptable for adoption. This adoption pathway should also be applied to other surgeries that utilize autografts from secondary surgical sites, such as posterior interbody lumbar fusion (PLIF). However, if the cervical spine is found to be an unacceptable replacement for the iliac crest autograft as the gold standard for ACDF, future studies should explore surgeries that use autografts from secondary surgical sites to mitigate morbidities associated with such sites, while continuing to develop a pipeline toward adopting the autograft gold standard.

References

[1] S. Rahman and J. M. Das, "Anatomy, Head and Neck: Cervical Spine," *StatPearls*, Aug. 2023, Accessed: May 29, 2024. [Online]. Available: https://www.ncbi.nlm.nih.gov/books/NBK557516/

[2] A. M. Wu *et al.*, "Global, regional, and national burden of neck pain, 1990–2020, and projections to 2050: a systematic analysis of the Global Burden of Disease Study 2021," *Lancet Rheumatol*, vol. 6, no. 3, pp. e142–e155, Mar. 2024, doi: 10.1016/S2665-9913(23)00321-1.

[3] W. Magnus, O. Viswanath, V. K. Viswanathan, and F. B. Mesfin, "Cervical Radiculopathy," *StatPearls*, Jan. 2024, Accessed: May 29, 2024. [Online]. Available: https://www.ncbi.nlm.nih.gov/books/NBK441828/

[4] J. L. Dieleman *et al.*, "US Health Care Spending by Payer and Health Condition, 1996-2016," *JAMA*, vol. 323, no. 9, p. 863, Mar. 2020, doi: 10.1001/JAMA.2020.0734.

[5] E. L. Hurwitz *et al.*, "Treatment of Neck Pain: Noninvasive Interventions: Results of the Bone and Joint Decade 2000–2010 Task Force on Neck Pain and Its Associated Disorders," *European Spine Journal*, vol. 17, no. Suppl 1, p. 123, Apr. 2008, doi: 10.1007/S00586-008-0631-Z.

[6] N. E. Epstein, "A Review of Complication Rates for Anterior Cervical Diskectomy and Fusion (ACDF)," *Surg Neurol Int*, vol. 10, no. 100, 2019, doi: 10.25259/SNI-191-2019.

[7] A. M. T. Chau and R. J. Mobbs, "Bone graft substitutes in anterior cervical discectomy and fusion," Apr. 2009. doi: 10.1007/s00586-008-0878-4.

[8] Z. Walterscheid *et al.*, "Anterior Cervical Discectomy With Fusion Using a Local Source for Cancellous Autograft: A Biomechanical Analysis of Vertebral Body Stability in an Osteopenic Bone Model," *Geriatr Orthop Surg Rehabil*, vol. 8, no. 3, pp. 128–134, Sep. 2017, doi: 10.1177/2151458517715739.

[9] C. N. O'Neill, Z. J. Walterscheid, and J. J. Carmouche, "A Novel Local Cancellous Autograft Source for Anterior Cervical Discectomy With Fusion," *Global Spine J*, vol. 12, no. 2, pp. 190–197, Mar. 2022, doi: 10.1177/2192568220947741.

[10] S. B. Fowler, P. Anthony-Phillips, D. Mehta, and K. Liebman, "Health-related quality of life in patients undergoing anterior cervical discectomy fusion.," *J Neurosci Nurs*, vol. 37, no. 2, pp. 97–100, Apr. 2005.

[11] R. Pollock *et al.*, "Donor site morbidity following iliac crest bone harvesting for cervical fusion: a comparison between minimally invasive and open techniques," *European Spine Journal*, vol. 17, no. 6, pp. 845–852, Jun. 2008, doi: 10.1007/s00586-008-0648-3.

[12] T. T. Roberts and A. J. Rosenbaum, "Bone grafts, bone substitutes and orthobiologics: The bridge between basic science and clinical advancements in fracture healing," *Organogenesis*, vol. 8, no. 4, p. 114, Oct. 2012, doi: 10.4161/ORG.23306.

[13] M. J. Turunen, V. Prantner, J. S. Jurvelin, H. Kröger, and H. Isaksson, "Composition and microarchitecture of human trabecular bone change with age and differ between anatomical locations," *Bone*, vol. 54, no. 1, pp. 118–125, May 2013, doi: 10.1016/J.BONE.2013.01.045.

[14] J. D. Boerckel, D. E. Mason, A. M. McDermott, and E. Alsberg, “Microcomputed tomography: approaches and applications in bioengineering,” *Stem Cell Res Ther*, vol. 5, no. 6, pp. 1–12, 2014, doi: 10.1186/SCRT534.
[15] C. H. Dreyer, M. Rasmussen, R. H. Pedersen, S. Overgaard, and M. Ding, “Comparisons of Efficacy between Autograft and Allograft on Defect Repair In Vivo in Normal and Osteoporotic Rats,” *Biomed Res Int*, vol. 2020, 2020, doi: 10.1155/2020/9358989.
[16] A. Bigham-Sadegh and A. Oryan, “Basic concepts regarding fracture healing and the current options and future directions in managing bone fractures,” *Int Wound J*, vol. 12, no. 3, p. 238, Jun. 2015, doi: 10.1111/IWJ.12231.
[17] R. B. Martin and J. Ishida, “The relative effects of collagen fiber orientation, porosity, density, and mineralization on bone strength,” *J Biomech*, vol. 22, no. 5, pp. 419–426, Jan. 1989, doi: 10.1016/0021-9290(89)90202-9.
[18] X. Wang, X. Shen, K. A. Athanasiou, and C. M. Agrawal, “Correlation of collagen network integrity with the biomechanical properties of bone,” in *Proceedings of the First Joint BMES/EMBS Conference. 1999 IEEE Engineering in Medicine and Biology 21st Annual Conference and the 1999 Annual Fall Meeting of the Biomedical Engineering Society (Cat. No.99CH37015)*, IEEE, p. 499. doi: 10.1109/IEMBS.1999.802577.
[19] T. Ito and H. Kimura-Suda, “Degree of orientations of collagen fibers and bone apatite crystals in rat femora by infrared dichroism imaging,” *J Oral Biosci*, vol. 61, no. 2, pp. 115–119, Jun. 2019, doi: 10.1016/J.JOB.2019.03.004.
[20] H. Haffer *et al.*, “Bone collagen quality in lumbar fusion patients: the association between volumetric bone mineral density and advanced glycation endproducts,” *Eur Spine J*, vol. 32, no. 5, p. 1678, May 2023, doi: 10.1007/S00586-023-07589-5.
[21] A. C. Ahn and A. J. Grodzinsky, “RELEVANCE OF COLLAGEN PIEZOELECTRICITY TO ‘WOLFF’S LAW’: A CRITICAL REVIEW,” *Med Eng Phys*, vol. 31, no. 7, p. 733, Sep. 2009, doi: 10.1016/J.MEDENGPHY.2009.02.006.
[22] S. Zhao *et al.*, “Standardizing compression testing for measuring the stiffness of human bone,” *Bone Joint Res*, vol. 7, no. 8, p. 524, Aug. 2018, doi: 10.1302/2046-3758.78.BJR-2018-0025.R1.
[23] E. F. Morgan, G. U. Unnikrisnan, and A. I. Hussein, “Bone Mechanical Properties in Healthy and Diseased States,” *Annu Rev Biomed Eng*, vol. 20, p. 119, Jun. 2018, doi: 10.1146/ANNUREV-BIOENG-062117-121139.
[24] S. Bailey and D. Vashishth, “Mechanical Characterization of Bone: State of the Art in Experimental Approaches—What Types of Experiments Do People Do and How Does One Interpret the Results?,” *Curr Osteoporos Rep*, vol. 16, no. 4, p. 423, Aug. 2018, doi: 10.1007/S11914-018-0454-8.
[25] “How does the spine work?,” Feb. 2019, Accessed: Mar. 03, 2024. [Online]. Available: https://www.ncbi.nlm.nih.gov/books/NBK279468/
[26] B. Jung, A. C. Black, and B. S. Bhutta, “Anatomy, Head and Neck, Neck Movements,” *StatPearls*, Nov. 2023, Accessed: Mar. 03, 2024. [Online]. Available: https://www.ncbi.nlm.nih.gov/books/NBK557555/

[27] J. T. Kaiser, V. Reddy, M. V. Launico, and J. G. Lugo-Pico, “Anatomy, Head and Neck: Cervical Vertebrae,” *StatPearls*, Oct. 2023, Accessed: Mar. 03, 2024. [Online]. Available: https://www.ncbi.nlm.nih.gov/books/NBK539734/
[28] “Vertebral column - Wikipedia.” Accessed: Mar. 12, 2024. [Online]. Available: https://en.wikipedia.org/wiki/Vertebral_column
[29] M. Angel and C. Fabre, “Development of Elderly Posture Male and Female Finite Element Neck Models and Assessment of Tissue-Level Response Under Impact Loading,” Jan. 2021, Accessed: Mar. 12, 2024. [Online]. Available: https://uwspace.uwaterloo.ca/handle/10012/16649
[30] A. G. Patwardhan *et al.*, “Load-Carrying Capacity of the Human Cervical Spine in Compression Is Increased Under a Follower Load,” *Spine (Phila Pa 1976)*, vol. 25, no. 12, 2000, [Online]. Available: https://journals.lww.com/spinejournal/fulltext/2000/06150/load_carrying_capacity_of_the_human_cervical_spine.15.aspx
[31] S. P. Moroney, A. B. Schultz, J. A. A. Miller, and G. B. J. Andersson, “Load-displacement properties of lower cervical spine motion segments,” *J Biomech*, vol. 21, no. 9, pp. 769–779, 1988, doi: 10.1016/0021-9290(88)90285-0.
[32] S. F. Ahrens, “The Effect of Age on Compression During,” 1994, Accessed: Mar. 13, 2024. [Online]. Available: www.jospt.org
[33] D. Ezra, Y. Masharawi, K. Salame, V. Slon, D. Alperovitch-Najenson, and I. Hershkovitz, “Demographic aspects in cervical vertebral bodies’ size and shape (C3-C7): a skeletal study,” *Spine J*, vol. 17, no. 1, pp. 135–142, Jan. 2017, doi: 10.1016/J.SPINEE.2016.08.022.
[34] J. A. Waxenbaum, V. Reddy, and B. Futterman, “Anatomy, Back, Intervertebral Discs,” *StatPearls*, Dec. 2023, Accessed: Mar. 13, 2024. [Online]. Available: https://www.ncbi.nlm.nih.gov/books/NBK470583/
[35] S. S. Rajaee, H. W. Bae, L. E. A. Kanim, and R. B. Delamarter, “Spinal fusion in the United States: Analysis of trends from 1998 to 2008,” *Spine (Phila Pa 1976)*, vol. 37, no. 1, pp. 67–76, Jan. 2012, doi: 10.1097/BRS.0B013E31820CCCFB.
[36] J. Fakhoury and T. J. Dowling, “Cervical Degenerative Disc Disease,” *StatPearls*, Aug. 2023, Accessed: Mar. 03, 2024. [Online]. Available: https://www.ncbi.nlm.nih.gov/books/NBK560772/
[37] “Herniated Cervical Disc, ruptured disc, bulging disc | Cincinnati, Ohio Mayfield Brain & Spine.” Accessed: Mar. 03, 2024. [Online]. Available: https://mayfieldclinic.com/pe-hcdisc.htm#
[38] F. J. Pencle and F. B. Mesfin, “Cervical Disc Injuries,” *StatPearls*, Jul. 2023, Accessed: Mar. 03, 2024. [Online]. Available: https://www.ncbi.nlm.nih.gov/books/NBK441971/
[39] S. Sharrak and Y. Al Khalili, “Cervical Disc Herniation,” *StatPearls*, Aug. 2023, Accessed: Mar. 03, 2024. [Online]. Available: https://www.ncbi.nlm.nih.gov/books/NBK546618/
[40] N. Yoganandan, H. Choi, Y. Purushothaman, D. Jebaseelan, J. Baisden, and S. Kurpad, “Effects of different severities of disc degeneration on the range of motion of cervical spine,” *J Craniovertebr Junction Spine*, vol. 11, no. 4, p. 269, Oct. 2020, doi: 10.4103/JCVJS.JCVJS_158_20.

[41] A. He *et al.*, “Comparison between cervical disc arthroplasty and conservative treatment for patients with single level cervical radiculopathy at C5/6,” *International Journal of Surgery*, vol. 54, pp. 124–128, Jun. 2018, doi: 10.1016/J.IJSU.2018.01.033.
[42] C. Y. Liu *et al.*, “Trends in Utilization and Cost of Cervical Spine Surgery Using the National Inpatient Sample Database, 2001 to 2013,” *Spine (Phila Pa 1976)*, vol. 42, no. 15, pp. E906–E913, Aug. 2017, doi: 10.1097/BRS.0000000000001999.
[43] S. Sharrak and Y. Al Khalili, “Cervical Disc Herniation,” *StatPearls*, Aug. 2023, Accessed: Mar. 03, 2024. [Online]. Available: https://www.ncbi.nlm.nih.gov/books/NBK546618/
[44] M. W. Peelle, B. A. Rawlins, and P. Frelinghuysen, “A Novel Source of Cancellous Autograft for ACDF Surgery: The Manubrium,” *J Spinal Disord Tech*, vol. 20, no. 1, pp. 36–41, Feb. 2007, doi: 10.1097/01.bsd.0000211230.89554.5c.
[45] S. T. Yoon *et al.*, “ACDF Graft Selection by Surgeons: Survey of AOSpine Members,” *Global Spine J*, vol. 7, no. 5, p. 410, Aug. 2017, doi: 10.1177/2192568217699200.
[46] A. R. Vaccaro *et al.*, “Bone grafting alternatives in spinal surgery,” *Spine Journal*, vol. 2, no. 3, pp. 206–215, May 2002, doi: 10.1016/S1529-9430(02)00180-8.
[47] M. S. Nickoli and W. K. Hsu, “Ceramic-Based Bone Grafts as a Bone Grafts Extender for Lumbar Spine Arthrodesis: A Systematic Review,” *Global Spine J*, vol. 4, no. 3, p. 211, Aug. 2014, doi: 10.1055/S-0034-1378141.
[48] S. Berven, B. K. Tay, F. S. Kleinstueck, and D. S. Bradford, “Clinical applications of bone graft substitutes in spine surgery: consideration of mineralized and demineralized preparations and growth factor supplementation,” *European Spine Journal*, vol. 10, no. Suppl 2, p. S169, 2001, doi: 10.1007/S005860100270.
[49] E. Truumees and H. N. Herkowitz, “Alternatives to Autologous Bone Harvest in Spine Surgery,” 1999, Accessed: Mar. 07, 2024. [Online]. Available: https://www.researchgate.net/publication/242429249
[50] S. A. Malca, P. H. Roche, E. Rosset, and W. Pellet, “Cervical interbody xenograft with plate fixation: evaluation of fusion after 7 years of use in post-traumatic discoligamentous instability,” *Spine (Phila Pa 1976)*, vol. 21, no. 6, pp. 685–690, Mar. 1996, doi: 10.1097/00007632-199603150-00004.
[51] P. J. Hubbell, B. Roth, and J. E. Block, “Comparative Evaluation of Mineralized Bone Allografts for Spinal Fusion Surgery,” *J Funct Biomater*, vol. 14, no. 7, Jul. 2023, doi: 10.3390/JFB14070384.
[52] S. A. Zadegan, A. Abedi, S. B. Jazayeri, A. R. Vaccaro, and V. Rahimi-Movaghar, “Demineralized bone matrix in anterior cervical discectomy and fusion: a systematic review,” *European Spine Journal*, vol. 26, no. 4, pp. 958–974, Apr. 2017, doi: 10.1007/S00586-016-4858-9/TABLES/2.
[53] H. M. Heneghan and J. P. McCabe, “Use of autologous bone graft in anterior cervical decompression: morbidity & quality of life analysis,” *BMC Musculoskelet Disord*, vol. 10, no. 1, p. 158, 2009, doi: 10.1186/1471-2474-10-158.
[54] K. J. Song and B. Y. Choi, “Current Concepts of Anterior Cervical Discectomy and Fusion: A Review of Literature,” *Asian Spine J*, vol. 8, no. 4, p. 531, 2014, doi: 10.4184/ASJ.2014.8.4.531.

[55] C. Myeroff and M. Archdeacon, “Autogenous bone graft: Donor sites and techniques,” *Journal of Bone and Joint Surgery*, vol. 93, no. 23, pp. 2227–2236, Dec. 2011, doi: 10.2106/JBJS.J.01513.
[56] N. E. Epstein, “Iliac crest autograft versus alternative constructs for anterior cervical spine surgery: Pros, cons, and costs,” *Surg Neurol Int*, vol. 3, no. 4, p. 143, 2012, doi: 10.4103/2152-7806.98575.
[57] A. Hosameldin, M. Mohammed Abdel-latif, and A. Abdel latif Osman, “Anterior cervical discectomy and fusion using interbody cage packed with autologous clavicle bone Graft: Novel technique,” vol. 29, p. 101570, 2022, doi: 10.1016/j.inat.2022.101570.
[58] J. S. Silber *et al.*, “Donor site morbidity after anterior iliac crest bone harvest for single-level anterior cervical discectomy and fusion,” *Spine (Phila Pa 1976)*, vol. 28, no. 2, pp. 134–139, Jan. 2003, doi: 10.1097/00007632-200301150-00008.
[59] Z. J. Li, Y. Wang, G. J. Xu, and P. Tian, “Is PEEK cage better than titanium cage in anterior cervical discectomy and fusion surgery? A meta-analysis,” *BMC Musculoskelet Disord*, vol. 17, no. 1, Sep. 2016, doi: 10.1186/S12891-016-1234-1.
[60] M. Cabraja, S. Oezdemir, D. Koeppen, and S. Kroppenstedt, “Anterior cervical discectomy and fusion: Comparison of titanium and polyetheretherketone cages,” *BMC Musculoskelet Disord*, vol. 13, no. 1, pp. 1–9, Sep. 2012, doi: 10.1186/1471-2474-13-172/TABLES/5.
[61] D. C. Tapscott and C. Wottowa, “Orthopedic Implant Materials,” *StatPearls*, Jul. 2023, Accessed: Mar. 10, 2024. [Online]. Available: https://www.ncbi.nlm.nih.gov/books/NBK560505/
[62] J. Lemcke, F. Al-Zain, U. Meier, and O. Suess, “Polyetheretherketone (PEEK) Spacers for Anterior Cervical Fusion: A Retrospective Comparative Effectiveness Clinical Trial,” *Open Orthop J*, vol. 5, no. 1, p. 348, Nov. 2011, doi: 10.2174/1874325001105010348.
[63] J. L. Goldberg *et al.*, “Titanium versus polyetheretherketone versus structural allograft in anterior cervical discectomy and fusion: A systematic review,” *Brain and Spine*, vol. 2, p. 100923, Jan. 2022, doi: 10.1016/J.BAS.2022.100923.
[64] “PEEK vs Titanium: How Do They Compare? - Genesis Medical Plastics.” Accessed: Mar. 10, 2024. [Online]. Available: https://www.genesismedicalplastics.com/markets-and-applications/peek-vs-titanium-which-best-medical-applications/
[65] S. T. Kujala, H. Song, R. A. Curto, and C. C. Edwards, “Treatment of cervical non-union with cervical disc replacement: A case series,” *Int J Surg Case Rep*, vol. 93, p. 106922, Apr. 2022, doi: 10.1016/J.IJSCR.2022.106922.
[66] J. D. Thomas and J. L. Kehoe, “Bone Nonunion,” *StatPearls*, Mar. 2023, Accessed: Mar. 11, 2024. [Online]. Available: https://www.ncbi.nlm.nih.gov/books/NBK554385/
[67] K. Kusel and A. Rezaee, “Fracture non-union,” *Radiopaedia.org*, Nov. 2018, doi: 10.53347/RID-64587.
[68] J. M. Larsen and D. A. Capen, “Pseudarthrosis of the Lumbar Spine,” *J Am Acad Orthop Surg*, vol. 5, no. 3, pp. 153–162, May 1997, doi: 10.5435/00124635-199705000-00004.

[69] E. Benzel, L. Gilbertson, and R. Mericle, “Enhancing spinal fusion,” in *Clinical neurosurgery*, vol. 55, 2008, pp. 63–71. Accessed: Mar. 11, 2024. [Online]. Available: https://www.researchgate.net/publication/24143338_Enhancing_spinal_fusion?_tp=eyJjb250ZXh0Ijp7ImZpcnN0UGFnZSI6Il9kaXJlY3QiLCJwYWdlIjoiX2RpcmVjdCJ9fQ#pf2

[70] F. Schulze, A. Lang, J. Schoon, G. I. Wassilew, and J. Reichert, “Scaffold Guided Bone Regeneration for the Treatment of Large Segmental Defects in Long Bones,” *Biomedicines*, vol. 11, no. 2, Feb. 2023, doi: 10.3390/BIOMEDICINES11020325.

[71] A. Oryan, S. Alidadi, A. Moshiri, and N. Maffulli, “Bone regenerative medicine: classic options, novel strategies, and future directions,” *J Orthop Surg Res*, vol. 9, no. 1, p. 18, Mar. 2014, doi: 10.1186/1749-799X-9-18.

[72] O. of D. E. United States Food and Drug Administration (USFDA), “Guidance Document for Industry and CDRH Staff for the Preparation of Investigational Device Exemptions and Premarket Approval Application for Bone Growth Stimulator Devices,” 1988.

[73] T. Albrektsson and C. Johansson, “Osteoinduction, osteoconduction and osseointegration,” *Eur Spine J*, vol. 10 Suppl 2, no. Suppl 2, pp. S96–S101, 2001, doi: 10.1007/S005860100282.

[74] S. P. Bruder, D. J. Fink, and A. I. Caplan, “Mesenchymal stem cells in bone development, bone repair, and skeletal regenaration therapy,” *J Cell Biochem*, vol. 56, no. 3, pp. 283–294, 1994, doi: 10.1002/JCB.240560303.

[75] A. Nahian and D. D. Davis, “Histology, Osteoprogenitor Cells,” *StatPearls*, Dec. 2022, Accessed: Mar. 17, 2024. [Online]. Available: https://www.ncbi.nlm.nih.gov/books/NBK559160/

[76] A. J. Burghardt, R. Krug, and S. Majumdar, “High-resolution imaging techniques for bone quality assessment,” *Vitamin D: Two-Volume Set*, vol. 1–2, pp. 891–925, Jun. 2011, doi: 10.1016/B978-0-12-381978-9.10050-2.

[77] R. T. Lubis, A. Azhari, and F. Pramanik, “Analysis of Bone Density and Bone Morphometry by Periapical Radiographs in Dental Implant Osseointegration Process,” *Int J Dent*, vol. 2023, 2023, doi: 10.1155/2023/4763961.

[78] R. J. van ’t Hof and E. Dall’Ara, “Analysis of bone architecture in rodents using micro-computed tomography,” *Methods in Molecular Biology*, vol. 1914, pp. 507–531, 2019, doi: 10.1007/978-1-4939-8997-3_28/FIGURES/13.

[79] M. L. Bouxsein, S. K. Boyd, B. A. Christiansen, R. E. Guldberg, K. J. Jepsen, and R. Müller, “Guidelines for assessment of bone microstructure in rodents using micro–computed tomography,” *Journal of Bone and Mineral Research*, vol. 25, no. 7, pp. 1468–1486, Jul. 2010, doi: 10.1002/JBMR.141.

[80] P. Hernandez-Cerdan *et al.*, “Methods for quantitative characterization of bone injury from computed-tomography images,” *Proc SPIE Int Soc Opt Eng*, vol. 10953, p. 40, Mar. 2019, doi: 10.1117/12.2513007.

[81] A. Poilliot, M. H. P. Gay-Dujak, and M. Müller-Gerbl, “The quantification of 3D-trabecular architecture of the fourth cervical vertebra using CT osteoabsorptiometry and micro-CT,” *J Orthop Surg Res*, vol. 18, no. 1, p. 297, Dec. 2023, doi: 10.1186/S13018-023-03760-2.

[82] I. H. Parkinson and N. L. Fazzalari, “Interrelationships Between Structural Parameters of Cancellous Bone Reveal Accelerated Structural Change at Low Bone Volume,” *Journal of Bone and Mineral Research*, vol. 18, no. 12, pp. 2200–2205, Dec. 2003, doi: 10.1359/JBMR.2003.18.12.2200.

[83] L. A. Feldkamp, S. A. Goldstein, M. A. Parfitt, G. Jesion, and M. Kleerekoper, “The direct examination of three-dimensional bone architecture in vitro by computed tomography,” *Journal of Bone and Mineral Research*, vol. 4, no. 1, pp. 3–11, Feb. 1989, doi: 10.1002/jbmr.5650040103.

[84] K. Keklikoglou *et al.*, “Micro-CT for Biological and Biomedical Studies: A Comparison of Imaging Techniques,” *J Imaging*, vol. 7, no. 9, Sep. 2021, doi: 10.3390/JIMAGING7090172.

[85] N. Chartain, “Designing Scaffolds for Directed Cell Response in Tissue Engineering Scaffolds Fabricated by Vat Photopolymerization,” 2019.

[86] C. Ghayor and F. E. Weber, “Osteoconductive Microarchitecture of Bone Substitutes for Bone Regeneration Revisited,” *Front Physiol*, vol. 9, no. JUL, Jul. 2018, doi: 10.3389/FPHYS.2018.00960.

[87] A. C. Y. Loenen *et al.*, “Early bone ingrowth and segmental stability of a trussed titanium cage versus a polyether ether ketone cage in an ovine lumbar interbody fusion model,” *Spine Journal*, vol. 22, no. 1, pp. 174–182, Jan. 2022, doi: 10.1016/J.SPINEE.2021.07.011.

[88] J. J. Kazama, R. Koda, S. Yamamoto, I. Narita, F. Gejyo, and A. Tokumoto, “Cancellous Bone Volume Is an Indicator for Trabecular Bone Connectivity in Dialysis Patients,” *Clin J Am Soc Nephrol*, vol. 5, no. 2, p. 292, 2010, doi: 10.2215/CJN.04150609.

[89] R. Oftadeh, M. Perez-Viloria, J. C. Villa-Camacho, A. Vaziri, and A. Nazarian, “Biomechanics and Mechanobiology of Trabecular Bone: A Review,” *J Biomech Eng*, vol. 137, no. 1, p. 0108021, Jan. 2015, doi: 10.1115/1.4029176.

[90] O. of the S. G. (US), “The Basics of Bone in Health and Disease,” 2004, Accessed: Mar. 24, 2024. [Online]. Available: https://www.ncbi.nlm.nih.gov/books/NBK45504/

[91] C. Chen *et al.*, “Quantitative imaging of peripheral trabecular bone microarchitecture using MDCT,” *Med Phys*, vol. 45, no. 1, p. 236, Jan. 2018, doi: 10.1002/MP.12632.

[92] M. V. Parisien, D. McMahon, N. Pushparaj, and D. W. Dempster, “Trabecular architecture in iliac crest bone biopsies: Infra-individual variability in structural parameters and changes with age,” *Bone*, vol. 9, no. 5, pp. 289–295, Jan. 1988, doi: 10.1016/8756-3282(88)90012-9.

[93] X. S. Liu, W.-J. Tseng, and M. Orthopaedic, “MicroCT 101: How to get most out of your scans PCMD MicroCT Imaging Core Learning Lunch Series,” 2019, doi: 10.1002/jbmr.141.

[94] T. Hildebrand, A. Laib, R. Müller, J. Dequeker, and P. Rüegsegger, “Direct Three-Dimensional Morphometric Analysis of Human Cancellous Bone: Microstructural Data from Spine, Femur, Iliac Crest, and Calcaneus,” *Journal of Bone and Mineral Research*, vol. 14, no. 7, pp. 1167–1174, Jul. 1999, doi: 10.1359/JBMR.1999.14.7.1167.

[95] R. W. E. Mellish, N. J. Garrahan, and J. E. Compston, “Age-related changes in trabecular width and spacing in human iliac crest biopsies,” *Bone Miner*, vol. 6, no. 3, pp. 331–338, 1989, doi: 10.1016/0169-6009(89)90038-X.
[96] “What is Micro-CT? An Introduction | Micro Photonics.” Accessed: Mar. 27, 2024. [Online]. Available: https://www.microphotonics.com/what-is-micro-ct-an-introduction/#
[97] A. K. Jha, N. C. Purandare, S. Shah, A. Agrawal, A. D. Puranik, and V. Rangarajan, “Identification of a unique cause of ring artifact seen in computed tomography trans-axial images,” *Indian J Nucl Med*, vol. 28, no. 4, p. 232, Oct. 2013, doi: 10.4103/0972-3919.121970.
[98] J. A. Meganck, K. M. Kozloff, M. M. Thornton, S. M. Broski, and S. A. Goldstein, “Beam Hardening Artifacts in Micro-Computed Tomography Scanning can be Reduced by X-ray Beam Filtration and the Resulting Images can be used to Accurately Measure BMD,” *Bone*, vol. 45, no. 6, p. 1104, Dec. 2009, doi: 10.1016/J.BONE.2009.07.078.
[99] S. C. Cowin, Ed., *Bone Mechanics Handbook*. CRC Press, 2001. doi: 10.1201/b14263.
[100] X. Lin, S. Patil, Y. G. Gao, and A. Qian, “The Bone Extracellular Matrix in Bone Formation and Regeneration,” *Front Pharmacol*, vol. 11, p. 521497, May 2020, doi: 10.3389/FPHAR.2020.00757/BIBTEX.
[101] S. Viguet-Carrin, P. Garnero, and P. D. Delmas, “The role of collagen in bone strength,” *Osteoporosis International*, vol. 17, no. 3, pp. 319–336, Mar. 2006, doi: 10.1007/s00198-005-2035-9.
[102] M. Tzaphlidou, “Bone Architecture: Collagen Structure and Calcium/Phosphorus Maps,” *J Biol Phys*, vol. 34, no. 1–2, p. 39, Apr. 2008, doi: 10.1007/S10867-008-9115-Y.
[103] X. Chen, O. Nadiarynkh, S. Plotnikov, and P. J. Campagnola, “Second harmonic generation microscopy for quantitative analysis of collagen fibrillar structure,” *Nat Protoc*, vol. 7, no. 4, pp. 654–669, Apr. 2012, doi: 10.1038/nprot.2012.009.
[104] H. Hino, J. Kuroda, and S. Kondo, “‘In Vivo Imaging of Bone Collagen Dynamics in zebrafish,’” *bioRxiv*, p. 2023.11.06.563068, Nov. 2023, doi: 10.1101/2023.11.06.563068.
[105] E. G. Pendleton, K. F. Tehrani, R. P. Barrow, and L. J. Mortensen, “Second harmonic generation characterization of collagen in whole bone,” *Biomed Opt Express*, vol. 11, no. 8, p. 4379, Aug. 2020, doi: 10.1364/BOE.391866.
[106] M. M. Kabir, V. V. G. K. Inavalli, T.-Y. Lau, and Jr. Kimani C. Toussaint, “Application of quantitative second-harmonic generation microscopy to dynamic conditions,” *Biomed Opt Express*, vol. 4, no. 11, p. 2546, Nov. 2013, doi: 10.1364/BOE.4.002546.
[107] G. Cox, E. Kable, A. Jones, I. Fraser, F. Manconi, and M. D. Gorrell, “3-Dimensional imaging of collagen using second harmonic generation,” *J Struct Biol*, vol. 141, no. 1, pp. 53–62, Jan. 2003, doi: 10.1016/S1047-8477(02)00576-2.
[108] H. Lee *et al.*, “OCIS codes: (170.3880) Medical and biological imaging; (180.4315) Nonlinear microscopy; (190.2620) Harmonic generation and mixing,” 2013, doi: 10.1364/BOE.4.000909.

[109] Y. Liu, A. Keikhosravi, G. S. Mehta, C. R. Drifka, and K. W. Eliceiri, “Methods for Quantifying Fibrillar Collagen Alignment,” *Methods Mol Biol*, vol. 1627, p. 429, 2017, doi: 10.1007/978-1-4939-7113-8_28.
[110] A. Aghigh, S. Bancelin, M. Rivard, M. Pinsard, H. Ibrahim, and F. Légaré, “Second harmonic generation microscopy: a powerful tool for bio-imaging,” *Biophys Rev*, vol. 15, no. 1, p. 43, Feb. 2023, doi: 10.1007/S12551-022-01041-6.
[111] P. Campagnola, “Second Harmonic Generation Imaging Microscopy: Applications to Diseases Diagnostics,” *Anal Chem*, vol. 83, no. 9, p. 3224, May 2011, doi: 10.1021/AC1032325.
[112] C. Y. Park, J. K. Lee, and R. S. Chuck, “Second Harmonic Generation Imaging Analysis of Collagen Arrangement in Human Cornea,” *Invest Ophthalmol Vis Sci*, vol. 56, no. 9, pp. 5622–5629, Aug. 2015, doi: 10.1167/IOVS.15-17129.
[113] W. P. Hansen and S. Fine, “Optical Second Harmonic Generation in Biological Systems,” *Applied Optics, Vol. 10, Issue 10, pp. 2350-2353*, vol. 10, no. 10, pp. 2350–2353, Oct. 1971, doi: 10.1364/AO.10.002350.
[114] I. Freund and M. Deutsch, “Second-harmonic microscopy of biological tissue,” *Optics Letters, Vol. 11, Issue 2, pp. 94-96*, vol. 11, no. 2, pp. 94–96, Feb. 1986, doi: 10.1364/OL.11.000094.
[115] A. C. Suarez, “Second Harmonic Generation Figure,” *Internal Virginia Tech report. Unpublished.*, 2024.
[116] T. L. Kivell, “A review of trabecular bone functional adaptation: what have we learned from trabecular analyses in extant hominoids and what can we apply to fossils?,” *J Anat*, vol. 228, no. 4, p. 569, Apr. 2016, doi: 10.1111/JOA.12446.
[117] T. M. Keaveny, E. F. Wachtel, C. M. Ford, and W. C. Hayes, “Differences between the tensile and compressive strengths of bovine tibial trabecular bone depend on modulus,” *J Biomech*, vol. 27, no. 9, pp. 1137–1146, Sep. 1994, doi: 10.1016/0021-9290(94)90054-X.
[118] L. Røhl, E. Larsen, F. Linde, A. Odgaard, and J. Jørgensen, “Tensile and compressive properties of cancellous bone,” *J Biomech*, vol. 24, no. 12, pp. 1143–1149, Jan. 1991, doi: 10.1016/0021-9290(91)90006-9.
[119] L. Røhl, E. Larsen, F. Linde, A. Odgaard, and J. Jørgensen, “Tensile and compressive properties of cancellous bone,” *J Biomech*, vol. 24, no. 12, pp. 1143–1149, Jan. 1991, doi: 10.1016/0021-9290(91)90006-9.
[120] H. H. Bayraktar, E. F. Morgan, G. L. Niebur, G. E. Morris, E. K. Wong, and T. M. Keaveny, “Comparison of the elastic and yield properties of human femoral trabecular and cortical bone tissue,” *J Biomech*, vol. 37, no. 1, pp. 27–35, Jan. 2004, doi: 10.1016/S0021-9290(03)00257-4.
[121] F. Linde, C. B. Gothgen, I. Hvid, and B. Pongsoipetch, “Mechanical properties of trabecular bone by a non-destructive compression testing approach,” *Eng Med*, vol. 17, no. 1, pp. 23–29, 1988, doi: 10.1243/EMED_JOUR_1988_017_008_02.
[122] N. H. Hart, S. Nimphius, T. Rantalainen, A. Ireland, A. Siafarikas, and R. U. Newton, “Mechanical basis of bone strength: influence of bone material, bone structure and muscle action,” *J Musculoskelet Neuronal Interact*, vol. 17, no. 3, p. 114, Sep. 2017, Accessed: May 22, 2024. [Online]. Available: /pmc/articles/PMC5601257/

[123] R. Belda, M. Palomar, J. L. Peris-Serra, A. Vercher-Martínez, and E. Giner, "Compression failure characterization of cancellous bone combining experimental testing, digital image correlation and finite element modeling," *Int J Mech Sci*, vol. 165, p. 105213, Jan. 2020, doi: 10.1016/J.IJMECSCI.2019.105213.
[124] L. Mosekilde and L. Mosekilde, "Normal vertebral body size and compressive strength: Relations to age and to vertebral and iliac trabecular bone compressive strength," *Bone*, vol. 7, no. 3, pp. 207–212, Jan. 1986, doi: 10.1016/8756-3282(86)90019-0.
[125] L. H. Yahia, G. Drouin, and P. Duval, "A methodology for mechanical measurements of technical constants of trabecular bone," *Eng Med*, vol. 17, no. 4, pp. 169–173, Oct. 1988, doi: 10.1243/EMED_JOUR_1988_017_044_02.
[126] T. M. Keaveny, T. P. Pinilla, R. P. Crawford, D. L. Kopperdahl, and A. Lou, "Systematic and random errors in compression testing of trabecular bone," *Journal of Orthopaedic Research*, vol. 15, no. 1, pp. 101–110, 1997, doi: 10.1002/JOR.1100150115.
[127] C. Öhman-Mägi, O. Holub, D. Wu, R. M. Hall, and C. Persson, "Density and mechanical properties of vertebral trabecular bone—A review," *JOR Spine*, vol. 4, no. 4, Dec. 2021, doi: 10.1002/JSP2.1176.
[128] T. S. Keller, "Predicting the compressive mechanical behavior of bone," *J Biomech*, vol. 27, no. 9, pp. 1159–1168, Sep. 1994, doi: 10.1016/0021-9290(94)90056-6.
[129] J. Lambert, J. M. Lamothe, R. F. Zernicke, R. N. Auer, and R. A. Reimer, "Dietary restriction does not adversely affect bone geometry and mechanics in rapidly growing male wistar rats," *Pediatr Res*, vol. 57, no. 2, pp. 227–231, Feb. 2005, doi: 10.1203/01.PDR.0000148715.61869.4E.
[130] V. P. W. Shim, L. M. Yang, J. F. Liu, and V. S. Lee, "Characterisation of the dynamic compressive mechanical properties of cancellous bone from the human cervical spine," *Int J Impact Eng*, vol. 32, no. 1–4, pp. 525–540, Dec. 2005, doi: 10.1016/J.IJIMPENG.2005.03.006.
[131] J. F. Liu, V. P. W. Shim, and P. V. S. Lee, "Quasi-static compressive and tensile tests on cancellous bone in human cervical spine," *Conference Proceedings of the Society for Experimental Mechanics Series*, vol. 5, pp. 109–118, 2013, doi: 10.1007/978-1-4614-4427-5_16/TABLES/1.
[132] S. A. Goldstein, "The mechanical properties of trabecular bone: Dependence on anatomic location and function," *J Biomech*, vol. 20, no. 11–12, pp. 1055–1061, Jan. 1987, doi: 10.1016/0021-9290(87)90023-6.
[133] E. Cendre *et al.*, "High-resolution computed tomography for architectural characterization of human lumbar cancellous bone: relationships with histomorphometry and biomechanics," *Osteoporos Int*, vol. 10, no. 5, pp. 353–360, 1999, doi: 10.1007/S001980050240.
[134] D. Hans *et al.*, "Ultrasound velocity of trabecular cubes reflects mainly bone density and elasticity," *Calcif Tissue Int*, vol. 64, no. 1, pp. 18–23, 1999, doi: 10.1007/S002239900572.
[135] S. Struhl, S. A. Goldstein, D. L. Dickie, M. J. Flynn, and L. S. Matthews, "The distribution of mechanical properties of trabecular bone within vertebral bodies and

iliac crest: correlation with computed tomography density.," *Transactions of the Orthopedic Research Society*, p. 262, 1987.
[136] C. Öhman-Mägi, O. Holub, D. Wu, R. M. Hall, and C. Persson, "Density and mechanical properties of vertebral trabecular bone—A review," *JOR Spine*, vol. 4, no. 4, Dec. 2021, doi: 10.1002/JSP2.1176.
[137] L. Mosekilde, A. Viidik, and L. Mosekilde, "Correlation between the compressive strength of iliac and vertebral trabecular bone in normal individuals," *Bone*, vol. 6, no. 5, pp. 291–295, 1985, doi: 10.1016/8756-3282(85)90317-5.
[138] M. A. K. Liebschner, "Biomechanical considerations of animal models used in tissue engineering of bone," *Biomaterials*, vol. 25, no. 9, pp. 1697–1714, Apr. 2004, doi: 10.1016/S0142-9612(03)00515-5.
[139] A. Akbay, G. Bozkurt, O. Ilgaz, S. Palaoglu, N. Akalan, and E. C. Benzel, "A demineralized calf vertebra model as an alternative to classic osteoporotic vertebra models for pedicle screw pullout studies," *Eur Spine J*, vol. 17, no. 3, pp. 468–473, Mar. 2008, doi: 10.1007/S00586-007-0545-1.
[140] L. C. da Costa Filho, R. Taga, and E. M. Taga, "Rabbit bone marrow response to bovine osteoinductive proteins and anorganic bovine bone.," *Int J Oral Maxillofac Implants*, vol. 16, no. 6, pp. 799–808, 2001.
[141] G. K. Jeong, H. S. Sandhu, and J. Farmer, "Bone Morphogenic Proteins: Applications in Spinal Surgery," *HSS Journal*, vol. 1, no. 1, p. 110, Sep. 2005, doi: 10.1007/S11420-005-0120-4.
[142] P. C. Cotterill, J. P. Kostuik, G. D'Angelo, G. R. Fernie, and B. E. Maki, "An anatomical comparison of the human and bovine thoracolumbar spine," *Journal of Orthopaedic Research*, vol. 4, no. 3, pp. 298–303, 1986, doi: 10.1002/JOR.1100040306.
[143] I. Kolkman, G. Hoflack, S. Aerts, R. D. Murray, G. Opsomer, and D. Lips, "Evaluation of the Rice pelvimeter for measuring pelvic area in double muscled Belgian Blue cows," *Livest Sci*, vol. 121, no. 2–3, pp. 259–266, Apr. 2009, doi: 10.1016/J.LIVSCI.2008.06.022.
[144] B. Zhang, Y. Du, J. Sun, J. Shen, T. Li, and Y. Zhou, "Change of Pelvic Sagittal Tilt after Total Hip Arthroplasty in Patients with Bilateral Crowe Type <scp>IV</scp> Developmental Dysplasia of the Hip," *Orthop Surg*, vol. 14, no. 5, pp. 919–926, May 2022, doi: 10.1111/os.13275.
[145] C. F. Schroeder, S. Z. Schmidtke, and M. W. Bidez, "Measuring the Human Pelvis: A Comparison of Direct and Radiographic Techniques Using a Modern United States-Based Sample," *J Phys Anthropol*, vol. 103, pp. 471–479, 1997, doi: 10.1002/(SICI)1096-8644(199708)103:4.
[146] B. J. Adams and P. J. Crabtree, "Human vs Cow," *Comparative Skeletal Anatomy*, pp. 29–44, 2008, doi: 10.1007/978-1-59745-132-1_3.
[147] M. L. Hillier and L. S. Bell, "Differentiating Human Bone from Animal Bone: A Review of Histological Methods," *J Forensic Sci*, vol. 52, no. 2, pp. 249–263, Mar. 2007, doi: 10.1111/J.1556-4029.2006.00368.X.
[148] D. Brits, M. Steyn, and E. N. L'Abbé, "A histomorphological analysis of human and non-human femora," *Int J Legal Med*, vol. 128, no. 2, pp. 369–377, 2014, doi: 10.1007/S00414-013-0854-3.

[149] A. Fedorov *et al.*, “3D Slicer as an image computing platform for the Quantitative Imaging Network,” *Magn Reson Imaging*, vol. 30, no. 9, pp. 1323–1341, Nov. 2012, doi: 10.1016/j.mri.2012.05.001.
[150] J. Schindelin *et al.*, “Fiji: An open-source platform for biological-image analysis,” *Nat Methods*, vol. 9, no. 7, pp. 676–682, Jul. 2012, doi: 10.1038/NMETH.2019.
[151] M. Maga, A. Summers, and D. Boyer, “SlicerMorph.” Accessed: May 29, 2024. [Online]. Available: https://slicermorph.github.io
[152] N. Otsu, “A Threshold Selection Method from Gray-Level Histograms,” *IEEE Trans Syst Man Cybern*, vol. 9, no. 1, pp. 62–66, Jan. 1979, doi: 10.1109/TSMC.1979.4310076.
[153] J.-B. Vimort, “BoneTextureExtension.” Accessed: May 29, 2024. [Online]. Available: https://www.slicer.org/wiki/Documentation/Nightly/Modules/ComputeBMFeatures
[154] R. Domander, A. A. Felder, and M. Doube, “BoneJ2 - refactoring established research software,” *Wellcome Open Res*, vol. 6, p. 37, Apr. 2021, doi: 10.12688/wellcomeopenres.16619.2.
[155] “Sigma Aldrich Product Information: 45359 Epoxy-Embedding Kit.”
[156] J. A. McGuire *et al.*, “Tear propagation in vaginal tissue under inflation,” *Acta Biomater*, vol. 127, pp. 193–204, Jun. 2021, doi: 10.1016/j.actbio.2021.03.065.
[157] C. J. Collins *et al.*, “The impact of age, mineralization, and collagen orientation on the mechanics of individual osteons from human femurs,” *Materialia (Oxf)*, vol. 9, p. 100573, Mar. 2020, doi: 10.1016/j.mtla.2019.100573.
[158] J. M. Patsch *et al.*, “Trabecular bone microstructure and local gene expression in iliac crest biopsies of men with idiopathic osteoporosis,” *Journal of Bone and Mineral Research*, vol. 26, no. 7, pp. 1584–1592, Jul. 2011, doi: 10.1002/jbmr.344.
[159] S. Weiner, T. Arad, I. Sabanay, and W. Traub, “Rotated plywood structure of primary lamellar bone in the rat: Orientations of the collagen fibril arrays,” *Bone*, vol. 20, no. 6, pp. 509–514, Jun. 1997, doi: 10.1016/S8756-3282(97)00053-7.
[160] M. M. Giraud-Guille, “Twisted plywood architecture of collagen fibrils in human compact bone osteons,” *Calcif Tissue Int*, vol. 42, no. 3, pp. 167–180, May 1988, doi: 10.1007/BF02556330/METRICS.
[161] Q. Ma, Z. Miri, H. J. Haugen, A. Moghanian, and D. Loca, “Significance of mechanical loading in bone fracture healing, bone regeneration, and vascularization,” *J Tissue Eng*, vol. 14, Jan. 2023, doi: 10.1177/20417314231172573.
[162] L. Song, “Effects of Exercise or Mechanical Stimulation on Bone Development and Bone Repair,” *Stem Cells Int*, vol. 2022, 2022, doi: 10.1155/2022/5372229.
[163] G. P. Panfilov *et al.*, “THE ELASTOPLASTIC PROPERTIES OF THE TRABECULAR BONE TISSUE,” *Frontier Materials & Technologies*, vol. 0, no. 4, pp. 45–51, Dec. 2019, doi: 10.18323/2073-5073-2019-4-45-51.
[164] S. S. Lee, X. Du, I. Kim, and S. J. Ferguson, “Scaffolds for bone-tissue engineering,” *Matter*, vol. 5, no. 9, pp. 2722–2759, Sep. 2022, doi: 10.1016/J.MATT.2022.06.003.
[165] W. J. Whitehouse, “The quantitative morphology of anisotropic trabecular bone,” *J Microsc*, vol. 101, no. 2, pp. 153–168, Jul. 1974, doi: 10.1111/J.1365-2818.1974.TB03878.X.

[166] J. L. Williams and J. L. Lewis, “Properties and an Anisotropic Model of Cancellous Bone From the Proximal Tibial Epiphysis,” *J Biomech Eng*, vol. 104, no. 1, pp. 50–56, Feb. 1982, doi: 10.1115/1.3138303.
[167] S. A. Zijderveld, C. M. Ten Bruggenkate, J. P. A. Van Den Bergh, and E. A. J. M. Schulten, “Fractures of the iliac crest after split-thickness bone grafting for preprosthetic surgery: report of 3 cases and review of the literature,” *Journal of Oral and Maxillofacial Surgery*, vol. 62, no. 7, pp. 781–786, Jul. 2004, doi: 10.1016/J.JOMS.2003.12.018.
[168] “Psoas Muscle: What It Is, Where It Is & Anatomy.” Accessed: Jun. 04, 2024. [Online]. Available: https://my.clevelandclinic.org/health/body/psoas-muscle

Appendix A – Curriculum Vitae

Jackson Comer

Jacksonsc@vt.edu | (513) 375-5257 | Blacksburg, VA, 24060 | LinkedIn.com/in/jackson-comer

EDUCATION

Virginia Tech *Blacksburg, VA*
M.S. in Biomedical Engineering | Overall GPA: **3.77/4.00** *June 2024*
B.S. in Biomedical Engineering; Minor in Engineering Science and Mechanics *May 2023*

EXPERIENCE

Collins Bone Biomechanics Lab at Virginia Tech *Blacksburg, VA*
Graduate Research Assistant and Lab Manager *May 2023 – Jul 2024*
- Enhancing the success of anterior cervical discectomy and fusion (ACDF) by mechanically characterizing the properties of human cervical spine (Cs) and iliac crest (Ic) autografts; *publication in progress*
- Reducing complications from ACDF associated morbidity at the secondary graft site by characterizing osteogenic properties and comparing strain distributions within the micromechanical niche of Cs and Ic autografts

Undergraduate Research Assistant and Lab Manager *January 2022 – May 2023*
- Quantified histotripsy safety for dogs with bone cancer by comparing ablated and nonablated tissues in a comparative oncology model to prevent amputations

University of Virginia Medical Center *Charlottesville, VA*
VA-K (Kidney) Tutor Intern *May 2021 – March 2022*
- Independently researched and curated an abstract on alarm fatigue in hemodialysis centers to increase patient rest, nurse productivity, and alarm importance
- Evaluated and developed a plan to engineer solutions on the effectiveness of different products and processes in multiple ICUs, the renal and hemodialysis units, and the renal lab

LEADERSHIP EXPERIENCE

impACCt Design Challenge *Blacksburg, VA*
Virginia Tech Mentor/Delegate *Sept 2020 – Dec 2023*
- One of 4 VT students chosen to collaborate with Clemson graduate architects, Boston College psychology students, and NC State industrial design students in the inaugural impACCt ACC-wide design challenge
- Designed various projects in the design team, including: a cohesive product focused on enhancing clean public drinking access, a culturally inclusive art installation connecting the U.S. and Mexico border, a product to combat food deserts
- Mentored 5 new Virginia Tech undergraduate students in ideation and prototyping

Virginia Tech Biomedical Engineering and Mechanics Department *Blacksburg, VA*
Graduate Teaching Assistant for Introduction to Problem Solving in Biomedical Engineering *January 2024 – May 2024*
- Designed coursework and exercises to teach advanced MATLAB techniques and applications to 66 students

Undergraduate Teaching Assistant for Introduction to Biomechanics *January 2023 – May 2023*
- Increased "A" passing rates by 11.9% by teaching and hosting office hours for the 33 students in the class

Biomedical Engineering Ambassador *September 2021 – Dec 2023*

Virginia Tech Together Design Challenge *Blacksburg, VA*
Team Leader/Creator *June 2020 – August 2020*
- Led and recruited a team of 8 students that prototyped an RFID system to track COVID-19 on campus
- Collaborated with 5 organizations on a virtual platform, delegated tasks to team members, collected data on scanning technology, and presented the prototype and research to a panel of Virginia Tech judges

Cincinnati Aquatic Club, Blacksburg Aquatic Center *Cincinnati, OH, Blacksburg, VA*
Swim Coach *May 2019 – August 2020, June 2022 – July 2024*

Sigma Phi Epsilon Fraternity *Blacksburg, VA*
Vice President of Member Development *January 2021 - December 2021*

SKILLS

3D Slicer, Python, Jupyter Notebooks, MATLAB, Solidworks, JMP, Microsoft Office (Word, PowerPoint)
Familiar with: Microsoft Excel, Autodesk Inventor, Vicon Imaging System

PUBLICATIONS/ABSTRACTS

- Determination of Biomechanical Effects of Histotripsy on Osteosarcoma in a Canine Comparative Oncology Model
- Comparing the Properties of Iliac Crest and Cervical Spine Bone: A Morphological Analysis of Autograft

Appendix B – Submitted Abstracts

ORS 2024 Abstract

Morphological Comparison of Iliac Crest and Cervical Spine Bone Grafts for ACDF

Haseeb E. Goheer[1], Jackson Comer[2], Jonathan J. Carmouche[1,3], Caitlyn J. Collins[2]
[1]Virginia Tech Carilion School of Medicine, Roanoke, VA, [2]Virginia Tech, Blacksburg, VA, [3]Carilion Clinic, Roanoke, VA
cjcollins@vt.edu

Disclosures: Haseeb E. Goheer (N), Jackson Comer (N), Jonathan J. Carmouche (N), Caitlyn J. Collins (N)

INTRODUCTION: Autologous bone graft (autograft) from the iliac crest is the gold standard for anterior cervical discectomy and fusion (ACDF). However, the use of iliac crest autograft requires a second surgical incision, which can contribute to higher morbidity. A novel ACDF technique has been developed using bone autograft from adjacent cervical vertebrae, eliminating the need for a second surgical incision [1]. While this site yielded a uniform osseous fusion in a previous, prospectively collected case series, the morphology of the cervical vertebral autograft tissue remains undetermined [2]. These structural and material properties impact mechanical support and the osteogenic properties of the graft. The purpose of this study is to compare the morphology of autologous iliac crest and adjacent cervical vertebrae bone grafts obtained during an ACDF at the tissue level to identify if microstructural equivalence exists between the bone graft donor site.

METHODS: Ten consecutive patients undergoing standard of care ACDF provided informed consent prior to participation in this Ethics Committee approved study. Autograft samples from both cervical vertebrae and iliac crest were excised using a 15-guage trephine needle and a 4 mm osteotome, respectively, and subjected to micro-computed tomography (microCT) imaging (Bruker SkyScan 1172, 60 kV, 167 mA, 17µm voxel size; Fig. 1). Images were reconstructed and then post-processed in 3D Slicer to determine the bone morphological and densitometric properties of each graft. Otsu's method was utilized to isolate bone tissue from background. Bone volume fraction (BV/TV), trabecular thickness (Tb.Th), and bone surface to bone volume ratio (BS/BV) were then determined. Python was utilized to generate a convex hull mask for the total volume used in the bone morphometric calculations using 3D Slicer and BoneJ2 (Fiji). Wilcoxon signed rank tests were used to identify mean differences in bone morphometric properties between the two sites. Statistical analysis was performed using R version 4.2.2.

RESULTS SECTION: Patient demographics and morphometric data are reported in Table 1. Macroscopically, the iliac crest autografts were larger and more intact compared to the smaller, fragmented local inferior cervical vertebral bone. On average, the sample obtained from the iliac crest was 5.222 mm^3 larger than from the cervical vertebra of the same patient. The autografts from the iliac crest had trends for greater mean difference in BS/BV (3.565%, p=0.076) and lower mean difference in Tb.Th (0.05820 mm, p = 0.2754) compared to those of the cervical vertebra. However, these differences were not significant.

DISCUSSION: Bone from the cervical vertebrae and iliac crest differed in volume and concavity macroscopically; meanwhile, the morphological measures did not significantly differ between the two harvest sites in trabecular or bone surface characteristics. Limitations of the study include the limited volume of cervical spine graft material compared to the iliac crest, attributed to the lack of standardized surgical biopsy tooling for the cervical vertebra. Analysis of cadaveric cervical and iliac crest autografts, excised using the same tools, may provide greater certainty in the equivalence of the microstructure of these two autografts. Further assessment of the transcriptional profile for genes known to act in bone repair and formation should also be evaluated to assess the viability of the cervical vertebrae as an alternative autograft. Given the current findings and positive clinical outcomes in pilot studies, autograft harvested from the inferior cervical vertebral body represents a potential alternative source of autologous bone graft for ACDF.

SIGNIFICANCE/CLINICAL RELEVANCE: This study provides the first direct structural comparison between cervical vertebral bone and iliac crest based on microCT analysis from same donor bone samples. The clinical relevance lies in demonstration of how these two harvest sites have similar structural features, thus potentially eliminating the need for a second surgical incision in 1-2 level ACDF procedures.

REFERENCES: [1] Walterscheid et al., *Geriatric Orthopaedic Surgery & Rehabilitation*, 2017. [2] O'Neill et al., *Global Spine Journal*, 2020.

ACKNOWLEDGEMENTS: This work has been supported by a Carilion Clinic Research Acceleration Program (RAP) 2023 grant and the National Center for Advancing Translational Science of the National Institutes of Health Award UL1TR003015/ KL2TR003016.

IMAGES AND TABLES

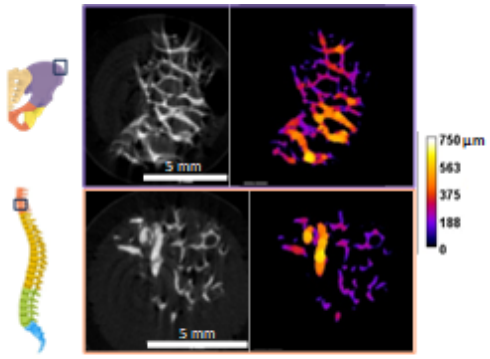

Figure 1. MicroCT images and Tb.Th (µm) heat maps from cervical spine (top) and iliac crest (bottom) from a single donor.

Table 1. The patient demographics and bone morphometric calculations for the ACDF surgery and the iliac crest and cervical spine grafts.

Demographics			
Age (yrs)	*Sex (M/F)*	*BMI*	*Smoke (Y:N)*
53.6 [38-62]	3/7	28.7	4:6

Morphometrics				
Graft	*BV/TV (%)*	*Tb.Th (mm)*	*BS/BV (%)*	*Volume (mm^3)*
Hip	21.5±3.63	0.276±0.083	21.56±4.69	29.97±31.78
Spine	25.3±6.45	0.334±0.071	18.00±4.08	24.75±10.00

VOS 2024 Abstract

Title: A Structural Comparison Between Iliac Crest and Cervical Spine Autograft Harvest: Implications for Anterior Cervical Discectomy and Fusion

Authors:
Haseeb E. Goheer, B.S. [1]
Jackson Comer, B.S.[2]
Caitlyn J. Collins, Ph.D. [2]
Jonathan J. Carmouche, M.D., M.B.A.[1,3]

[1]Virginia Tech Carilion School of Medicine, 2 Riverside Circle, Roanoke, Virginia, 24016, United States of America
[2]Department of Biomedical Engineering and Mechanics, Virginia Tech, Blacksburg, Virginia, 24060, United States of America
[3]Department of Orthopaedic Surgery, Institute for Orthopaedics & Neurosciences, Carilion Clinic, 2331 Franklin Road Southwest, Roanoke, Virginia, 24014, United States of America

Introduction:
Autologous bone graft (autograft) from the iliac crest (IC) is the gold standard for anterior cervical discectomy and fusion (ACDF). However, the use of IC autograft requires a second surgical incision, which can contribute to higher morbidity. We developed a novel ACDF technique using bone autograft from adjacent cervical vertebrae, eliminating the need for a second surgical incision. While this site yielded a uniform osseous fusion in a previous prospectively collected case series, the morphological characteristics of the cervical vertebral autograft remain undetermined. These structural and material properties impact mechanical support and the osteogenic properties of the graft. The purpose of this study is to compare autologous iliac crest and adjacent cervical vertebrae bone grafts obtained during ACDF at the tissue level to identify if equivalence exists between the two graft sites.

Methods:
Ten consecutive patients undergoing standard of care ACDF, provided bone samples from both cervical vertebrae and IC. Samples underwent micro-computed tomography (microCT) imaging (Bruker SkyScan 1172, 60 kV, 167 mA, 17µm voxel size). Using 3D Slicer, an Otsu threshold was applied to all reconstructed microCT images to isolate bone tissue from background. Bone volume fraction (BV/TV), trabecular thickness (Tb.Th), trabecular separation (Tb.S), trabecular number (Tb.N), and bone surface to bone volume ratio (BS/BV) were then determined. Paired sample t-tests for continuous variables were used to identify mean differences in bone morphometric properties between the two sites. The study has been approved by the Carilion Clinic Institutional Review Board (IRB).

Results: Seven of the ten patients undergoing ACDF were female and three were male, with a mean age of 54 years (range: 38-62 years). Four patients had a history of smoking. Macroscopically, the IC autograft was consistently larger with more integrity compared to the smaller fragmented inferior cervical vertebral bone. The sample obtained from the IC was on average 5.222 (mm^3) larger than the spine autograft bone from the same patient. The IC had a trend for greater mean difference of BS/BV (3.565%, p=0.076) compared to the spine while the cervical spine had a trend for greater mean differences of Tb.Th (2.064 um, p = .0739) compared to the IC. However, these differences were not significant.

Discussion:
Bone from the cervical vertebrae and IC differ in shape and concavity macroscopically; the morphological measures did not significantly differ between the two harvest sites in trabecular and bone surface characteristics. Limitations of the study include the limited volume of cervical spine graft material compared to the IC. Cadaveric analysis of cervical and IC autografts may reveal greater differences or similarities in the bone microarchitecture. Given the current findings and positive clinical outcomes in pilot studies, the use of cervical spine autograft may be justified.

AAOS 2024 Abstract

Title: Autologous Bone Graft Obtained from the Iliac Crest and Cervical Vertebrae of the Same Patient Exhibit Similar Molecular and Structural Characteristics

Authors:
Haseeb E. Goheer, B.S.[1], Jackson Comer, B.S.[2], Sharon K. Michelhaugh, Ph.D.[3], Linsen T. Samuel, M.D., M.B.A [4], Jennifer M. Munson, Ph.D. [2, 3], Caitlyn J. Collins, Ph.D. [2], Jonathan J. Carmouche, M.D., M.B.A.[1,4]

[1]Virginia Tech Carilion School of Medicine, Roanoke, Virginia, 24016, United States of America
[2]Department of Biomedical Engineering and Mechanics, Virginia Tech, Blacksburg, Virginia, 24061, United States of America
[3]Fralin Biomedical Research Institute, Virginia Tech, Roanoke, Virginia, 24016, United States of America
[4]Department of Orthopaedic Surgery, Carilion Clinic, Roanoke, Virginia, 24014, United States of America

Introduction: Anterior cervical discectomy and fusion (ACDF) is one of the most common cervical spine procedures. Autologous bone graft (autograft) from the iliac crest (IC) is considered the historical gold standard for ACDF procedures because the tissue has osteoconductive, osteoinductive, and osteogenic properties; however, the required secondary surgical site is associated with both short- and long-term complications. To mitigate IC harvest site complications, the use of an adjacent cervical vertebral body as an alternative donor site has been previously identified. While successful fusion has been demonstrated clinically for this site in previous studies, a comparative assessment of the osteoinductive and osteoconductive properties of cervical vertebral tissue compared to the IC has not been investigated. Therefore, the purpose of this study is to compare the molecular and cellular characteristics of autograft from the IC and cervical vertebrae.

Methods: A prospective study was performed on twelve consecutive skeletally mature patients undergoing ACDF, from whom autograft material was harvested from both the inferior cervical vertebrae and iliac crest. Portions of each autograft sample were assessed using 1) quantitative reverse transcriptase-polymerase chain reaction (qRT-PCR) and 2) micro-computed tomography (micro-CT) imaging to quantify and compare the osteogenic gene expression and bone morphological properties of both tissues, respectively. For qRT-PCR, tissue from both sites was digested and RNA was extracted prior to assessment of the following genes: mitochondrial membrane ATP synthase F (1)F(0) Complex V (ATP5F1), alkaline phosphatase (ALP), Bone Morphogenetic Protein 2 (BMP-2), vascular endothelial growth factor A (VEGFA), runt-related transcription factor 2 (RUNX2), and tumor necrosis factor superfamily member 11 (TNFSF11). The expression level of each target gene was calculated relative to that of ATP5F1 (housekeeping gene) in each sample. For the micro-CT analysis, imaging was performed using a Bruker SkyScan 1172 (60 kV, 167 mA, 17µm voxel size). Images were reconstructed and then post-processed in 3D Slicer and ImageJ to determine the bone morphological properties of each graft. Otsu's method was utilized to isolate bone tissue from background. Bone volume fraction (BV/TV), trabecular thickness (Tb.Th), trabecular separation (Tb.S), and bone surface to bone volume ratio (BS/BV) were then determined. Differences between the two groups were identified using student t-tests for qRT-PCR data and paired t-tests for micro-CT data. Significance was defined as 0.01 using Bonferroni correction to account for multiple exploratory comparisons.

Results: A total of twelve patients, of which eight were female and four were male with a mean age of 53.9 ± 6.9 years, consented to participate and were enrolled in this study. Six patients had a history of tobacco use. Macroscopically, the iliac crest autografts were larger and more intact compared to the smaller, fragmented local inferior cervical vertebral bone. The qRT-PCR analysis of the bone autografts revealed no differences in ALP, BMP2, RUNX2, VEGFA, and TNFSF11 expression between the cervical vertebrae and iliac crest ($p > 0.01$). Finally, micro-CT analysis of the cervical vertebrae and iliac crest autografts showed no statistically significant differences between groups for BV/TV, Tb.Th, Tb.S, and BS/BV ($p > 0.01$).

Discussion and Conclusion: This study provides the first direct comparison between cervical vertebral bone and iliac crest based on micro-CT and qRT-PCR analysis from same donor bone samples. Given the lack of significant differences in gene expression and morphometric properties between bone from the cervical vertebrae and those for bone harvested from the iliac crest, the cervical vertebrae continue to represent an alternative source of autologous bone graft.

Category: **Spine**